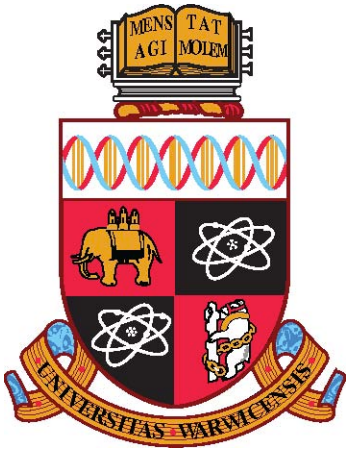

Regulation of KIF1C transport

by
Nida Siddiqui

Supervisors:
Dr. Anne Straube
Dr. Robert Cross

Thesis
Submitted to The University of Warwick for the degree of
Doctor of Philosophy
Jan 2018

CONTENTS

List of Tables

List of Figures

ACKNOWLEDGEMENTS

I would like to thank my supervisor Dr. Anne Straube for providing me with this opportunity to learn and grow as a researcher. Thank you for the guidance and never ending support and encouragement. I would like to thank Dr. Robert Cross, my second supervisor and our collaborator for valuable comments and helpful discussions over the past three years. I would also like to thank Dr. Algirdas Toleikis and Hamdi Hussain for collaborating with us and providing invaluable expertise. Special thanks to Dr. Hauke Drechsler for helping me with insect cell culture.

I would like to acknowledge everyone at CMCB, especially the past and present members of the Straube lab for keeping the atmosphere in the lab lively with active discussions. Special thanks to Dr. Alice Bachmann, Daniel Roth and Hamdi Hussain. I would like to thank the cake club for scrumptious cakes week after week and introducing me to the world of baking.

I would like to thank Dr. Anup Das and Dr. Rucha Sawlekar for making Coventry a home away from home. I will always cherish the time we spent together.

Finally, I would like to thank my family, especially my parents for their encouragement, love and support in fulfilling my PhD.

DECLARATION

This thesis is submitted to the University of Warwick in support of my application for the degree of Doctor of Philosophy. It has been composed by myself and has not been submitted in any previous application for any degree.

The work presented (including data generated and data analysis) was carried out by the author except in the cases outlined below:

- pKan-CMV-KIF1C$_{1\text{-}610}$GFP and pFastBac-M13-KIF1CGFP-MBN were cloned by Daniel Roth.
- Cross-link mass spectrometry was carried out in collaboration with Hamdi Hussain (HH), McAinsh Lab, CMCB, University of Warwick. The reactions were setup in parallel with HH. The samples were run by the proteomics facility, University of Warwick using HH's method. The analysis of the spectra was done together with HH.
- The Optical Trapping of KIF1C was carried out in collaboration with Dr. Algirdas Toleikis (AT), Cross Lab, CMCB, University of Warwick. The experiments were done together with AT and the code used to analyse trapping data was developed by AT unless mentioned otherwise.

Parts of this thesis have been published by the author:

- Parts of Chapter 1 are published in "Siddiqui, N. and Straube, A., 2017. Intracellular cargo transport by kinesin-3 motors. *Biochemistry (Moscow)*, *82*(7), pp.803-815".

ABSTRACT

KIF1C is a kinesin-3 family motor protein that accumulates at the tip of the tail in migrating cells and transports α5β1-integrins into cellular protrusions and is therefore required for the regulation of cell adhesion structures. KIF1C also transports dense core vesicles (DCVs) in neurons. Consistent with its function in long distance transport, mutations in KIF1C causes hereditary spastic paraplegia (HSP) and cerebellar dysfunction in humans. Previous data generated in the Straube lab (Bachmann et al, unpublished) show that PTPN21, a scaffolding phosphatase restores KIF1C mediated α5-integrin transport when overexpressed in KIF1C-depleted cells. In this study, the hydrodynamic analysis of recombinant full-length KIF1C and crosslinking mass spectrometry reveals that KIF1C is a stable dimer that adopts an autoinhibited conformation by interaction of its tail with the motor domain. Next, we show that KIF1C is a processive plus-end directed motor in single molecule assays and confirm that the scaffold phosphatase PTPN21 is a positive regulator of KIF1C-mediated transport. We also investigate the structural domains of KIF1C contributing to the rear accumulation in cells and show that the proline rich domain at the C-terminus of KIF1C is required for the tail localisation of KIF1C, but that the binding of 14-3-3 proteins to the tail domain negatively regulates KIF1C. Finally, using optical trapping we show that a single KIF1C can generate forces up to 5.5 pN and the HSP-causing mutations are processive but weak motors.

List of Abbreviations

ATP	Adenosine-5'-triphosphate
FERM	4.1 protein Ezrin Radixin Moesin-like domain
FHA	Forkhead-associated domain
HA	Human influenza hemagglutinin
HSP	Hereditary spastic paraplegia
MAPs	Microtubule-associated proteins
MT	Microtubule
MTOC	Microtubule-organising center
PCR	Polymerase chain reaction
PTPN21	Tyrosine-protein phosphatase non-receptor type 21
PH	Pleckstrin homology domain
PX	Phosphoinositide-binding structural domain
START	StAR-related lipid-transfer domain
Ni-NTA	Nickel-nitrilotriacetic acid

Amino acid abbreviation

A	Ala	Alanine
C	Cys	Cysteine
E	Glu	Glutamate
G	Gly	Glycine
H	His	Histidine
K	Lys	Lysine
L	Leu	Leucine
P	Pro	Proline
R	Arg	Arginine
S	Ser	Serine
W	Trp	Tryptophan

CHAPTER 1 INTRODUCTION

1.1. Cytoskeleton and Intracellular transport

The cytoskeleton is the supporting structure of the cell that provides shape as well as spatial organization to carry out fundamental functions. The cytoskeletal system is comprised of microtubules, actin microfilaments and intermediate filaments. Microtubules are polymers of alpha and beta tubulin heterodimers (Luduena and Woodward, 1975). They have a growing plus end which extends to the periphery of a cell whereas most of the minus ends are anchored at the Microtubule organizing centre (MTOC). Microfilaments are polar, tightly packed polymers of filamentous actin (F-actin). Actin microfilaments are predominantly present in the edges of the cell and they contribute to cell motility (Carlier and Pantaloni, 2007). Microtubules and actin microfilaments act as tracks for intracellular transport driven by molecular motors. Kinesins and dynein drive transport along microtubules, whereas myosins drive actin based transport. Intermediate filaments are formed of multiple types of related monomer units and they are called so since their mean diameter (~10 nm) lies in between that of actin microfilaments (~8 nm) and microtubules (~25 nm). Intermediate filaments have higher tensile strength than microtubules and protect the cell from shearing stresses and opposing forces (Herrmann et al., 2007). Together, these three components of the cytoskeleton contribute towards the maintenance of cell structure and help perform vital functions.

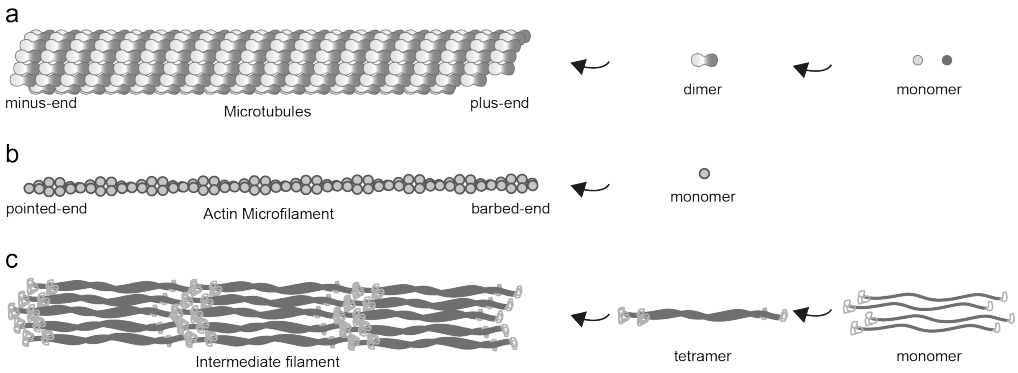

Figure 1.1: Cytoskeletal filaments

The three major classes of cytoskeletal filaments are depicted. (a) Microtubules, composed of alpha (light grey) and beta tubulin (dark grey) subunits. (b) Actin microfilaments, composed of G-actin monomers. (c) Intermediate filaments, composed of various monomer units. Adapted from (Insall and Machesky, 2001).

1.2. Microtubule based transport

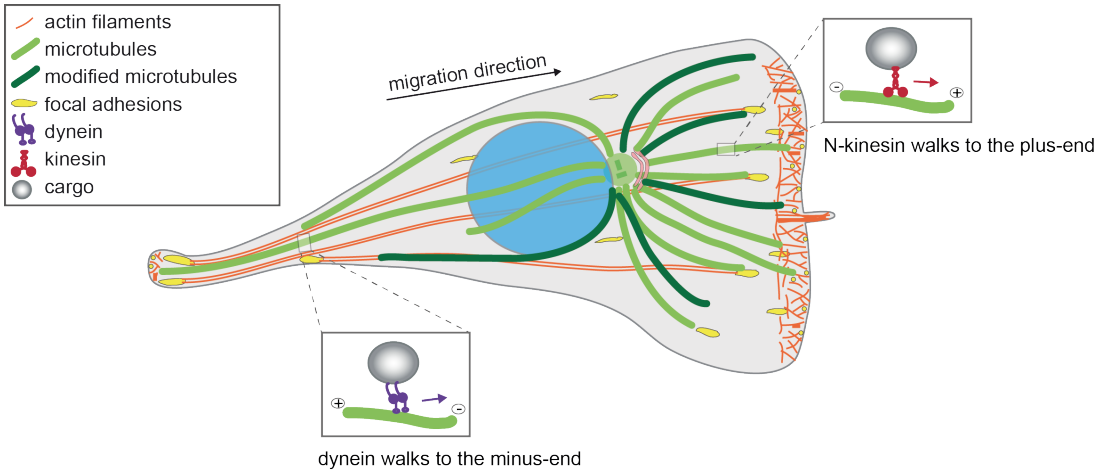

Figure 1.2: Microtubule based cellular transport in a migrating cell

Cytoskeleton network in a migrating cell. Motors transport cargo directionally along microtubules. Kinesins walk to the plus-ends and dynein to the minus-end of the microtubules. Adapted from (Bachmann and Straube, 2015).

Microtubules carry out a range of functions such as supporting the cell shape, providing intracellular tracks for the translocation of cargo, and in participating in cell division and cell migration (Vicente-Manzanares et al., 2005). These diverse functions are mediated by Microtubule-associated proteins (MAPs) (Etienne-Manneville, 2010) and post-translational modifications on alpha and beta tubulin sub units (Janke, 2014). Molecular motors are a class of MAPs that directionally transport cargo along

microtubule tracks. Dynein and kinesin are examples for molecular motors (Hirokawa, 1998) (Figure 1.2).

Kinesin motors are present in all eukaryotes and are crucial for cell functionality since they transport intracellular cargo such as chromosomes, mitochondria (Nangaku et al., 1994) and secretory vesicles (Lo et al., 2011). They utilize ATP to generate mechanical force and step along microtubules (Cross, 2016). Kinesins have been classified into 15 families based on the sequence homology and position of their motor domain (Lawrence et al., 2004, Wickstead et al., 2010). In general, N-kinesins have the motor domain at the amino terminal and walk towards the plus-end of the microtubule, C-kinesins possess the motor domain to the carboxy end and walk to the minus-end whereas the M-kinesins have the motor domain in the middle and they destabilize microtubules (Bringmann et al., 2004) (Hirokawa et al., 2009). However, there are a few exceptions such as Cin8, Cut7 and KlpA. Kinesin-5 motor protein Cin8 and Cut7 have a N-terminal motor domain but can walk bi-directionally (Gerson-Gurwitz et al., 2011, Roostalu et al., 2011, Britto et al., 2016). Whereas kinesin-14 motor protein KlpA which possesses a C-terminal motor domain has been reported to walk along the plus end-directed microtubules (Popchock et al., 2017). Members of the kinesin- 1, 2 and 3 families have emerged to be vital in shuttling cargo in cells (Lipka et al., 2016, Elluru et al., 1995, Scholey, 2013). In particular, for kinesin -3 family motors, it is becoming clear that their main function is the long-distance transport of membranous cargo since they are highly processive, i.e. the distance they walk before falling off the microtubule track. This makes them particularly suited for long-haul tasks and their implication in neuronal diseases (Reid et al., 2002, Dor et al., 2014, Caballero Oteyza et al., 2014) has led to the need to understand the mechanism of motor activity and regulation.

1.3. Kinesin-3 family

UNC-104 was the first member of the kinesin-3 family to be identified in *Caenorhabditis elegans* as a result of the mutation affecting the transport of synaptic vesicles to the axon terminal (Hall and Hedgecock, 1991, Tsunetoshi

et al., 1991), following which other kinesins from different species were established based on homology to the motor domain of the UNC-104 (Miki et al., 2005). The kinesin-3 family comprises of six subfamilies in mammals KIF1, KIF13, KIF14, KIF16, KIF28 and a fungal-specific group of short kinesin-3-like proteins (Fuchs, 2004) (Figure 1.3), making it one of the largest kinesin super families (Miki et al., 2005). The mammalian kinesin-3 motors have been reported to be involved in a wide array of cellular functions. KIF1A (*Ce*UNC-104 homolog in mammals) is involved in transport of vesicles (Lo et al., 2011, Okada et al., 1995) and viral particles (Kratchmarov et al., 2013), KIF1B transports mitochondria (Nangaku et al., 1994), KIF1C is involved in neuronal transport, integrin transport and cell migration (Theisen et al., 2012, Kopp et al., 2006, Lipka et al., 2016), KIF14 in cytokinesis (Gruneberg et al., 2006, Xu et al., 2014) and in Rap1a-Radil signalling during breast cancer progression (Ahmed et al., 2012) , KIF13A and KIF16A in mitosis (Sagona et al., 2010, Torres et al., 2011), and KIF16B for early embryonic development (Ueno et al., 2011).

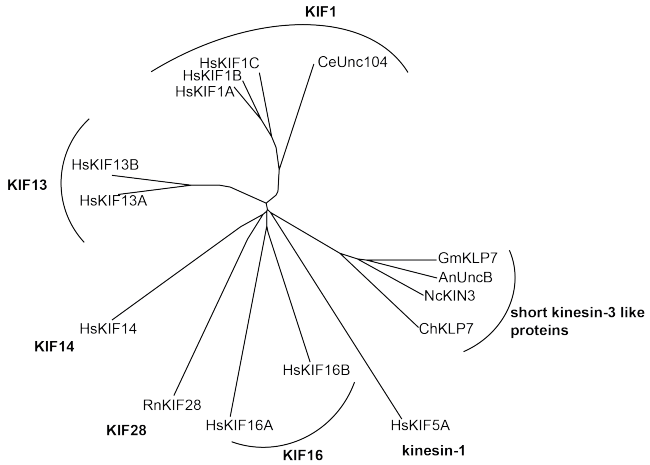

Figure 1.3: Kinesin-3 family tree.

Phylogenetic tree of selected kinesin-3 family members. Homo sapiens (Hs), Caenorhabditis elegans (Ce), Aspergillus nidulans (An), Neurospora crassa (Nc), Rattus norvegicus (Rn), Gibberella moniliformis (Gm), and Cochliobolus heterostrophus (Ch). Bold font indicates subfamilies. Human KIF5A, a kinesin 1, was used as root. Adapted from (Siddiqui and Straube, 2017).

1.3.1. Kinesin-3 family - Cellular function and human disease

Kinesin-3-mediated transport is required for neuronal morphogenesis and function; mutations in any of the KIF1 motors KIF1A, KIF1B or KIF1C

cause neurological disorders, spastic paraplegia or multiple sclerosis both in human patients and mouse models (Dor et al., 2014, Yonekawa et al., 1998, Niwa et al., 2008, Caballero Oteyza et al., 2014, Aulchenko et al., 2008). *C. elegans* worms require axonal transport by UNC-104 for the coordination of their movement (Tsunetoshi et al., 1991). In addition, kinesin-3 motors have been shown to regulate signalling processes and the orderly progression of cell division. For example, KIF16A tethers the pericentriolar material to the daughter centriole during mitosis thereby preventing PCM fragmentation and enabling the formation of a bipolar mitotic spindle (Torres et al., 2011); and KIF13A translocates a component of the cell abscission machinery to the spindle midzone thereby controlling cytokinesis (Sagona et al., 2010). Likewise, deletion of the sole kinesin-3 in *Ustilago maydis* results in a cell separation defect (Wedlich-Soldner, 2002). Important cargoes of kinesin-3 proteins are summarised in Table 1 and range from mitochondria and viruses to vesicles containing a variety of receptors, pre-synaptic signalling proteins, microtubule regulators and phospholipids (Okada et al., 1995, Drerup et al., 2016, Fehling et al., 2013, Theisen et al., 2012, Horiguchi et al., 2006, Lo et al., 2011, Nangaku et al., 1994, Ueno et al., 2011).

Motor	Cargo	Cell type	Reference
KIF1A	Tyrosine kinase A receptor (TrkA)	Mouse dorsal root ganglion neurons	(Tanaka et al., 2016)
	Synaptotagmin and synaptophysin	Rat spinal nerves (cauda equina)	(Okada et al., 1995)
	Dense core vesicles	Rat primary hippocampal neurons	(Lo et al., 2011)
	Beta secretase-1	Mouse SCG neurons	(Hung and Coleman, 2016)
	AMPA receptors	Rat brain	(Shin et al., 2003)
KIF1B	mitochondria	Mouse Neuro2a cells	(Nangaku et al., 1994)
	SCG10 / Stathmin-2	Sensory axons in zebrafish	(Drerup et al., 2016)
	lysosomes	Cos7 African green monkey fibroblast cells	(Matsushita et al., 2004)
KIF1C	$\alpha 5\beta 1$-integrin	RPE1 human epithelial cell line	(Theisen et al., 2012)
	Dense core vesicles	Rat primary hippocampal neurons	(Lipka et al., 2016)

KIF13A	Serotonin type 1A receptor	Mouse hippocampal neurons	(Zhou et al., 2013)
	Viral matrix proteins	Huh7 human hepatoma cell line	(Fehling et al., 2013)
	Mannose-6-phosphate receptors	MDCK canine epithelial cell line	(Nakagawa et al., 2000)
	FYVE-CENT	HeLa human cervical cancer cell line	(Sagona et al., 2010)
KIF13B	Human discs large (hDlg) tumour suppressor	In vitro reconstitution with purified human KIF13B	(Yamada et al., 2007)
	PtdIns(3,4,5)P_3-containing vesicles	Rat PC12 cells and in vitro reconstitution	(Horiguchi et al., 2006)
	Vascular endothelial growth factor receptor 2	Human umbilical vein endothelial cells (HUVECs)	(Yamada et al., 2014)
	Transient receptor potential vanilloid 1	CHO cells, rat dorsal root ganglion neurons	(Xing et al., 2012)
KIF16B	Fibroblast growth factor receptor	Mouse embryonic stem cells	(Ueno et al., 2011)

Table 1: Kinesin-3 cargoes.

List of cargoes identified to be transported by selected kinesin-3 family members.

1.3.2. Structure of kinesin-3 motors

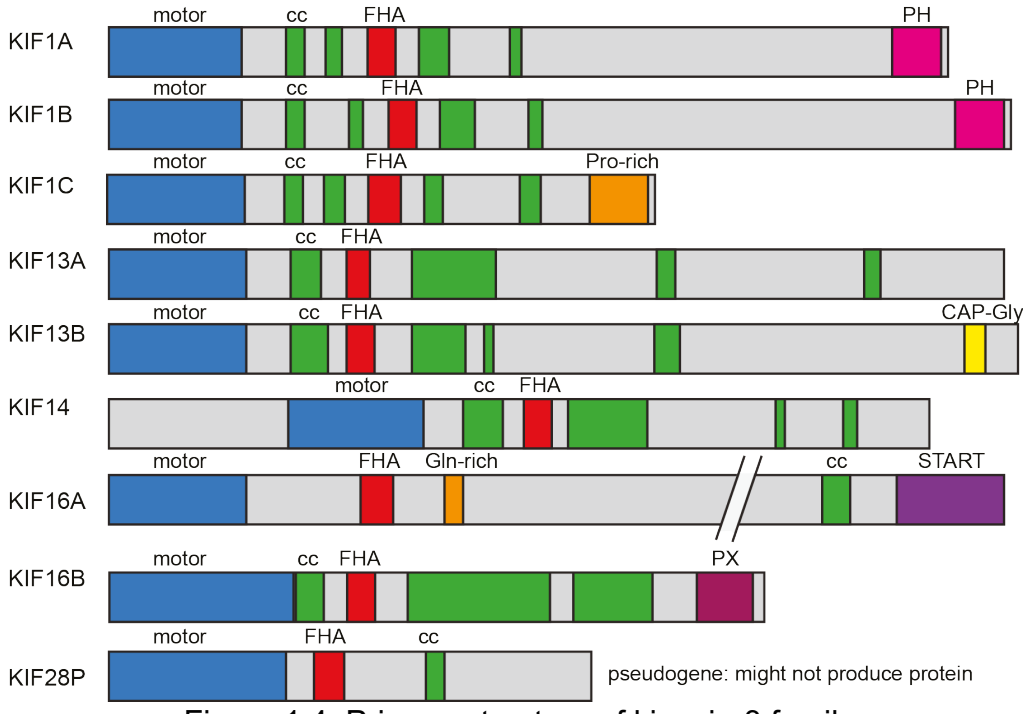

Figure 1.4: Primary structure of kinesin-3 family

Schematic representation of the different kinesin-3 family members and their structural domain organization is depicted here. Blue-motor domain, green-coiled coil, red-FHA domain, pink-pleckstrin homology, orange-proline-rich, yellow-CAP-Gly, purple-START domain.

All kinesin motors that walk towards the plus end of microtubules have their motor domain at the N-terminus of the molecule. This is also true for kinesin-3 family motors. What sets kinesin-3 motors apart from other kinesins is the organisation of the neck region, which contains a β-strand as well as a helix (Miki et al., 2005), and the presence of a forkhead-associated (FHA) domain (Westerholm-Parvinen et al., 2000) in the tail. In addition to the FHA domain, the tail region contains a number of short coiled-coils and diverse protein and lipid interaction domains that mediate binding to cargo and regulators.

The motor domain binds to the microtubule and the energy from ATP hydrolysis is used to produce directional movement (Endow, 1999, Vale et al., 2000). A characteristic feature of the kinesin-3 family is the presence of a stretch of positively charged lysine residues designated as the K-loop in loop 12 of the motor domain. This loop is ideally positioned so that it can make contact with the negatively charged glutamate-rich (E-hook) C-terminal tail of β-tubulin. The K-loop was proposed to enable processive motion of monomeric KIF1A by mediating diffusive interaction to microtubules throughout the ATPase cycle (Okada and Hirokawa, 1999, Okada and Hirokawa, 2000). However, reports suggest that the K-loop in KIF1, KIF13 and KIF16 increase microtubule affinity (Soppina and Verhey, 2014, Rogers et al., 2001, Matsushita et al., 2009). An increase in processivity could not be attributed to the K-loop where these motors are working as dimers since the mutation of K-loop leads to decreased microtubule affinity but the processivity of motor remains unaffected (Soppina and Verhey, 2014). Instead, the K-loop promotes microtubule-binding and enables kinesin-3 motors to effectively work in teams (Rogers et al., 2001, Soppina and Verhey, 2014). Recent comparative high-resolution cryo electron microscopy structures of kinesin-1 (KIF5A) and kinesin-3 (KIF1A) motor domains bound to microtubules in different nucleotide states paired with molecular dynamics simulations, ascertained which family-specific residue changes result in the 200-fold increased affinity of kinesin-3 motors to microtubules relative to kinesin-1 (Scarabelli et al., 2015, Atherton et al., 2014). These residues reside in loops L2, L7, L8, L11, L12 and α-helices α4 and α6. Thus, the contribution of

multiple sites increases kinesin-3's interaction surface with microtubules and results in a large effect on affinity. This increased affinity then increases the processivity of dimeric kinesin-3 motors (Atherton et al., 2014). Key residues that result in a 10-fold increased processivity of kinesin-3 versus kinesin-1 are Arg167 in loop 8, Lys266 in loop 11 and Arg346 in α-helix 6 of KIF1A (Scarabelli et al., 2015).

Coiled coils are important structural features that mediate motor dimerisation (Peckham, 2011). Kinesin-3 motors tend not to contain the extended coiled coils that are typical for the tails of other kinesins, but instead contain a number of smaller predicted coiled-coil regions scattered along the tail. It is presently unclear whether all of these contribute to dimer formation. So far, the only direct test of this was performed with the fourth coiled-coil domain of KIF1C, which is sufficient to drive dimerisation in a yeast-two-hybrid assay (Dorner et al., 1999). In KIF1A, KIF13A and KIF13B, the coiled-coil domains seem to interfere with dimerisation. It has been shown that instead, the neck coil alone efficiently dimerises these motors (Hammond et al., 2009, Soppina et al., 2014).

FHA domains are small protein modules that recognise phospho-threonine epitopes on proteins and mediate protein-protein interactions (Li et al., 2000, Hammet et al., 2003). FHA domains have been found in more than 200 different proteins with diverse cellular functions such as transcription, DNA repair and protein degradation (Durocher and Jackson, 2002). Besides fulfilling a structural role in kinesin-3 proteins, the FHA domain also confers specific cargo interactions. For example, the FHA domain of KIF13B medicates binding to its cargo transient receptor potential vanilloid 1 (TRPV1). Interestingly, this interaction depends on phosphorylation of KIF13B at T506 in the FHA domain by cyclin-dependent kinase 5 (Cdk-5). (Xing et al., 2012). A point mutation that is likely to alter the folding of the FHA domain of KIF1C has been reported to change the anthrax susceptibility in mice. Ectopic expression of a resistant allele of KIF1C was shown to partially rescue anthrax susceptible macrophages (Durocher and Jackson, 2002, Watters et al., 2001) suggesting the importance of FHA domain, however more recently in vitro

assays with macrophages and in vivo assays in mice rule out kif1c gene as a candidate for anthrax toxin susceptibility (Nakajima and Tanaka, 2010). The role of the point mutation in the FHA domain remains unclear.

Several kinesin-3 tails contain domains that allow direct interaction with membranes: e.g. KIF16A contains a START/lipid sterol-binding domain at the C-terminus (Torres et al., 2011). KIF1A and KIF1B have a pleckstrin homology (PH) domain that is important for binding cargo vesicles (Xue et al., 2010), probably through specific interaction with phosphatidylinositol 4,5-bisphosphate (PtdIns(4,5)-P_2) (Klopfenstein et al., 2002). KIF16B possesses a phosphoinositide-binding structural domain (PX), which binds to PtdIns(3,4,5)P_3 and is involved in the trafficking of early endosomes (Blatner et al., 2007, Hoepfner et al., 2005).

Other kinesin-3 tails contain protein interaction domains, such as a CAP-Gly domain at the C-terminus of KIF13B. CAP-Gly domains bind to sequence motifs at the C-terminus of tubulin and EBs, zinc-finger motifs and proline rich sequences (Steinmetz and Akhmanova, 2008). KIF1C possesses a proline-rich region at the C-terminus. Proline-rich regions play a structural role and also act as binding sites for protein interaction (Williamson, 1994). In the case of KIF1C, this domain mediates several protein interactions, including the cargo adapter protein BICDR1, 14-3-3 proteins and Rab6 (Schlager et al., 2010, Dorner et al., 1999, Lee et al., 2015).

Surprisingly, a monomeric motor construct of KIF1A has been observed to undergo processive plus-end directed movement along microtubules (Okada and Hirokawa, 1999). This is thought to be possible due to the presence of the K-loop and a stable microtubule interaction surface that persists throughout the ATPase cycle (Atherton et al., 2014, Okada and Hirokawa, 2000). However, monomeric KIF1A only moves very slowly (0.15 µm/s) and weakly (~0.15 pN) along microtubules, while multiple KIF1A motors transport cargo at 1.5 µm/s (Okada et al., 2003, Okada et al., 1995). Teams of 10 monomeric KIF1A motors have been proposed to become approximately 100-fold stronger than a single monomeric motor (Oriola and Casademunt, 2013), however, experimental data on the force generation of kinesin-3 teams are

lacking. There is evidence suggesting that kinesin-3 motors exist as inactive monomers in cells until activated by dimerisation (Soppina et al., 2014, Al-Bassam et al., 2003, Rashid et al., 2005, Tomishige et al., 2002). Other studies suggest that KIF1A motors are dimeric *in vivo*, but in an autoinhibited state until activated by cargo binding (Hammond et al., 2009, Pollock et al., 1999). Thus, the extent to which individual kinesin-3 family members exist as monomers or dimers in cells remains to be elucidated. However, it is clear that a single monomeric motor cannot achieve the high processivity of kinesin-3 mediated cargo transport observed in cells. Thus these would need either to work in teams formed by recruitment of several monomeric motors to the same cargo, or to form dimers.

1.3.3. Regulation of Cargo Transport

1.3.3.a. Mechanism of autoinhibition

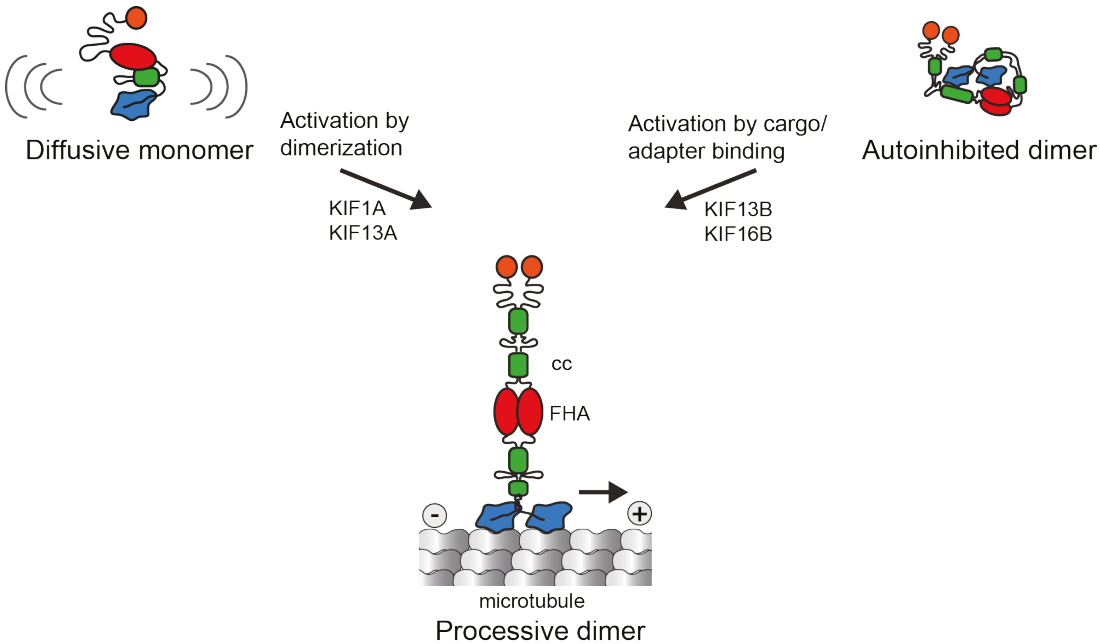

Figure 1.5: Models of Autoinhibition

The two known models for autoinhibition are depicted here. A monomer to dimer switch model, where the motor is a diffusive monomer and is activated by dimerization and the autoinhibited dimer activated by cargo and/or adapter binding.

Early work and biochemical characterisation of conventional kinesin revealed that the molecule exists in two conformations: a folded inactive

conformation and an extended active one (Hirokawa et al., 1989, Hackney et al., 1992). Consistent with an autoinhibited state, a small peptide region in the tail of kinesin-1 binds to the motor domain to inhibit it (Friedman and Vale, 1999, Stock et al., 1999, Coy et al., 1999). Crystal structure of kinesin-1 dimeric motor heads reveals a “double lockdown” mechanism where the movement of the motor heads is restricted due to the cross-linking at the coiled coil region and tail domains (Kaan et al., 2011). While kinesin-3 motors do not contain such an extensive coiled-coil region with a hinge that allows neat folding and unfolding of the tail, inactive kinesin-3 motors have been shown to adopt a compact conformation with a crumpled tail (Hirokawa and Noda, 2008), which is likely to extend when activated and/or under load. That the pool of motors exists in an autoinhibited state in cells is important because in the absence of cargo, motor activity needs to be tightly regulated to avoid microtubule crowding and futile ATP consumption.

Currently, there are two models of autoinhibition that apply to kinesin-3 motors. In the monomer-dimer switch model, intramolecular interactions involving neck and tail regions hold some kinesin-3 motors in a monomeric, inactive state. Upon activation, these motors dimerise with their neck coil and tail regions undergoing intermolecular interactions. In the alternative tail block model, the motors are stable dimers, but regions of the tail interact with the motor or neck domains and interfere with motor activity until cargo binding occupies the tail region and releases the motor. Evidence exists for both models and the picture emerging is that different kinesin-3 motors might use either or a combination of both of these methods of autoinhibition.

Most KIF1 and KIF13 motors are thought to undergo a monomer-dimer switch. Consistently with an autoinhibited state, full length UNC-104 from *C. elegans* and murine KIF1A are inactive in motility assays (Hammond et al., 2009, Okada et al., 1995). As a monomeric motor domain construct of KIF1A could produce some directional motion by itself and work as a processive motor when dimerised artificially (Okada and Hirokawa, 1999, Tomishige et al., 2002), regions of the neck or tail interfere with motor activity. Indeed, in UNC-104, the two neck helices can form an intramolecular coiled-coil, thereby

inhibiting the ATPase and microtubule binding cycle of the motor and holding the motor in a monomeric state (Al-Bassam et al., 2003). The neck helices can also form an intermolecular coiled-coil thereby enabling the switch from monomer to dimer, which is required to obtain a processive UNC-104 motor (Al-Bassam et al., 2003). In murine KIF1A, a similar switch through intra- and intermolecular coiled-coil formation is proposed to occur between the neck coil region and the first coiled coil domain (CC1). Surprisingly, the truncation of the entire tail results in processive dimeric motors of KIF1A, KIF13A and KIF13B, while all longer constructs containing CC1 result in monomers that only show diffusive movement, suggesting that the CC1 makes contacts with the neck region to keep the motors in a monomeric state (Hammond et al., 2009, Soppina et al., 2014). If autoinhibition is prevented by deletion of the flexible hinge between the neck helices in *C. elegans* UNC-104, the motility of the motor *in vitro* is unperturbed, but transgenic worms show severe defects in the coordination of their movement (Al-Bassam et al., 2003). Likewise, mutations in the CC1 segment of KIF1A result in activation of the motor (Huo et al., 2012, Yue et al., 2013). In the KIF13 subfamily, a proline residue at the junction of neck coil and CC1 provides the flexibility to enable CC1 to fold back and interact with the neck coil. Deletion of this proline residue results in dimerisation via the neck coil domains and active, processive motors (Soppina et al., 2014, Ren et al., 2016). Control of the autoinhibited state of the KIF1A motor might also involve the FHA domain and the following coiled coil CC2. A tandem construct of CC1 and FHA domains forms a very stable dimer. Furthermore, the dimerisation of CC1-FHA sequesters the CC1 region and makes it unavailable for the autoinhibition of the neck coil region (Huo et al., 2012). Also, CC2 can fold back to interact with the FHA domain, which disrupts the motor activity (Hammond et al., 2009). Disruption of the CC1-FHA dimer severely impairs synaptic vesicle transport and locomotion in *C. elegans* worms, suggesting that robust dimerisation is crucially important for KIF1A function *in vivo* (Yue et al., 2013).

Evidence for a tail block mechanism exists for KIF13B and KIF16B. In KIF16B, microtubule binding is inhibited by the interaction of the second and third

coiled-coil with the motor domain in an ATP dependent manner. This tail-mediated inhibition is important for the correct localisation of early endosomes to somatodendritic regions in neurons and the recycling of AMPA and NGF receptors (Farkhondeh et al., 2015). An interaction of a tail domain with the motor domain also contributes to the autoinhibition of KIF13B (Yamada et al., 2007, Yoshimura et al., 2010). Upon phosphorylation of KIF13B close to its C-terminus by Par1b/MARK2 (microtubule affinity-regulating kinase), 14-3-3β binds and promotes the intramolecular interaction of KIF13B motor and tail domains. This in turn negatively regulates KIF13B microtubule binding, resulting in the dispersal of the motor in the cytoplasm and a reduction in cell protrusion and axon formation (Yoshimura et al., 2010). Also, KIF1C, which is known to exist as a stable dimer, interacts with 14-3-3 proteins in a phosphorylation-dependent manner (Dorner et al., 1999). However, whether this mediates an auto inhibitory tail – motor interaction similarly to KIF13B remains to be elucidated.

Taken together, these data suggest specific autoinhibition mechanisms for each kinesin-3 family member. These might require different interaction partners to achieve release from autoinhibition and activate the motors for transport of specific cargoes.

1.3.3.b. Activation by cargo interaction

Many kinesins are activated upon cargo binding. Full-length KIF13B, also known as guanylate kinase-associated kinesin (GAKIN) exists in an autoinhibited state in solution. It is activated by the direct binding of its cargo human discs large (hDlg) tumour suppressor (Yamada et al., 2007). In contrast to KIF1A, full-length KIF13B is active in a gliding assay. This could be because the binding of the C-terminus to the glass surface might mimic the cargo-bound state, thus relieving autoinhibition (Yamada et al., 2007). In contrast, KIF16B is a monomer in the cytoplasm and dimerises at the cargo surface. The localised dimerisation of KIF16B on early endosomes has been directly observed using Förster resonance energy transfer (FRET) in live cells (Soppina et al., 2014). Thus, these examples support the idea that due to the

diverse cargo binding tail, the different kinesin-3 family members use diverse means of autoinhibition and cargo-dependent release of inhibition, involving changes in the dimerisation status for some members and competitive binding of a peptide region that weakly interacts with the motor domain for others. The mechanisms of cargo-mediated activation thus require to be elucidated for each family member.

While some motors bind their cargo directly, often cargo adapter proteins mediate both the motor activation and cargo recruitment. For *C. elegans* kinesin-3 motor UNC-104, a number of adapter proteins are known that are involved in cargo loading; a bimolecular fluorescence complementation assay (BiFC) was employed to show that binding of different adapters UNC-16 (JIP3), DNC-1 (DCTN-1/Glued) and SYD-2 (Liprin-α) to UNC-104 results in translocation to different sub-cellular compartments in neuronal cells. This suggests that adaptor proteins are able to recruit the motor to their cargo and steer their transport (Wagner et al., 2009, Hsu et al., 2011). Further, binding of LIN-2 (CASK) and SYD-2 was shown to positively regulate the UNC-104 motor by increasing its velocity and binding of LIN-2 also increased run lengths. The cargo transport of synaptobrevin-1 (SNB-1) was markedly reduced in the neurons of LIN-2 knockout worms implying that LIN-2 is an activator of UNC-104 motor (Wu et al., 2016). In *Ustilago maydis*, the cargo adapter Hook protein (Hok1) mediates the recruitment of Kin3 and dynein to early endosomes and regulates bi-directional motility. Hok1 releases Kin3 and this allows for dynein to bind and drive the subsequent change in directionality (Bielska et al., 2014). Similar to Kin3, KIF1C binds to another dynein adapter protein, Bicaudal-D-related protein 1 (BICDR-1) (Schlager et al., 2010). BICDR-1 also binds Rab6A vesicles, thus linking both motors to secretory vesicles and controlling the bi-directional vesicle transport in developing neurons (Schlager et al., 2010). Centaurin α1 (CENTA1) acts as a cargo adapter for KIF13B and recruits the motor to PtdIns(3,4)P_2 / PtdIns(3,4,5)P_3-containing vesicles (Horiguchi et al., 2006, Tong et al., 2010). CENTA1 contains two PH domains that bind the head groups of phosphoinositides, and PH1 also directly binds the FHA domain of KIF13B in a phosphorylation-

independent manner (Tong et al., 2010). As KIF13B FHA simultaneously interacts with the ArfGAP domain of a second CENTA1 molecule, CENTA1-KIF13B form a heterotetrameric transport complex for PtdIns(3,4,5)P_3-rich vesicles (Horiguchi et al., 2006, Tong et al., 2010).

1.3.3.c Regulation by Rab GTPases

The members of the Rab family of GTPases are known to control the localization of vesicles/organelles in a nucleotide-dependent manner. Rab proteins act at all stages including vesicle formation, motility and tethering of vesicles to the designated compartment (Hutagalung and Novick, 2011). Rab GTPases exist in either GTP or GDP bound states, and are activated by GEFs (GTP/GDP exchange factors) and switched off by GAPs (GTPase activating factors) (Novick and Zerial, 1997). Once activated, the Rab proteins bind to vesicles that are translocated to the destination compartment, where they dock and fuse. The Rab proteins are then recycled back via a cytosolic intermediate (Zerial and McBride, 2001).

KIF1A and KIF1Bβ both transport Rab3-coated vesicles in the axon. Rab3 is a synaptic vesicle protein that controls the exocytosis of synaptic vesicles (Fischer von Mollard et al., 1991, Stettler et al., 1994, Schluter et al., 2004). It has been found that DENN/MADD (Differentially expressed in normal and neoplastic cells/MAP kinase activating death domain), a GEF for Rab3, binds to Rab3 and the tail domain of KIF1A and KIF1Bβ and is thought to mediate the transport to the axon terminal while maintaining Rab3 in the GTP-bound form (Niwa et al., 2008).

Rab6 binds to KIF1C at two sites, to the motor domain and near the C-terminus. Rab6 binding to the motor domain disrupts the motor's ability to bind microtubules (Lee et al., 2015), while the binding to the C-terminus might activate cargo loading and relief from autoinhibition. Secretory Rab6-vesicles are transported bi-directionally and it is thought that the dual ability of Rab6 to activate and inhibit KIF1C might regulate the directional switch. KIF1C also transports Rab11-positive vesicles for the recycling of integrins (Theisen et al.,

2012). Whether Rab11 is directly involved in controlling the activity of KIF1C is as yet unclear.

KIF13A binds to the active GTP-bound recycling endosomes associated with Rab11 and controls endosomal sorting and recycling of endosomal cargo (Delevoye et al., 2014). KIF16B transports Rab5-positive early endosomes and Rab14-positive vesicles in non-neuronal cells (Hoepfner et al., 2005, Ueno et al., 2011). To which extent these Rabs affect kinesin remains to be understood.

1.3.3.d. Specificity for a subset of microtubule tracks

The microtubule tracks on which kinesin motors walk are not uniform. Depending on the cell type or its differentiation status, cells express different tubulin isoforms, accumulate microtubules with different posttranslational modifications (PTMs) and also express different microtubule-associated proteins (MAPs) that decorate the microtubules. Kinesins are known to be sensitive to both changes to tubulin and MAP composition.

Tubulin undergoes a diverse range of chemical modifications known as posttranslational modifications subsequent to polymerization into microtubules. These modifications mainly occur on the C-terminal tails of both alpha- and beta-tubulin and include the removal of terminal amino acids, such as detyrosination, and the addition of polyglutamate and polyglycine side chains (Hallak et al., 1977, Edde et al., 1990, Redeker et al., 1994). Considering that the kinesin-3-specific K-loop is thought to interact with the C-terminal tail of β-tubulin, it is expected that changes in this region would impact kinesin-3 binding. Further modification at other sites of tubulin have been described such as the acetylation of K40 in α-tubulin and phosphorylation of tubulin at various sites (L'Hernault and Rosenbaum, 1985). These modifications may change the stability of microtubules and act as signposts for motor transport by selectively increasing or decreasing the affinity of certain motors to the microtubule (Janke, 2014). In line with this idea, knockdown of polyglutamylase PGs1 in ROSA22 mice decreases the localisation of KIF1A to neurites (Ikegami et al., 2007). However, in COS cells, the truncated,

constitutively active KIF1A (1-393) was a non-selective motor (Cai et al., 2009). Similar to the finding in COS cells, the negative result could be due to the lack of modified microtubules in these cells rather than a different property of the motor and would require further investigation to elucidate.

The subcellular localisation of KIF1C is regulated by acetylation in primary human macrophages in a way that suggests that tubulin acetylation is a negative signal for KIF1C transport (Bhuwania et al., 2014). Likewise, KIF1Bβ and KIF1A have been reported to drive lysosomal transport preferentially along tyrosinated (i.e. non-modified) microtubules (Guardia et al., 2016). These data suggest that most kinesin-3 motors are sensitive to tubulin PTMs, but with different preferences.

MAPs regulate the assembly and disassembly kinetics of microtubules as well as the interactions of motors with microtubules (van der Vaart et al., 2009, Atherton et al., 2013). Lattice-decorating MAPs such as the neuronal protein tau regulate the attachment rate and can act as roadblocks that affect motors differently, depending on their ability to take side or backwards steps to circumvent the roadblock (Schneider et al., 2015, Dixit et al., 2008, Seitz et al., 2002).

For kinesin-3, MAPs known to regulate the motor include doublecortin like kinase-1 (DCLK-1), which regulates KIF1 transport of dense core vesicles (DCVs) along dendrites in neurons. DCLK-1 specifically binds to microtubules in dendrites, which acts as a positive signal to promote dendritic transport of KIF1 cargoes. In the absence of DCLK-1, KIF1 motors predominantly transport DCVs into the axon (Lipka et al., 2016). The microtubule plus end tracking protein CLASP is required to stimulate the trafficking of KIF1C (Efimova et al., 2014). KIF1C has also been described to move with growing microtubule plus ends in cells (Kopp et al., 2006). This could be either due to the preference for unmodified (i.e. freshly assembled) microtubules (Bhuwania et al., 2014), or due to its fast transport speed and thus ability to catch up with the growing microtubule end (Rogers et al., 2001) or due to its interaction with CLASP (Efimova et al., 2014).

1.3.3.e. Cooperation of motors

Kinesin-3s have been implicated in the bi-directional transport of cargo. This means that when a specific kinesin-3 is inhibited or depleted, the transport of its cargo both towards the plus and the minus end of the microtubule is impaired (Theisen et al., 2012, Ally et al., 2009, Tien et al., 2011). It has been suggested that kinesin-3 cooperates with dynein in the bi-directional transport of cargoes, but the mechanism underlying the mutual activation of these opposite-polarity motors remains to be elucidated (Hancock, 2014). It has been suggested that cooperation depends on the opposing force generated, resulting in a mechanical activation wherein any two opposite polarity motors that move along microtubules were able to activate their counterpart and drive bi-directional transport (Ally et al., 2009). Other proposed models include a steric inhibition mechanism whereby the direct interaction of the opposing motor or accessory protein relieves autoinhibition, and a microtubule tethering mechanism whereby the opposing motor is in a weakly bound state and acts as a processivity factor (Hancock, 2014). This is different to the idea of tug-of-war that has been proposed and reconstituted for kinesin-1 and dynein-mediated transport, where the motors pull against each other and the strongest team wins, i.e. the number of motors of each type loaded to a cargo molecule and the force that each motor can produce determine the net movement of the cargo (Amrute-Nayak and Bullock, 2012, Derr et al., 2012). Potential linkers to facilitate cooperation of dynein and kinesin-3 include Hook and Bicaudal, cargo adaptor proteins that have been identified to interact with both dynein and kinesin-3 tail domains (Bielska et al., 2014, Schlager et al., 2010, Splinter et al., 2010, Fu and Holzbaur, 2014). Interestingly, the presence of BICD2 increases the force generation and processivity of dynein/dynactin (Belyy et al., 2016, Schlager et al., 2014), demonstrating that these cargo adaptor proteins regulate motor activity and could act as switches to control transport directionality within a complex containing two opposing motors. Other control mechanisms could come from accessory proteins such as kinesin binding protein (KBP), which has been shown to bind KIF1C, stimulate KIF1B, but inhibit KIF1A-mediated

bi-directional transport (Kevenaar et al., 2016, Drerup et al., 2016). If the activity of such regulatory proteins was spatially controlled, this would enable directional switching of transport complexes in the presence of opposing motors.

1.4. KIF1C

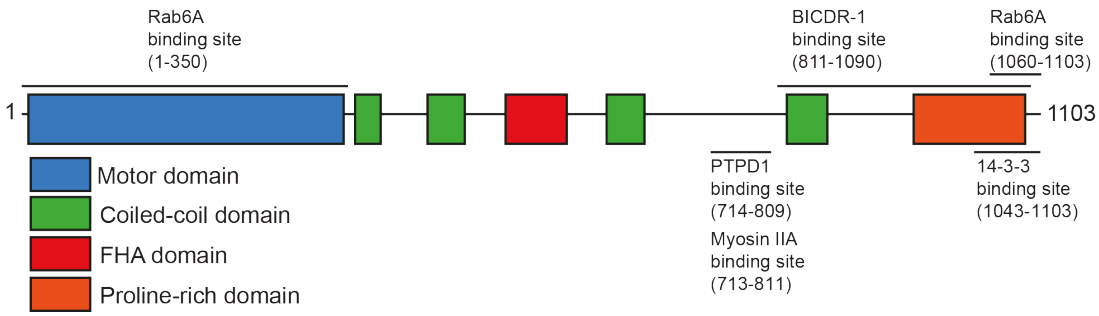

Figure 1.6: Primary Structure of KIF1C

Schematic representation of the primary structure of KIF1C depicting different structural domains. The different proteins that are known to interact with KIF1C are depicted. Rab6A binds at the N and C-terminus (Lee et al., 2015), PTPD1 and Myosin IIA binds between the third and fourth coiled coil domain (Dorner et al., 1998) (Kopp et al., 2006), BICDR-1 and 14-3-3 proteins bind at the C-terminus (Schlager et al., 2010) (Dorner et al., 1999).

In a yeast two-hybrid screen using the FERM domain of a protein tyrosine phosphatase (PTPN21) as bait, KIF1C was identified as an interacting partner for the FERM domain (Dorner et al., 1998). KIF1C is a 1103 amino acid long N-kinesin, comprising of an N-terminal motor domain, a central FHA domain with coiled coil domains at either side and a proline rich domain towards the carboxy terminal of the protein (Fig 1.6). Among the various kinesin-3 family members, KIF1C is most similar to KIF1A and KIF1B in its sequence homology (Dorner et al., 1998). Kinesin-3 family members are implicated in long-distance cargo transport (Lipka et al., 2016, Theisen et al., 2012) and consistent with this function, mutations in KIF1C have been reported to cause hereditary spastic paraplegia (HSP) and cerebral dysfunction in humans (Dor et al., 2013). Functional characterisation for these mutations are lacking.

Cell lysate treatment with cross-linking agents detected endogenous KIF1C dimers, suggesting that KIF1C may be a dimeric motor protein (Dorner et al,

1999). KIF1C localizes to the Golgi apparatus and has been shown to be involved in the cargo transport from Golgi to endoplasmic reticulum (ER) (Dorner et al., 1998). However, knockout experiments in mice did not reveal any deleterious effects and fibroblasts from these mice had a functional Golgi to ER transport (Nakajima et al., 2002). This suggests that KIF1C is not the only motor involved in Golgi to ER transport and the pathway can be rescued by other motor proteins. More recently, KIF1C has been reported to be a key player in maintaining the Golgi structure along with Rab6, a direct KIF1C interacting partner (Lee et al., 2015). Depletion of either Rab6 or KIF1C resulted in Golgi fragmentation suggesting a co-operation between these two proteins. KIF1C has also been implicated in neuronal transport as an unbiased and fast neuronal cargo transporter as it can walk along axons and dendrites (Lipka et al., 2016).

KIF1C also regulates podosome dynamics in macrophages and vascular smooth muscle cells (Kopp et al., 2006; Efimova et al., 2014; Bhuwania et al., 2014) and tubulin acetylation has been shown to influence the subcellular localisation of KIF1C positive vesicles in primary macrophages (Bhuwania et al., 2014). KIF1C has also been shown to interact with Myosin IIA (Kopp et al., 2006) which also localizes to podosomes (Kopp et al., 2006). Myosin IIA generates contractile forces involved in rear retraction (Vicente-Manzanares et al., 2009. It has been reported that in vascular smooth muscle cells (VSMCs) KIF1C fails to accumulate at the cell cortex in CLASP-depleted cells (Efimova et al.,2014) and recent reports from our lab show that KIF1C and PTPN21, a scaffolding phosphatase co-operate to mediate podosome formation in VSMCs (Bachmann et al, unpublished).

KIF1C associates with different regulatory proteins, but the functional significance of these interactions is not very well understood. KIF1C and BICDR-1 (Bicaudal-D-related protein 1) are known to interact and to play a role in the bi-directional transport of secretory vesicles in young neurons (Schlager et al., 2010). BICDR-1 is a dynein cargo adapter and has been recently shown to recruit two dynein molecules by cryo electron microscopy (Grotjahn et al., 2017, Urnavicius et al., 2017). BICDR-1 also binds Rab6A

vesicles, which act as an intermediary protein that links the motor to the cargo (Schlager et al., 2010) and recently it was reported that KIF1C also binds Rab6 at the motor domain and cargo-binding domain (Lee et al., 2015). Another binding partner for KIF1C that was identified recently was Hook3 which also binds dynein (Redwine et al., 2017). Whether Hook3 plays a similar role to that of BICDR-1 in bi-directional transport remains to be seen.

KIF1C has been shown to bind to 14-3-3 scaffold family proteins via the phosphorylation carboxy-terminal serine 1092 (Dorner et al., 1999). 14-3-3 proteins recognise and bind to phospho-serine and phospho-threonine proteins. They act as scaffolding proteins and mediate protein-protein interactions thereby regulating motor and cargo transport activity (Fu et al., 2000, Tzivion and Avruch, 2002).

KIF1C has also been implicated in regulating cellular adhesions in migrating cells. KIF1C transports α5β1- integrins into cellular protrusions and localizes to the tip of the tail in migrating cells (Theisen et al., 2012). The α5β1- integrin transport aids in maturation of trailing adhesions and maintenance of cell tails. Depletion of KIF1C in these cells hampers the tail stability and results in loss of directional persistence (Theisen et al., 2012). In addition to this, reports from our lab show that PTPN21 rescues KIF1C dependent α5 integrin transport in KIF1C depleted cells. PTPN21 emerges as an activator of KIF1C function in cells (Bachmann et al., unpublished).

It is evident that KIF1C has a pivotal role to play in the regulation of cellular processes. Hence, it is important to elucidate the mechanism of kinesin activity, its interactions with other proteins to better understand intracellular cargo transport which is known to play a key role in the pathogenesis of neurological disorders and axonopathies.

1.5. Outline of this work

Previously it has been shown that (Bachmann et al, unpublished) PTPN21, a scaffolding phosphatase restores KIF1C mediated α5-integrin transport when overexpressed in KIF1C-depleted cells. Here, using hydrodynamic analysis the oligomeric status of KIF1C is elucidated. Next,

using purified proteins and single molecule motility assays the activation of KIF1C by PTPN21 is described. In cells, using structural domain analysis the region contributing to the tail localization of KIF1C is determined along with the negative regulation of KIF1C activity by 14-3-3 proteins. Finally, the mechanical properties of KIF1C and behaviour of HSP causing patient mutants are determined using the optical trapping system.

CHAPTER 2 MATERIALS AND METHODS

2.1. Cell Biology

2.1.1. Mammalian cell maintenance

The hTERT RPE-1 cells (Clonetech) were cultured in (DMEM/Nutrient F-12 Ham (Sigma) supplemented with 10 % FBS (Sigma), 2 mM L-Glutamine (Sigma), 2.3 g/l Sodium Bicarbonate (Sigma), 100 U/ml Penicillin (Sigma), 100 µg/ml Streptomycin (Sigma) with 5 % CO_2 in a humidified incubator. For cell maintenance, the RPE-1 cells were grown to 70 % confluency, washed with PBS and incubated with 0.05 % Trypsin and 0.02 % EDTA (w/v) solution (Sigma). Using an inverted microscope cell detachment was assessed and reseeded 1 in 10 in fresh pre-warmed RPE-1 growth medium.

2.1.2. DNA transfection

Cells were seeded onto flourodishes coated with 10 µg/ml fibronectin (Sigma) 24 hours before DNA transfection and the medium was replaced with fresh pre-warmed growth medium prior to DNA transfection. Fugene6 (Promega) was used for plasmid transfection as described in Table 2. DNA was resuspended in Opti-MEM (Gibco) before Fugene6 addition. The transfection reaction was mixed well by pipetting and incubated for 30 minutes at room temperature before addition to cells.

	35 mm quadrant fluorodish – per well
Opti-MEM	37.5 µl
Fugene6	1.125 µl
DNA	0.375 µg

Table 2 : Mammalian cell transfection

2.1.3. Insect cell maintenance

SF9 cells (Invitrogen) were cultured in SF900 serum free medium (Gibco) supplemented with 100 U/ml Penicillin (Sigma), 100 µg/ml Streptomycin (Sigma) in a shaking incubator at 28°C and 105 rpm. Cells were grown up to a density of 1.5×10^6 cells/ml and split 1 in 3 in fresh SF900 serum free medium.

2.1.4. Insect cell transfection and generation of virus stocks

The bacmid DNA and Escort IV (Sigma) were mixed well and added to cells resuspended at a density of 1×10^6 cells per well in a 24- deep well plate as described in Table 3. The transfection reaction was mixed well by pipetting and incubated for 30 minutes at room temperature before addition to cells.

	24- deep well plate, per well
Escort IV	12 µl
SF900 media	1.125 µl
DNA	7 µl

Table 3 : Insect cell transfection

After 5 to 7 days, the cells are spun down and the supernatant harbouring the virus is passed through a 0.45 µm filter and P1 (passage 1) virus stocks are collected. SF9 cells are then infected with 50 µl of P1 virus at a density of 0.5×10^6 cells/ml. Post 36hrs the cells are harvested, resuspended in 70% SF900 SFM, 20% FBS and 10% DMSO, aliquoted as 500 µl and frozen in a cooling pot (Nalgene) and stored in -80ºC. These stocks are referred to as BIICs (Baculovirus Infected Insect Cells).

2.2. Molecular Biology

2.2.1. PCR

PCR amplification was carried out using High-fidelity Phusion DNA polymerase (NEB) for cloning and Taq DNA polymerase (Fermentas) for gene expression analysis. The PCR mix was prepared in a total volume of 50 µl as in Table 4 and the cycling conditions used are described in Table 4. PCR

product amplification was confirmed by visualising 5 µl of PCR reaction mixed with 1 µl 6X Orange G loading buffer on an agarose gel. The product size was compared to the GeneRuler 1 kb ladder (Fermentas). When needed, PCR products were purified using PureLink Quick Gel Extraction Kit and/or PureLink Quick PCR Purification Kit as per manufacturers' guidelines (Invitrogen) and resuspended in 50µl ddH_2O. Primers used for PCR are listed in Table 5.

PCR Mix	Final Concentration	Step	Temperature	Time
DNA	300 pM	Denaturation	98ºC	2 min
Forward & Reverse primer	0.2 µM	Annealing	60ºC	30 s
dNTP	0.2 mM	Extension	72ºC	30 s/kb
Buffer	1X	Step 2 to 4 repeated 34 times		
Phusion polymerase	1U	Final extension	72ºC	10 min

Table 4 : PCR cycling conditions

Name	Primer sequence	Remark
UT05 KIF1C F	CAACACGGAGTCCCAGATTG	
UT170 KIF1C R	ACTGACCTTCTCCGAGTCC	
AS83 eGFP R	GCCGTTTACGTCGCCGTC	
AS358 KIF1C-1479 R	GAAGggatCCACAGTTCCCCCATCCTC	BamHI
AS359 KIF1C-1837 R	GGGGatCCCCTCGTTCCCGTTCC	BamHI
AS370 KIf1C-2033 F	CGGGGtcGACTCTGACAAGCGCTCTTG	SalI
AS376 KIF1C F	CTGCGGGTCtGGGAGCACC	R169W
AS416 PTPN21-296 F	TTGGAGTGGTGTTTTATGTGC	
AS460 KIF1C-811 R	CTCCACCTCCCCCGCTGTCCGAGTCTGC	
AS495 KIF1C-950 R	TGCgGatCCTGCAGCCGTAGCTGCTC	BamHI
AS496 KIF1C-1043 R	GCAGgAtCCGCTCCCCGGGATCGG	BamHI
AS497 KIF1C R	GACGGCAGCGTgCTGCCCCTGACC	S1092A
AS498 KIF1C R	GACGGCAGCGTgagGCCCCTGACCTC	S1092E

AS528 KIF1C R	CTGCACGTACaGGCCCAGGATG	P176L
AS529 pFB MCS F	GATTACGATATCCCAACGACC	
AS556 HA-Ezrin	GAAACCCATATGGGATACCCATACGATGTTCCA GATTACGCTGTGGTGCCGAAACCAATCAATGTC	NdeI
AS557 Ezrin-FERM R	CGGTTgcggccgcTTTCTTCTCTGTTTCCAGCTG	NotI
AS558 HA-tag	AAGCTTcatATGGGATACCCATACGATGTTC	NdeI
AS559 PTPN21-FERM R	GAAGAAGCggccGcTTCTGTATAATGTCCATTATAGTG	NotI
AS592 PTPN21-381 R	GAGGTCAgcggccGCTCTATCCAAGCTTGTCTG	NotI
AS627 KIF1C R	CAGGGCTTCTGTCTcGgcTAGCTTCTCCTC	R463A K464E
AS628 KIF1C R	GTGATGGGCgAGAACCACGTTTTC	K591E
AS629 KIF1C R	CATAAAGCTGGcAATGGcGgcGgcGCTGCAGGATC	E642A E644A K645A

Table 5 : List of primers used

The table depicts list of primers used in this study. Lower case indicates restriction sites and mutations. F – forward primer, R – reverse primer.

2.2.2. Mutagenesis PCR

Mutagenesis PCR was used to generate pKan-CMV-KIF1C$_{S1092A}$GFP, pKan-CMV-KIF1C$_{S1092E}$GFP, pFastBac-M13-KIF1C$_{R463AK464E}$GFP, pFastBac-M13-KIF1C$_{K591E}$GFP and pFastBac-M13-KIF1C$_{E642AE644AK645A}$GFP plasmids as described in 2.2.3 using the High-fidelity Phusion Polymerase (NEB). The PCR was carried out as indicated in Table 6. PCR product amplification was confirmed loading on an agarose gel.

PCR Mix	Final concentration
DNA	300 pM
Upstream primer	0.2 µM
Mutagenic primer	0.2 µM
dNTP	0.2 mM
Buffer	1X
Phusion polymerase	1U

Table 6 : Mutagenesis PCR Mix

Cycle Step	Temperature	Time
Initial denaturation	98ºC	2min
Denaturation	98ºC	10 s
Annealing	60ºC	30 s
Extension	72ºC	30 s/kb
Step 2 to 4 repeated 9 times		
72ºC, pause - Addition of 1 µM downstream primer		
Denaturation	98ºC	10 s
Annealing	60ºC	30 s
Extension	72ºC	20 s
Step 6 to 8 repeated 9 times		
72ºC, pause - Addition of 1 µM upstream primer		
10	98ºC	10 s
11	65ºC	30 s
12	72ºC	20 s
Step 10 to 12 repeated 9 times		
72ºC, 10 min		

Table 7: Mutagenesis PCR conditions

2.2.3. Cloning

Briefly, PCR products were digested with restriction enzymes from NEB and used as per manufacturer's instructions. The digested backbone plasmids and inserts were visualized on an agarose gel and extracted using PureLink Quick Gel Extraction Kit. The fragments were ligated for 1 hr at 22ºC using T4 DNA ligase (Thermo Scientific) and transformed into chemically competent TOP10 cells (Invitrogen) by subjecting to heat shock treatment at 42ºC for 45

s. The transformed mix was allowed to propagate for 1hr at 37ºC before plating it on a LB agar plate with suitable antibiotic. Single colonies from the plate were then picked and the DNA was extracted by Plasmid DNA Miniprep kit (Bio Basic), followed by restriction digestion and sequencing to confirm positive clones.

pKan-RIP-KIF1C$_{1\text{-}950}$GFP was generated by using primers UT05 and AS495 on the template pKan-RIP-KIF1CGFP. The insert and vector were digested with SalI - BamHI and ligated.

pKan-RIP-KIF1C$_{1\text{-}1043}$GFP was generated by using primers UT05 and AS496 on the template pKan-RIP-KIF1CGFP. The insert and vector were digested with SalI - BamHI and ligated.

pKan- RIP -KIF1C$_{\Delta 623\text{-}\Delta 679}$GFP was generated by using primers AS370 and AS83 on the template pKan-RIP-KIF1CGFP. The insert and vector were digested with SalI - BamHI and ligated.

pKan- RIP -KIF1C$_{S1092A}$GFP was generated by using primers UT05 and AS83 along with mutagenic primer AS497 on the template pKan-RIP-KIF1CGFP. The insert and vector were digested with SalI - BamHI and ligated.

pKan- RIP -KIF1C$_{S1092E}$GFP was generated by using primers UT05 and AS83 along with mutagenic primer AS498 on the template pKan-RIP-KIF1CGFP. The insert and vector were digested with SalI - BamHI and ligated.

pFastBac-M13-KIF1CGFP-MBN was generated by digesting pKIF1C-GFP with EcoRI - MfeI and replacing it in the backbone of pFastBac-M13. The positive clone was then subjected to mung bean nuclease at the EcoRI site to correct the frame shift in the ORF. The positive clones were transformed with DH10Bac (Invitrogen) competent cells and plated on LB supplemented with kanamycin (30 µg/ml), gentamycin (7 µg/ml), tetracycline (10 µg/ml), IPTG (40 µg/ml), X-Gal (100 µg/ml) for blue-white screening. Positive bacmid transformants (white colonies) were screened by PCR using M13 forward and reverse primers and internal gene primers for the integration into the viral genome.

pFastBac-M13-KIF1C$_{R463AK464E}$GFP was generated by using primers AS359 and pFB5' along with mutagenic primer AS627 on the template pFastBac-M13-KIF1CGFP-MBN. The insert and vector were digested with BsiWI-NdeI and ligated.

pKan-RIP-KIF1C$_{R463AK464E}$GFP was generated by Daniel Roth by digesting pFastBac-M13-KIF1C$_{R463AK464E}$GFP with BsiWI-BamHI and replacing it in pKan-RIP-KIF1CGFP. The insert and vector were ligated.

pFastBac-M13-KIF1C$_{K591E}$GFP was generated by using primers AS460 and pFB5' along with mutagenic primer AS628 on the template pFastBac-M13-KIF1CGFP-MBN. The insert and vector were digested with BsiWI-SalI and ligated.

pKan- RIP-KIF1C$_{K591E}$GFP was generated by Daniel Roth by digesting pFastBac-M13-KIF1C$_{K591E}$GFP with BsiWI-BamHI and replacing it in pKan-RIP-KIF1CGFP. The insert and vector were ligated.

pFastBac-M13-KIF1C$_{E642AE644AK645A}$GFP generated by using primers UT05 and AS83 along with mutagenic primer AS629 on the template pFastBac-M13-KIF1CGFP-MBN. The insert and vector were digested with SalI-BamHI and ligated.

pKan- RIP -KIF1C$_{E642AE644AK645A}$GFP was generated by Daniel Roth by digesting pFastBac-M13-KIF1C$_{E642AE644AK645A}$GFP with BsiWI-BamHI and replacing it in pKan-RIP-KIF1CGFP. The insert and vector were ligated.

pFastBac-M13-KIF1CGFP$_{P176L}$ was generated by using primers AS358 and pFB5' along with mutagenic primer AS528 on the template pFastBac-M13-KIF1CGFP-MBN. The insert and vector were digested with AscI-StuI and ligated.

pFastBac-M13-KIF1CGFP$_{R169W}$ was generated by using primers UT170 and pFB5' along with mutagenic primer AS376 on the template pFastBac-M13-KIF1CGFP-MBN. The insert and vector were digested with AscI-BsiWI and ligated.

pET22b-HA-PTPN21$_{1-378}$6HIS was generated by using AS558 and AS559 on the template pHA-PTPN21-eGFP. The insert and vector were digested with NdeI - NotI followed by ligation, transformation and screening

for positive clones. The positive close was transformed with BL21 DE3 competent cells for expression.

pET22b-HA-PTPN21$_{1-381}$6HIS was generated by using AS416 and AS592 on the template pHA-PTPN21-eGFP. The insert and vector (pET22b-HA-PTPN21$_{1-378}$6His) were digested with BsrGI - NotI followed by ligation, transformation and screening for positive clones. The positive clone was transformed with BL21 DE3 competent cells for expression.

pET22b-HA-Ezrin$_{1-328}$6HIS was generated by using AS556 and AS557 on the template pRSETC_6HISEzrin. The insert and vector were digested with NdeI-NotI followed by ligation, transformation and screening for positive clones. The positive clone was transformed with BL21 DE3 competent cells for expression.

2.2.4. Protein Expression

SF9 cells were infected with BIIC stocks and protein expression was monitored for 120 hr by taking a sample out every 24hr followed by SDS-PAGE and immunoblotting to determine the peak of protein expression. For large-scale expression, 500ml of SF9 cells at a density of 1-1.5×10^6 cells/ml were infected with one vial of BIIC as described in (Wasilko et al., 2009). Post 72hrs, cells were harvested by spinning at 252 × g for 20 min. The weight of the cell pellet was noted. The pellet was resuspended in 4 ml of SF9 lysis buffer (Table 7) per gram of the cell pellet, supplemented with 0.1 mM ATP and protease inhibitor cocktail (Roche) to prevent proteolytic degradation and snap frozen in liquid nitrogen until further use.

Bacterial expression plasmids transformed with BL21 DE3 and were grown overnight as 3ml starter cultures. The starter cultures were diluted 1:100 and grown in 200 ml of 2×YT (yeast extract, tryptone) at 37ºC, 180 rpm until they reached an optical density (OD_{600}) of 0.5. The cultures were then induced with IPTG (Isopropyl β-D-1-thiogalactopyranoside; Melford) at a final concentration of 500 µM and the temperature was reduced to 16ºC for overnight expression. Next morning the cells we harvested at 1500 × g and resuspended in bacterial lysis buffer (Table 7) supplemented with 200 mM

phenylmethanesulfonyl fluoride (PMSF; Melford) at a dilution of 1:200 to inhibit proteolytic degradation and snap frozen in liquid nitrogen until further use.

2.2.5. Protein Purification

Protein purification was carried out in a two-step process. Harvested cell pellets were resuspended in SP lysis buffers according to the requirement. The cells were lysed using a douncer (Wheaton) with 20 strokes. Bacterial cell pellets were sonicated at 4ºC. Lysates were then cleared by spinning at 38000 × g for 30min at 4ºC. SP Sepharose beads (GE Healthcare) were equilibrated with the lysis buffer and the cleared lysate obtained after the spin is mixed with the beads and batch bound for 1hr at 4ºC. Next, the beads were loaded onto a 5ml disposable polypropylene gravity column (Thermo Scientific) and washed with 10 - CV (column volume) until the OD_{280} is below 0.05. The protein was then eluted from the beads by the addition of SP elution buffer (Table 9, 11). The peak fractions obtained were pooled and diluted to the Ni-NTA lysis buffer and batch bound with the Ni-NTA beads (Qiagen) for 1hr at 4ºC. Next, the beads were loaded onto a gravity column and washed with 10CV until the OD_{280} is below 0.05. The protein was then eluted from the beads with the Ni-NTA elution buffer (Table 10, 12). The peak fractions were run on a SDS-PAGE gel for visualisation and protein was aliquoted and flash frozen.

SF9 lysis buffer	Bacterial lysis buffer
50 mM Sodium phosphate pH 7.5	50 mM Sodium phosphate pH 7.5
150 mM Sodium Chloride	50 mM Sodium Chloride
20 mM Imidazole	20 mM Imidazole
0.1% Tween 20,1.5 mM $MgCl_2$	1.5 mM $MgCl_2$

Table 8: Lysis Buffers used

SF9 SP wash buffer	SF9 SP elution buffer
50 mM Sodium phosphate pH 7.5	50 mM Sodium phosphate pH 7.5
150 mM Sodium Chloride	300 mM Sodium Chloride

Table 9: SF9 SP buffers

SF9 Ni-NTA wash buffer	SF9 Ni-NTA elution buffer
50 mM Sodium phosphate pH 7.5 150 mM Sodium Chloride 50 mM Imidazole 10% glycerol	50 mM Sodium phosphate pH 7.5 150 mM Sodium Chloride 150 mM Imidazole 0.1 mM ATP, 10% glycerol

Table 10: SF9 Ni-NTA buffers

Bacterial SP wash buffer	Bacterial SP elution buffer
50 mM Sodium phosphate pH 7.5 50 mM Sodium Chloride	50 mM Sodium phosphate pH 7.5 200 mM Sodium Chloride

Table 11: Bacterial SP buffers

Bacterial Ni-NTA wash buffer	Bacterial Ni-NTA elution buffer
50 mM Sodium phosphate pH 7.5 50 mM Sodium Chloride 20 mM Imidazole 10% glycerol	50 mM Sodium phosphate pH 7.5 50 mM Sodium Chloride 150 mM Imidazole 10% glycerol

Table 12: Bacterial Ni-NTA buffers

2.3. Biochemistry

2.3.1. Size exclusion chromatography (SEC)

To determine the stokes radius, SEC was carried out using Superdex 200 (GE Healthcare) column on the AKTApurifier10 FPLC with a UNICORN control system (GE Healthcare). The column was equilibrated with the SEC Buffer (Table 13). Protein was injected into the column and the fractions were collected using the fraction collector. 100 µl of 5 mg/ml standard proteins were injected individually. The Stokes radius for the standard proteins used were as follows thyroglobulin-8.5 nm, apoferritin-6.1 nm, glucose oxidase-4.3 nm, bovine serum albumin-3.48 nm. The fractions were run on a SDS-PAGE gel for visualisation, where necessary immunoblotting was carried out. Stokes radius R_s was determined according to (Erickson, 2009).

SEC Buffer
35 mM Sodium phosphate pH 7.5
150/500 mM Sodium Chloride
1.5 mM $MgCl_2$

Table 13: SEC buffer

2.3.2. Analytical ultracentrifugation/ Glycerol gradients

10 - 40% vol/vol glycerol gradients were made using the Gradient master (Biocomp) with the buffer listed in Table 13. The 5 ml polyallomer tubes (Beckman) were marked using the metal marker in the middle at 2.5 ml. Next, 2.5 ml of 10% glycerol buffer was added into the tube using a syringe. Next, 2.5 ml of 40% glycerol buffer was added to the bottom of the tube containing the 10% glycerol buffer until the 2.5 ml mark. Where necessary the salt concentration was adjusted. The protein sample was loaded on top of the gradient and the samples were spun at 364496 × g for 16 hrs at 4ºC. 100 µl of 5mg/ml standard proteins were loaded individually on separate gradients. The sedimentation co-efficient of standard proteins were as follows – apoferritin- 16.6 S, catalase-11.3 S, glucose oxidase-8 S, bovine serum albumin-4.6 S. The next day, 250 µl aliquots were carefully taken out from the top of the gradient tubes and the A_{280} was measured to determine the peak in the gradient. The samples were processed for SDS-PAGE and immunoblotting where necessary. The frictional ratio was determined $f/f_{min} = S_{max}/S$ with $S_{max} = 0.00361 \cdot M^{2/3}$ in Svedberg for a protein of mass M in Daltons (Erickson, 2009).

Analytical Ultracentrifugation buffer	
35 mM Sodium phosphate pH 7.5	35 mM Sodium phosphate pH 7.5
1.5 mM $MgCl_2$	1.5 mM $MgCl_2$
50 mM Sodium Chloride	50 mM Sodium Chloride
0.1 mM ATP	0.1 mM ATP
1 mM EGTA	1 mM EGTA
40% glycerol	10% glycerol

Table 14: Analytical Ultracentrifugation buffer

2.3.3. Crosslinking mass-spectrometry

The two cross-linkers that were used were BS3 (bis (sulpho-succinimidyl) suberate) and EDC (1-Ethyl-3-(3-dimethylaminopropyl) carbodiimide). BS3 has a spacer arm of 11 Å and reacts with primary amines in lysine side chains. EDC cross-links with amines (lysine, protein N-terminus) and directly cross-links atoms of the protein with each other in a 3 Å cross-link. Freshly prepared cross-linker (5 mM) was mixed by pipetting with the protein of interest (500 nM) in solution. For EDC cross-linking, N-hydroxysulfosuccinnimide (3 mM) was added to improve efficiency of the cross-linking. The reaction was incubated at room temperature for an hour shaking at 400 rpm and quenched with Tris buffer pH 7.5 to a final concentration of 50 mM. Next, the protein was diluted in 50 mM Ammonium bicarbonate and reduced using 1 mM DTT for 60 min at room temperature. The sample was then alkylated with 5.5 mM iodoacetamide for 20 min in the dark at room temperature and digested using (1 µg per 100 µg of protein) trypsin (sequencing grade; Promega) overnight at 37°C. The Cross-linked peptides were de-salted using C18 stage tips (Rappsilber et al., 2007). The samples were then analysed in the Proteomics facility (WPH RTP), University of Warwick. Briefly, an aliquot containing 20 µl of extracted peptides (total sample volume 50 µl) from each sample was analysed by nano LC-ESI-MS/MS using the Ultimate 3000/Orbitrap Fusion instrumentation (Thermo Scientific) using a 60 minute LC separation on a 50cm column. The resulting sequences are visualized using Scaffold (Proteome software) for percentage coverage and purity followed by analysis using StavroX (Gotze et al., 2015).

2.3.5. *In-vitro* Tubulin polymerisation

Tubulin was prepared from porcine brains according to protocols published (Gell et al., 2011). Microtubules were polymerised in MRB80 buffer (Table 14) in a two-step reaction to generate long microtubules. First 16 µM pig-brain tubulin was polymerised with 1 mM GTP (Jena Biosciences) at 37°C for 30 minutes, stabilized by addition of 100 µM Paclitaxel (Sigma) to generate seeds. These unlabelled polymerised microtubule seeds (0.16 µM) were mixed with pig-brain tubulin, biotin-tubulin (Cytoskeleton Inc.), Hilyte647-labelled tubulin (Cytoskeleton Inc.), in the molar ratio of 25:1:2 in the presence of 1 mM GTP (Jena Biosciences) and incubated at 37°C for 30 minutes. Microtubules were stabilized by addition of 100 µM Paclitaxel (Sigma). To remove free tubulin, microtubules were pelleted at 100,000 × g for 10 min at room temperature in an airfuge (Beckmann Coulter), washed with and resuspended in MRB80 and 100 µM Taxol.

MRB80 Buffer
80 mM K-Pipes pH 6.8
4 mM $MgCl_2$
1 mM EGTA

Table 15: MRB80 Buffer

2.3.6. Single molecule motility assay

Flow chambers were made using clean glass slides and double sided sticky tape (Scotch 3M) as shown in Figure 2.1. Coverslips (22×22) were cleaned by incubating in 2.3 M hydrochloric acid overnight at 60ºC. The next day, coverslips were washed with Millipore water and sonicated at 60ºC for 5 min. The wash cycle was repeated 5 times. The coverslips were dried using a Spin Clean (Technical video) and plasma cleaned using Henniker plasma clean (HPT-200) for 3 min and placed on top of the glass slide making a 100 µm deep flow chamber. The surface was coated with (0.2 mg/ml) PLL(20)-g[3.5]-PEG(2)/PEG(3.4)-Biotin (50%) (Susos AG). Biotin-647-microtubules were attached to this surface with streptavidin (5mg/ml) and the surface was blocked with κ-casein (1 mg/ml) (Sigma). KIF1C, PTPN21 and Ezrin-FERM

were pre-spun. KIF1C was incubated with either buffer or PTPN21 or Ezrin-FERM for 15min at room temperature, following which the motility mix (Table 16) was flown in and the chamber was sealed with candle wax.

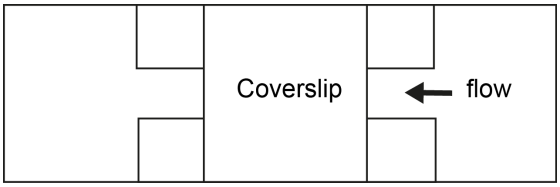

Figure 2.1: Motility flow chamber

Schematic representation of a single molecule motility chamber. A clean glass slide was taped with double sided sticky tape was and a clean coverslip to make a flow chamber.

Motility Mix
3-10 nM Motor protein
1 mM ATP
5 mM Phosphocreatine
7 U/ml Creatine phosphokinase
0.2 mg/ml Catalase
0.4 mg/ml Glucose oxidase
4 mM DTT
50 mM Glucose
25 mM KCl
100 μM Taxol
0.2 mg/ml κ-casein

Table 16: Motility mix

2.4. Microscopy and Data Analyses

2.4.1. Live-cell Imaging

Live cells were imaged using a 60x oil NA 1.4 objective on an Olympus Deltavision microscope (Applied Precision, LLC). The microscope is equipped with eGFP, mCherry filter sets and a CoolSNAP HQ2 camera (Roper Scientific) under the control of SoftWorx (Applied Precision). The environment was tightly controlled at 37ºC and 5% CO_2 using a stage-top incubator (Tokai Hit) and a weather station (Precision control). Images were acquired with 500ms exposure every 2 s for 180 s. The fluorescent intensity was measured

at the tail and front of the cell and corrected for background in the GFP and mCherry channel using ImageJ software (Fig 2.2). To determine the ratio of accumulation at the tail or front, the mean intensities measured at the tail and the front in the GFP channel was divided to mean intensity measured at the tail and the front in the mCherry channel.

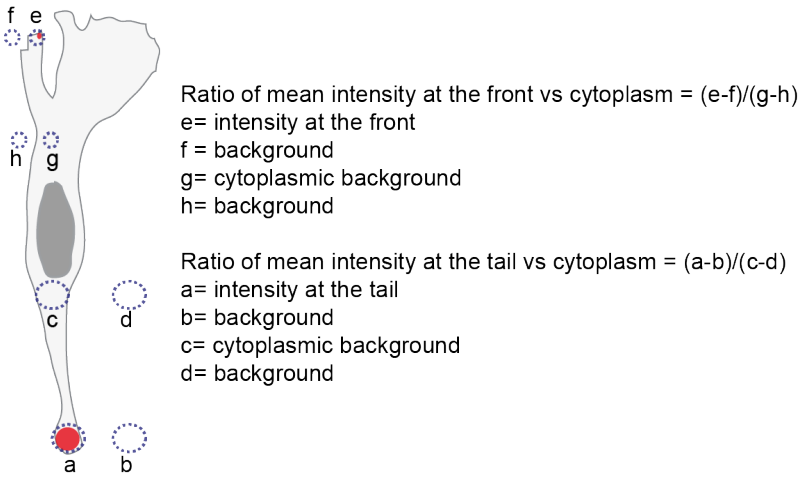

Figure 2.2: Intensity measurements

Schematic representation of the measurement of the ratio of mean intensity at the front or tail of a cell. A region of interest was drawn manually surrounding the accumulation observed and the mean intensity was measured at the tail, front, cytoplasm and background in both channels. Similarly, for cells that were more or less round (deletion constructs) the mean intensity was measured at the accumulation peaks.

2.4.2. TIRF Microscopy and Image analysis

Single molecule motility assay was observed on an Olympus TIRF system using a 100x NA 1.49 objective, 1x additional magnification, 488 nm, and 640 nm laser lines, an ImageEM emCCD camera (Hamamatsu Photonics), an environmental chamber and a stage-top-incubator (Okolab, Ottaviano, Italy) under the control of xcellence software (Olympus). Images were acquired every 100 ms for 180 s at an exposure of 60 ms unless otherwise mentioned. The images were analysed by drawing kymographs on microtubules of line width 11, which covers and averages intensity over 11 pixels using the Kymograph plugin (Seitz and Surrey, 2006). The runs were identified manually by scoring the kymographs for runs and static motors. The speed and run length was calculated from the length and slope of each run

using a macro written by Dr. Anne Straube. The runs with “stop & go” events were analysed as separate phases to distinguish between the two events. Blind analysis was also carried out independently for an unbiased scoring of the data sets.

2.5. Optical Trapping

560 nm Polystyrene beads and motor protein were incubated together in the assay buffer containing 80 mM PIPES (Piperazine-1,4-bis (2-ethanesulfonic acid)) pH 7, 2 mM $MgSO_4$, 1 mM EGTA, 1 mM DTT, 3 mg/ml D-glucose, 0.2 mg/ml κ-casein and 1 μM ATP. The concentration of motor was decreased such that only 20-30% of the beads moved. Flow cells were constructed using plasma cleaned coverslips and Dow Corning High Vacuum Grease. Two lines of grease were applied to the base coverslip (22 x 50 mm) using a syringe, the top coverslip (22 x 22 mm) was placed, forming a flow cell of approximately 10 μl capacity. Glutaraldehyde (8%) was added to the chamber and incubated for 2 hr followed by washing the flow cell with 200 μl of Millipore water. The microtubules were diluted to the required concentration and were introduced to the flow cell and allowed to adsorb on to the surface coated with glutaraldehyde. The microtubules were incubated for an hour to allow for adsorption. Next, 0.2 μl of bead-motor protein solution was diluted in 20 μl of assay buffer composed of BRB80, 1 mM ATP, 0.4 mg/ml κ-casein, 10 μM taxol and 0.4 μl of the oxygen scavenger (1 mg/ml catalase, 5 mg/ml Glucose oxidase, 3 mg/ml D-glucose, 50% glycerol in the assay buffer). The beads were then introduced to the cell using capillary action to draw the solution through. The flow chamber was viewed immediately using the Optical Trap setup (Carter and Cross, 2005). The images were acquired at 20 kHz for 180 s and the image analysis was carried out using code written in R by Dr. Algirdas Toleikis unless otherwise mentioned. Briefly, a moving window t-test algorithm (Carter and Cross, 2005) was used which identifies a step based on a t-test with the following parameters – t-test score threshold=30, minimum step size=5 nm, minimum force=1 pN, moving average, n=20. The size of the window and the threshold are varied to determine accurate steps.

2.6. Statistical Analysis and figure preparation

Statistical data analyses and graphs were generated using Origin Pro 8.5 (OriginLab) unless otherwise mentioned. Box plots show quartiles, 10-90% data. All statistical significance analyses were carried out using two-sample t-tests assuming equal variance unless otherwise mentioned. Figures were prepared using Adobe Illustrator.

CHAPTER 3 CONFIRMATION OF PTPN21 FERM DOMAIN AS AN ACTIVATOR OF KIF1C

The two well-known modes of kinesin motor activation are the tail-block model and the monomer to dimer switch model. In the tail-block model, the protein is a stable dimer and the tail interacts with the head to keep the motor in an autoinhibited state. Upon binding by an adapter protein or cargo the motor is activated (Yamada et al., 2007, Hammond et al., 2009, Farkhondeh et al., 2015, Yoshimura et al., 2010). In the monomer to dimer switch model, the intramolecular interactions between the neck and tail regions hold the kinesin motors in a monomeric, inactive state. Upon activation by cargo, these motors dimerize with their neck coil and tail regions (Soppina et al., 2014, Okada and Hirokawa, 1999, Tomishige et al., 2002).

However, it remains to be elucidated what the mode of activation is for KIF1C. Previous reports from our lab show that KIF1C transports integrin vesicles (Theisen et al., 2012) and further to this, KIF1C depletion leads to a decrease in integrin vesicle motility as tested in two different cellular models. This phenotype could be rescued by expressing the FERM domain of a phosphatase – PTPN21, which compensates for KIF1C depletion. The addition of FERM domain of PTPN21 could either activate and mobilize the remaining KIF1C pool present in the cell or there is another motor that is being activated (unpublished data, Straube Lab).

To test in-vitro whether PTPN21 FERM domain activates KIF1C directly and to determine the mechanism of activation, it was essential to purify full-length KIF1C and determine the hydrodynamic properties.

3.1. Purification of KIF1C

KIF1C was expressed in SF9 insect cells with an amino-terminal hexa-histidine tag and a carboxy-terminal GFP tag. Purification was carried out in a two-step process by anion exchange chromatography using SP-Sepharose beads and affinity chromatography using Ni-NTA beads.

In the first trial, affinity chromatography was performed to selectively bind KIF1C via the 6His tag. This was followed by anion exchange chromatography to remove the non-specific proteins contaminating the Ni-NTA purification. The resulting protein obtained still contained impurities and buffer exchange was required to bring the protein in a suitable buffer for subsequent experiments. Hence, in the second trial, anion chromatography was carried out first (Fig 3.1 a) followed by affinity chromatography (Fig 3.1 b) to yield a clean protein at 154kD as visualized by SDS-PAGE. To determine the purity of the sample, in-solution mass spectrometry was carried out and KIF1C-GFP was confirmed to be the most abundant protein (Table 17).

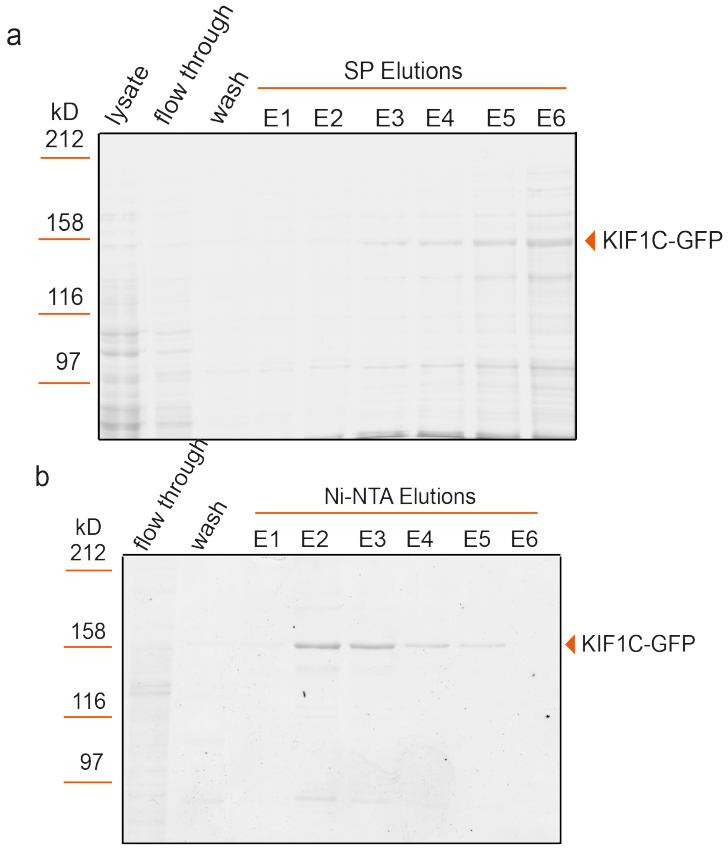

Figure 3.1: Purification of full-length KIF1C

(a) Coomassie gel of 6His-KIF1C-GFP after anion exchange chromatography. The lysate was bound to SP-Sepharose beads and the column was washed with 150 mM

NaCl SF9 SP wash buffer and eluted with 300 mM NaCl. Elutions E3-E6 were pooled and bound to Ni-NTA beads for affinity chromatography. (b) Coomassie gel of 6His-KIF1C-GFP after affinity chromatography. The elutions E3-E6 from SP were bound to Ni-NTA beads and washed with 50 mM Imidazole SP Ni-NTA Buffers and eluted with 150 mM Imidazole. Elutions E2 – E5 were stored for subsequent experiments.

Name of protein identified	Peptide count
KIF1C	70
Trypsin	3
Fragile X mental retardation syndrome related protein	2

Table 17: Mass-spec analysis of KIF1C-GFP for purity

The protein was digested with trypsin and mass-spectrometry was carried out. The peptide count gives the total number of unique peptides identified by Scaffold software. KIF1C dominated the list of peptides that were identified. The other proteins that were identified were trypsin, which was used to digest KIF1C and a Fragile X mental retardation syndrome related protein.

3.2. Hydrodynamic Analysis

The two modes of motor activation can be distinguished by determining if the motor is a monomer or a dimer. To do this, hydrodynamic analysis of KIF1C was carried out. Hydrodynamic analysis involves techniques such as size exclusion chromatography which determines the stokes radius and glycerol gradient centrifugation which gives the sedimentation co-efficient of the protein. From these parameters the size, shape and the conformation state of the motor protein can be estimated (Erickson, 2009).

3.2.1. Determining Stokes Radius by Size exclusion chromatography

Size exclusion chromatography separates proteins on the basis of the Stokes radius (R_S) of the molecule (Fig 3.2). For a given protein of interest, this can be calculated relative to the Stokes radii of the standard proteins run independently on the size exclusion column.

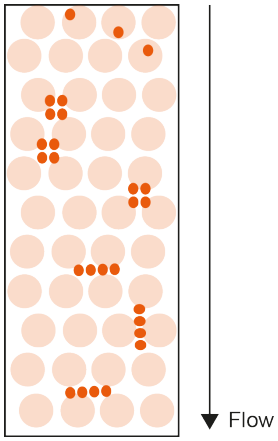

Figure 3.2: Size exclusion chromatography

Proteins are separated based on their shape and mass. Proteins with different shapes but similar molecular mass elute at different rates.

To estimate the stokes radius for KIF1C-GFP, the protein was expressed from insect cells and subjected to a single step Ni-NTA purification process and the elution was run on the size exclusion column at two different salt concentrations. The elution fractions were measured in the NanoDrop 3300 Fluorospectrometer (Thermo Scientific) to confirm the presence of KIF1C-GFP (Fig 3.3).

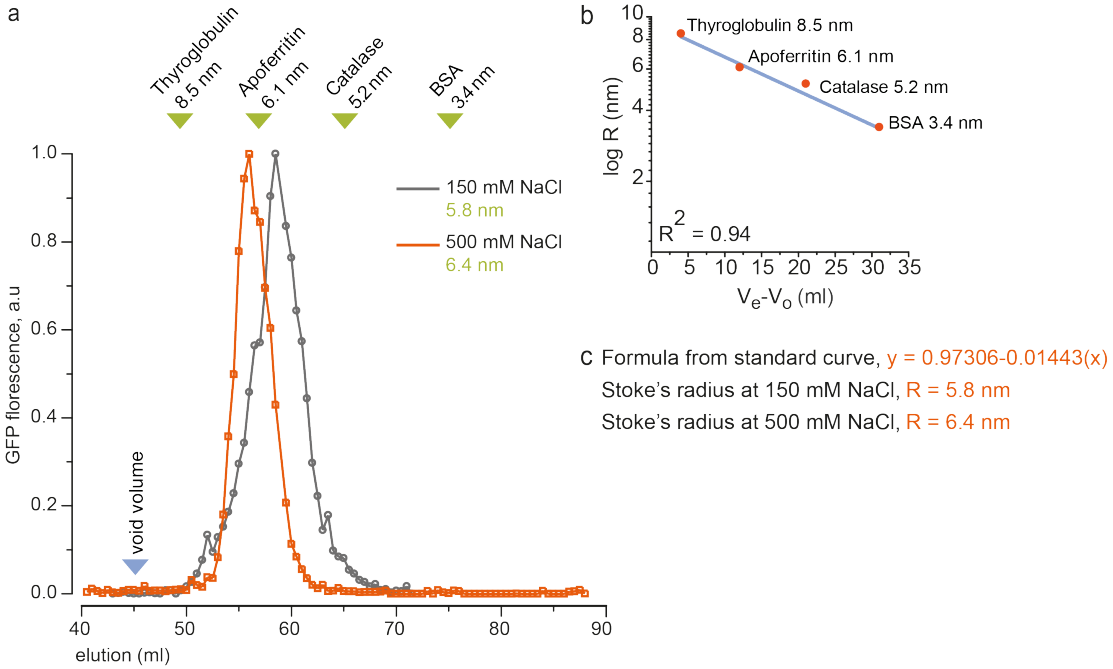

Figure 3.3: Determination of R_S for KIF1C-GFP

(a) KIF1C-GFP was injected into a size exclusion column at physiological and a high salt concentration of 150 mM NaCl and 500 mM NaCl respectively. The fractions containing KIF1C-GFP were measured in the NanoDrop 3300 Fluorospectrometer.

The elution volume at 150 mM NaCl for KIF1C-GFP was found to be 58.5 ml whereas with 500 mM NaCl it was 56 ml as indicated by grey and orange profile respectively. (b) Standard proteins were run on the size exclusion column independently to determine elution volume, which is plotted against known Stokes radii. (c) The Stokes radius for KIF1C-GFP was calculated from the formula derived from the standard curve to be 5.8 nm at 150 mM NaCl and 6.4 nm at 500 mM NaCl.

The stokes radius for KIF1C-GFP was calculated by plotting elution volume versus known stokes radii of the standard proteins (Erickson, 2009). At physiological levels (150 mM NaCl) the stokes radius for KIF1C-GFP was found to be 5.8 nm and increasing the ionic strength to 500 mM NaCl resulted in a stokes radius of 6.4 nm (Fig 3.3). The experiment has been independently repeated twice and similar elution profiles were observed. The profile of KIF1C-GFP at 150 mM salt versus at 500 mM salt depicts a shift in the elution volume suggesting that KIF1C-GFP possibly changes conformation at a higher salt concentration. Increasing the ionic strength could either lead to the motor transitioning to a monomer or if the motor is compact, it could become elongated. But, in the former case, the monomer protein molecules would elute after the dimeric peak of KIF1C. Since, there was no detectable monomer peak of KIF1C observed, another possibility could be that the motor is in an equilibrium between two states which results in a peak (orange) that elutes just before the dimeric peak of KIF1C (grey). Next, to validate these results and to estimate the molecular mass, glycerol gradient centrifugation was carried out.

3.2.2. Determining Sedimentation co-efficient by Glycerol gradient centrifugation

Sedimentation co-efficient (S) as revealed by a glycerol gradient centrifugation determines how fast a protein moves through a gradient. (Fig 3.4). Bulky and compact molecules travel farther down the gradient whereas lighter and linear molecules sediment slower. The sedimentation co-efficient for a target protein can be determined relative to the S values of the standard proteins of known sedimentation co-efficient that are run across independent gradients.

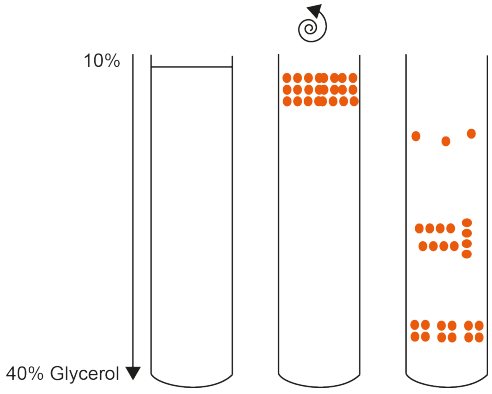

Figure 3.4: Glycerol gradient sedimentation

Proteins are separated based on their rate of sedimentation. Higher molecular mass proteins sediment faster than lower ones while linear molecules sediment slower than compact protein molecules.

KIF1C-GFP was purified by a single step Ni-NTA column and the elutions were loaded onto a gradient of 10-40% glycerol at different salt concentrations. The standard proteins of known sedimentation co-efficients were run independently in separate gradients and the sedimentation co-efficient for KIF1C-GFP was calculated from the standard curve. There was a shift in the migration pattern that was observed with the increase in ionic strength (Fig 3.5). At physiological conditions (0-150 mM NaCl), KIF1C-GFP was found to have a sedimentation co-efficient of 11 S and at higher ionic strength (500 mM) the sedimentation co-efficient reduced to around 8 S (Fig 3.5b). A similar observation has been reported for kinesin-1 in which the motor protein transitions from 9 S to 6 S as the ionic strength increases (Hackney et al., 1992). For kinesin-1, this results in a conformation change from a folded to an extended one. Our data suggests a similar effect could be occurring in case of KIF1C-GFP as well, where the motor is compact and transitions to an elongated state resulting in a lower sedimentation rate.

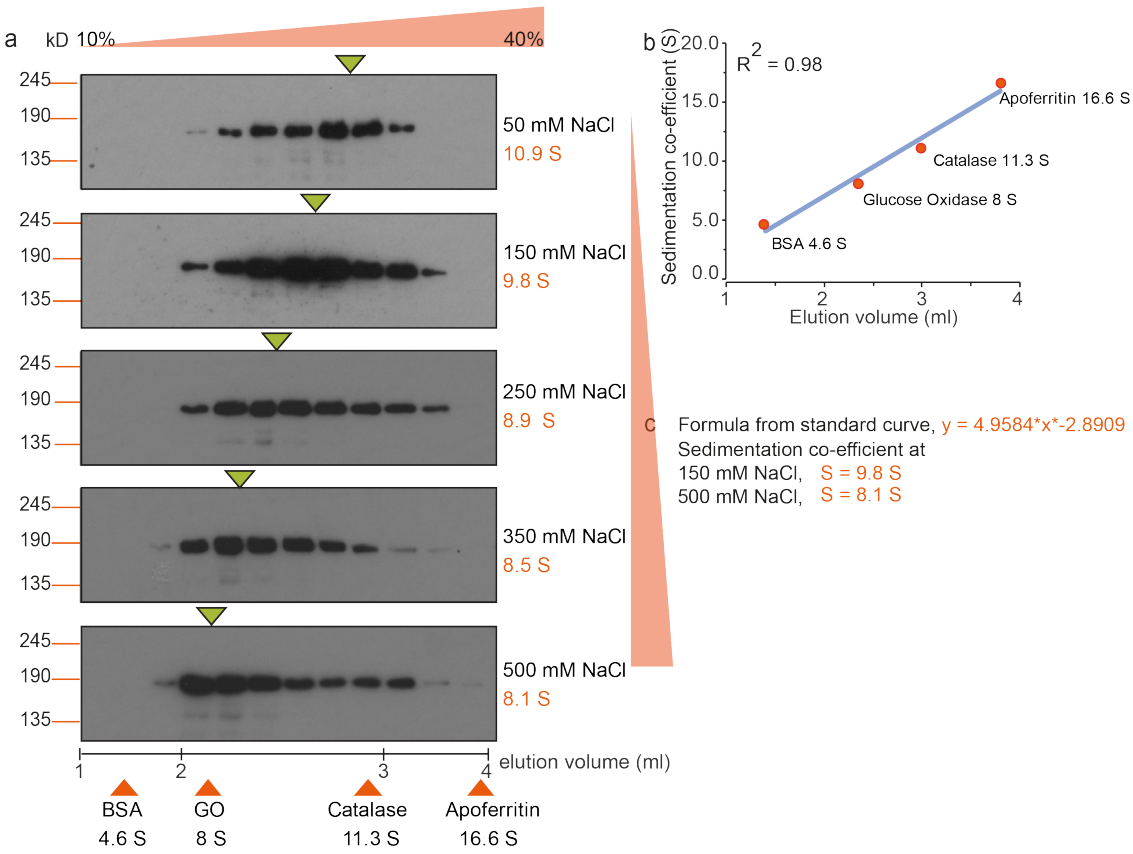

Figure 3.5: Behaviour of KIF1C at increasing concentration of NaCl

(a) KIF1C-GFP was loaded onto a 10-40 % glycerol gradient at increasing salt concentrations in separate gradients. Fractions were collected from the top of the gradients and run on a SDS-PAGE followed by immunoblotting to determine the profile at different salt concentrations. The standards were run independently at 150 mM salt concentration. GO – Glucose oxidase, BSA – Bovine serum albumin. The peak elution volumes at different salt concentrations are indicated by green arrow heads. (b) Standard proteins were run on a 10-40 % gradient independently to determine elution volume, which is plotted against known sedimentation co-efficient. (c) The sedimentation co-efficient for KIF1C-GFP was calculated from the formula derived from the standard curve to be 9.8 S at 150 mM NaCl and 8.1 S at 500 mM NaCl. The sedimentation co-efficient calculated at different salt concentrations is depicted in orange.

3.2.3. Calculation of molecular mass

From the stokes radius and sedimentation co-efficient obtained from size exclusion chromatography and glycerol gradient centrifugation, the molecular mass for KIF1C-GFP was calculated using the formula M=4205×R×S (Erickson, 2009) (Table 18).

KIF1C-GFP	R_S (nm)	S (S)	M=4205×R_S×S (kD)
150 mM NaCl	5.8	9.8	239
500 mM NaCl	6.4	8.1	218

Table 18: Molecular mass calculation for KIF1C-GFP

At 150 mM NaCl the stokes radius and sedimentation co-efficient were calculated to be 5.8 nm and 9.8 S, whereas at 500 mM NaCl it was found to be 6.4 nm and 8.1 S. From these values, the molecular mass was calculated to be around 239 kD and 218 kD respectively. R_S=Stokes radius, S=Sedimentation co-efficient.

The predicted mass of a KIF1C-GFP monomer is 154 kD and 308 kD for a dimer. Using the hydrodynamic properties, our analysis suggests that KIF1C-GFP is a dimer with a calculated mass of 239 kD at 150 mM and 218 kD at 500 mM salt conditions. There was a difference in migration pattern that was observed at different salt conditions in size exclusion chromatography as well as glycerol gradient centrifugation. This suggested that the protein undergoes a transition to a different state. The frictional co-efficient determines if the protein is globular (1.2-1.3), slightly elongated (1.5-1.9) or very elongated (2-3). This was calculated for KIF1C-GFP under different salt conditions that were tested (Fig 3.6).

Salt (mM)	S_{max}/S
50	1.5
150	1.6
250	1.8
350	1.9
500	2.0

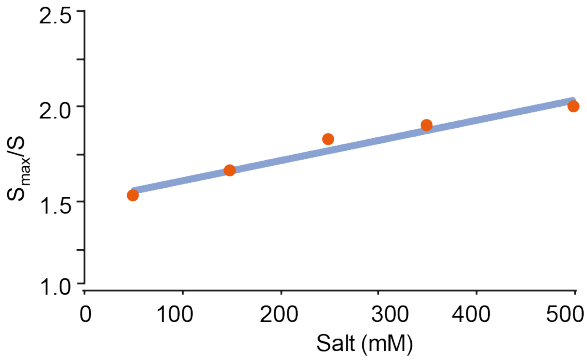

Figure 3.6: Frictional co-efficient of KIF1C-GFP

The S_{max}/S ratio was calculated at increasing salt concentrations and plotted against different salt concentrations. S_{max} is the sedimentation co-efficient of the protein if it was a sphere. From the plot, it is evident that KIF1C-GFP becomes elongated with the increase in salt concentration.

For KIF1C-GFP, it was observed that increasing the ionic strength increases the frictional co-efficient of the protein molecule from 1.5 to 2.0 (Fig 3.6) suggesting a change from a folded to an extended form. From both

molecular mass calculations, it is likely that KIF1C-GFP is a dimeric motor protein that undergoes a conformation change to become more elongated at high salt concentrations. However, the deviations observed from the predicted molecular mass could be since the formula assumes the molecules to be a sphere and the kinesin motor proteins are not strictly spherical. An additional factor could be that since the glycerol gradient centrifugation was carried out in a high concentration of glycerol as opposed to size exclusion chromatography, this could influence the conformation state of the motor protein.

The hydrodynamic analysis gave insight into the size and shape of KIF1C-GFP. It indicated that KIF1C-GFP is most likely dimeric in nature and might exist in a autoinhibited state in solution. To validate the folded autoinhibition state and to identify potential interaction sites between the tail and motor domain, cross-link mass spectrometry was employed.

3.3. Cross-link mass spectrometry of KIF1C-GFP

Cross-link mass spectrometry was carried out in collaboration with Hamdi Hussain (HH), McAinsh Lab, CMCB, University of Warwick. The reactions were setup in parallel with HH. The samples were run by the proteomics facility, University of Warwick using HH's method. The analysis of the spectra was done together with HH.

Cross-link mass spectrometry is a powerful tool to study protein interactions and to identify potential interaction surfaces (Rappsilber, 2011). To gain better understanding of the conformation state of KIF1C-GFP, cross-link mass spectrometry was performed with BS3 that crosslinks peptides in the vicinity of 11Å. KIF1C-GFP (500 nM) eluted with 50 mM sodium phosphate pH 7.5, 150 mM NaCl, 150 mM imidazole, 0.1 mM ATP and 10% glycerol with a final pH of 8.5 was mixed with 5 mM of BS3 (bis (sulpho- succinimidyl) suberate) and in-solution cross-linking and digestion was carried out as described in the Methods section.

The cross-linked peptides were screened on the basis of a high score and good fragmentation. The b ions extend from the amino terminus and the y ions extend from carboxy terminus. A peptide is designated as an α peptide based on the fragmentation observed between the two cross-linked peptides. Higher fragmentation peptides are labelled as α whereas the lower fragmented peptide is labelled β. Scoring is achieved based on the observed fragmentation ions. A score of at least 100 is used as a cut-off which is based on the following, (a) Fragmentation ion series, which should be observed for both peptides, specifically those fragment ions that include the cross-linker and the attached second peptide. (b) Observed fragmentation ions should be within ~20 ppm of expected fragment ions and there should be 3 or more ion fragments for b or y ions in the α peptide. (c) Fragmentation ions observed should account for most of the high intensity peaks present in the spectra. There should only be a few unidentified high intensity signals in the spectra. (c) There should be little noise in spectra.

A representative spectrum obtained for a cross-linked peptide IVmGK-LKEGANINK for KIF1C-GFP shows the precursor ion in green which was fragmented well (reduction in relative intensity), b and y ions colour coded for the two peptides observed (Fig 3.7).

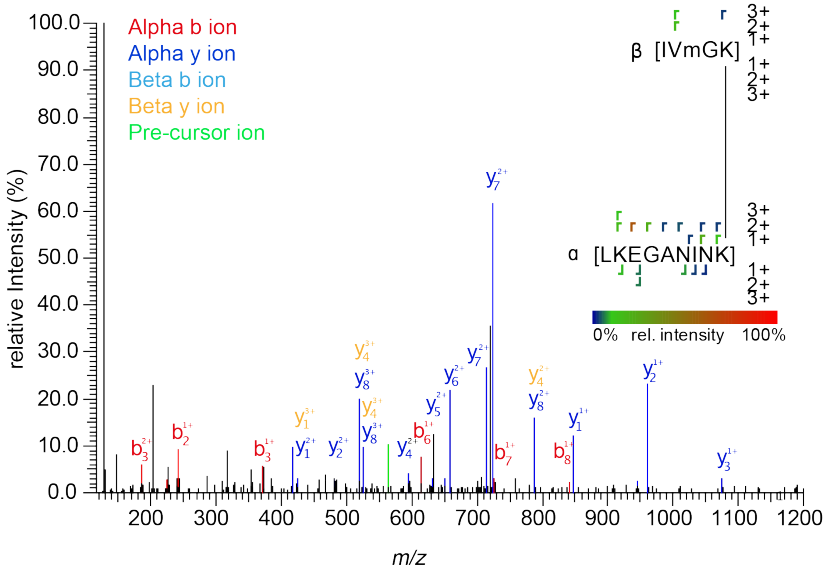

Figure 3.7: Fragmentation spectra of a cross-linked peptide in KIF1C

For the cross-linked peptide IVmGK-LKEGANINK, the precursor ion is shown in green, the peaks are labelled in colour and the b and y-ions are labelled with the peptide fragment name.

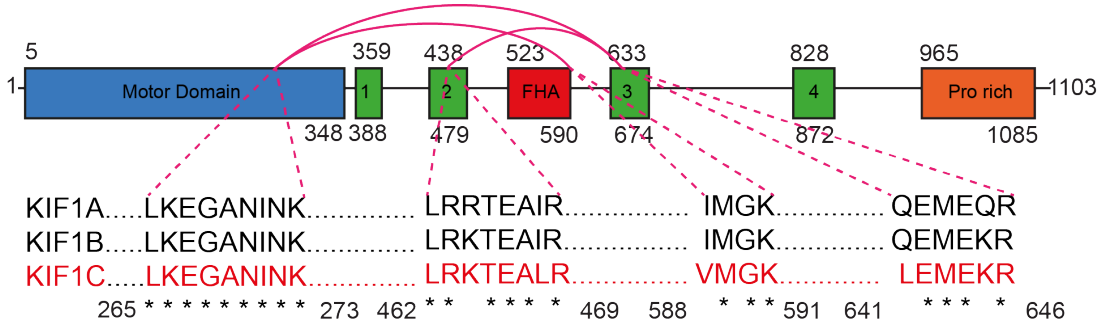

Figure 3.8: Primary structure of KIF1C showing crosslinks

Crosslinks with a high threshold identified using BS3 (pink) are depicted in the primary structure of KIF1C along with sequence conservation between KIF1 family

On the basis of the score and fragmentation state, there were three cross-links that were identified with high confidence. These are shown in Fig 3.8 as pink arches for BS3 cross-links. Also shown is the sequence conservation of the peptides between other KIF1 family members KIF1A and KIF1B.

One of the cross-links that was identified was Lysine 645 in the peptide $_{641}$LEMEKR$_{646}$ of the third coiled coil region (CC3), which made contact with Lysine 464 of the peptide $_{462}$LRKTEALR$_{469}$ in the second coiled coil region (CC2). The CC2 region has been reported to fold back and disrupt motor activity in KIF1A (Hammond et al., 2009). Similarly, the other two cross-links ($_{588}$IVmGK$_{591}$ in the FHA domain and $_{641}$LEMEKR$_{646}$ in the CC3 region) make contacts with Lysine 273 in the peptide sequence $_{265}$LKEGANINK$_{273}$ in loop 11 in the motor domain. This sequence is highly conserved between the KIF1 family. Previously it has been reported that Lysine 266 from the $_{265}$LKEGANINK$_{273}$ peptide is essential for the increased processivity in KIF1A family motors (Scarabelli et al., 2015). From the structure (Fig. 3.9) it is evident that Lysine 266 makes contacts with the microtubule surface and blocking this site with the tail could potentially keep the motor in an autoinhibited state.

Taken together, these results suggested that KIF1C exists in an autoinhibited tail-block state.

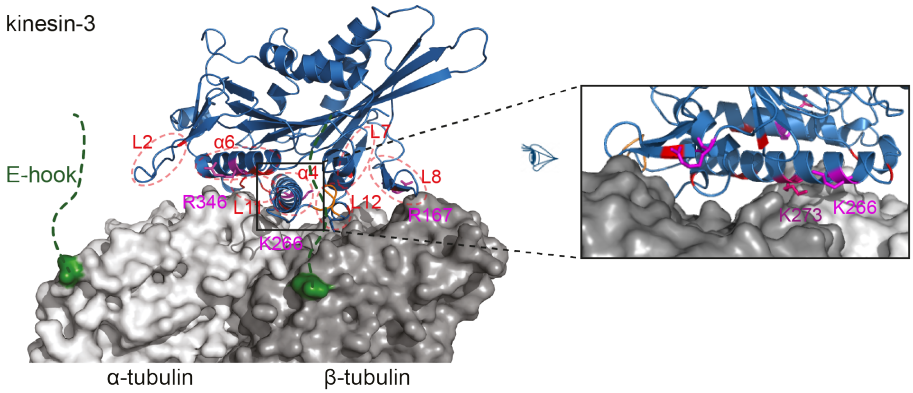

Figure 3.9: Structure of Kinesin-3 motor domain binding to the microtubule
Residues of the kinesin motor domain (blue) that are known to contribute to the interaction with microtubules (grey) are shown in pink (Scarabelli et al., 2015) and the residue K273 shown to crosslink with the KIF1C tail is highlighted in magenta. PDB accession numbers: 4UXP. Adapted from (Siddiqui and Straube, 2017).

3.4. Cross-link mass spectrometry with KIF1C-GFP and PTPN21 FERM

The KIF1C-GFP cross-links support the idea that the motor protein is in an autoinhibited tail-block state. To test whether the addition of FERM domain of PTPN21 would activate KIF1C, $PTPN21_{1-381}$ was purified from *E. coli* and cross-link mass spectrometry was performed with the two proteins.

3.4.1. PTPN21-FERM purification

$PTPN21_{1-381}$ which is the FERM domain of PTPN21 was expressed in *E. coli* BL21 DE3 with an amino-terminal HA tag and a carboxy-terminal 6His tag. Purification was carried out in a two-step process with anion chromatography followed by affinity chromatography similar to KIF1C-GFP purification. The protein was visualized on SDS-PAGE as a 46 kD protein (Fig 3.10).

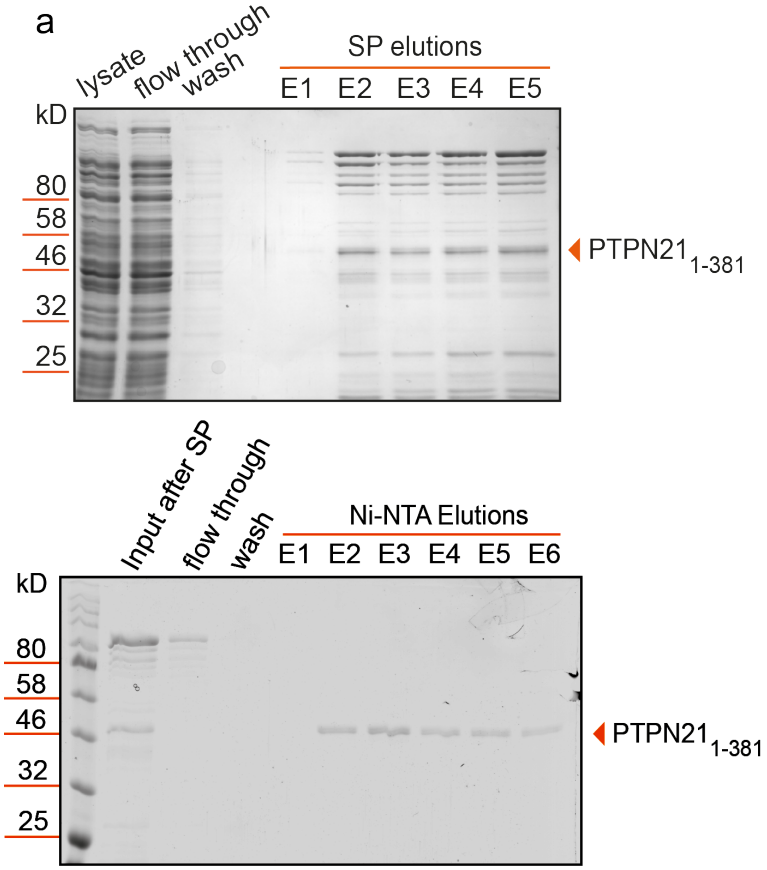

Figure 3.10: Purification of PTPN21 FERM domain

(a) Coomassie gel of HA-PTPN21$_{1-381}$-6His after anion exchange chromatography. The lysate was bound to SP-Sepharose beads and the column was washed with wash buffer containing 50 mM NaCl and eluted with 200 mM NaCl. Elutions E2-E5 were pooled and bound to Ni-NTA beads for affinity chromatography. (b) Coomassie gel of HA-PTPN21$_{1-381}$-6His after affinity column purification. The elutions E2-E5 from SP-Sepharose were bound to Ni-NTA beads which was washed with 20 mM Imidazole containing wash buffer and eluted with 150 mM Imidazole. Elutions E2-E6 were stored and used for subsequent experiments.

3.4.2. Crosslink mass spectrometry with KIF1C-GFP and PTPN21$_{1-381}$

KIF1C-GFP and PTPN21$_{1-381}$ were mixed in equimolar amounts and 5 mM of the cross-linker BS3 and 5 mM of EDC were added in separate reactions and in-solution cross-linking was carried out as described in the Methods section.

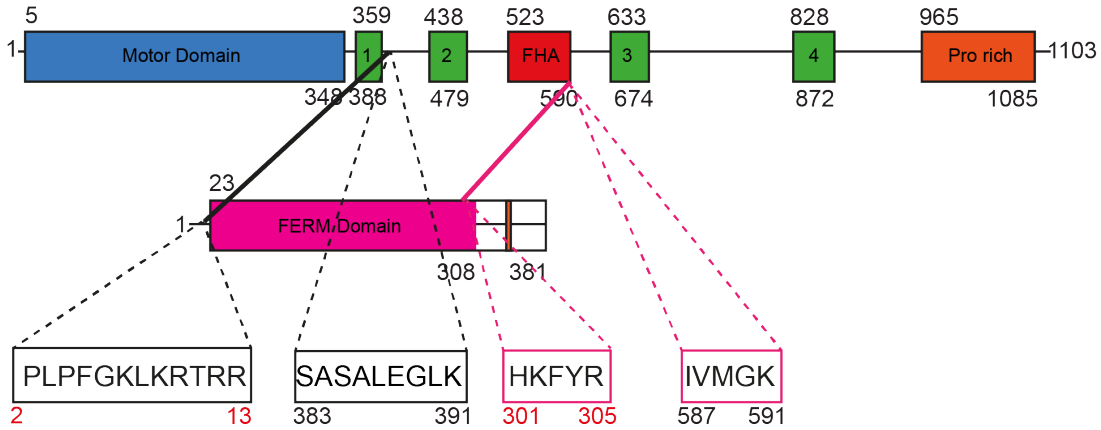

Figure 3.11: Primary structure of KIF1C and PTPN21 showing cross-links
Cross-links identified between KIF1C and PTPN21$_{1-381}$ are depicted in pink for BS3 and in black for EDC. Sequence numbers in red represent PTPN21 and sequence numbers in black represent KIF1C.

From the spectra and the fragmentation score, there were cross-links that were identified between KIF1C-GFP and PTPN21$_{1-381}$ which validated the binding of the two proteins (Fig.3.11). This is consistent with reports published previously which identified the region between 362 and 1103 of KIF1C binding to FERM domain of PTPN21 in a yeast two hybrid screen (Dorner et al., 1998). The peptide $_{588}$IVmGK$_{591}$ in the FHA domain of KIF1C which crosslinked with the motor domain along with other tail cross-links of KIF1C to keep the motor in an autoinhibited state, was observed to make links with $_{301}$HKFYR$_{305}$ sequence from the FERM domain. The lack of KIF1C-GFP specific cross-links that were observed previously and the new cross-links with the FERM domain of PTPN21 suggests that the binding of PTPN21 could possibly relieve the autoinhibition. However, the crosslink mass spectrometry has been performed only once, repetitions with varying concentrations of the KIF1C and PTPN21 FERM domain are required to validate these interactions.

3.4.3. Ionic strength of different buffers

The final pH and ionic strength of the different buffers used in this study are listed below. The hydrodynamic analysis was carried out in 35 mM sodium phosphate buffer pH 7.5 with 1.5 mM $MgCl_2$ at different salt concentrations between 150 and 500 mM NaCl whereas the cross-linking mass spectrometry

was performed with protein eluted in 50 mM sodium phosphate buffer pH 7.5, 150 mM NaCl and 150 mM Imidazole, with a final pH of 8.5. It is important to note that the buffer composition is different between the two techniques and our results suggest that changes in salt concentrations affect the conformation state of KIF1C. It is important to carry out experiments in the low salt conditions in which KIF1C was observed to be in a folded state and the cross-link mass spectrometry data is consistent with this result. It would also be interesting to perform cross-link mass spectrometry at high salt conditions in which the protein adopts an elongated conformation as observed by glycerol gradient centrifugation.

Buffer	pH	Ionic strength
Ni-NTA elution buffer	8.5	0.36
Size exclusion chromatography 150 mM NaCl	7.5	0.25
500 mM NaCl	7.2	0.60
Glycerol gradient centrifugation 50 mM NaCl	7.5	0.17
150 mM NaCl	7.5	0.27
250 mM NaCl	7.5	0.37
350 mM NaCl	7.5	0.47
500 mM NaCl	7.5	0.62
Cross – link mass spectrometry	8.5	0.37

Table 19: Ionic strength of different buffers

The ionic strength of the various buffers used was calculated using the formula $I = ½ \Sigma c_i z_i^2$, where c_i is the molar concentration of the ion and z_i is the charge. The pH was measured after all components were added.

3.5. Single-molecule behaviour of KIF1C

To confirm that the FERM domain of PTPN21 activates KIF1C, the single molecule behaviour of KIF1C-GFP was characterized first and subsequently experiments with PTPN21-FERM were carried out using total internal reflection microscopy (TIRF). Single molecule motility assay with KIF1C-GFP on Hilyte647-labelled microtubules showed that KIF1C is a processive, plus-end accumulating motor (Fig 3.12).

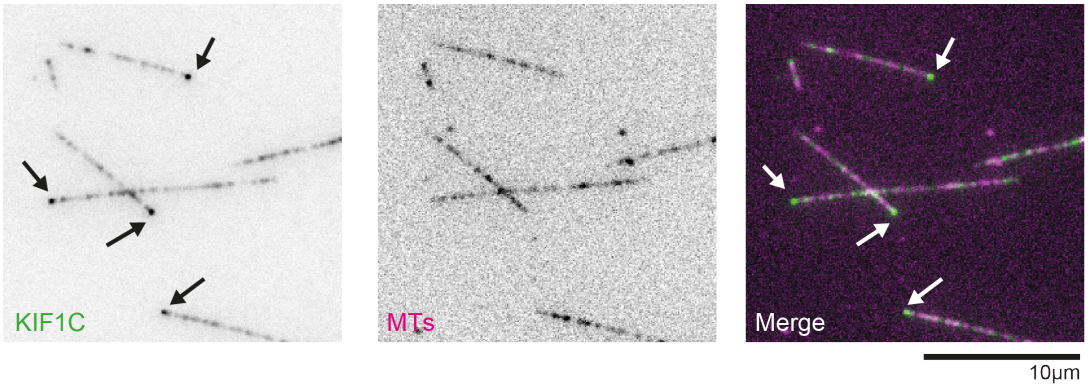

Figure 3.12: KIF1C-GFP accumulates at plus-ends of microtubules
KIF1C-GFP was added to a chamber with microtubules (MT) immobilised on a glass surface. KIF1C was observed walking to the plus-ends of the microtubules Arrow heads indicate KIF1C-GFP accumulation at microtubule plus-ends. KIF1C is in green and microtubules in magenta.

3.5.1. Buffer optimisation

It is known from the literature that kinesin motors are sensitive to salt concentrations (Gilbert et al., 1995, A et al., 2014, Ma and Taylor, 1995, Vale, 1996). To determine the optimal buffer condition for single molecule motility of KIF1C-GFP, various salt concentrations were tested and the velocities and run lengths were calculated for comparison.

Single molecule motility assay was first carried out in MRB80 buffer without the addition of any extra salt. From the Fig 3.13 (a) the velocity and run length of the motors was found to be 0.51 µm/s and 1.9 µm respectively. All motors were found to bind the microtubules. With the increase of salt concentration to 25 mM there was no significant change in velocity and run length (0.48 µm/s and 1.9 µm respectively Fig 3.13 (b)) but there was a reduction in the number of static/dead motors observed. With another step increase with KCl concentration to 50 mM, there was an increase observed in the velocity but no significant difference in run length of the motors (0.74 µm/s and 1.8 µm respectively (Fig 3.13 (c)). There was a further reduction in the number of motors binding and with the final increase to 75 mM KCl in the assay, there were very less binding events observed (Fig 3.13 (d)). From these data, the optimal buffer condition was chosen as MRB80 with the addition of 25 mM KCl.

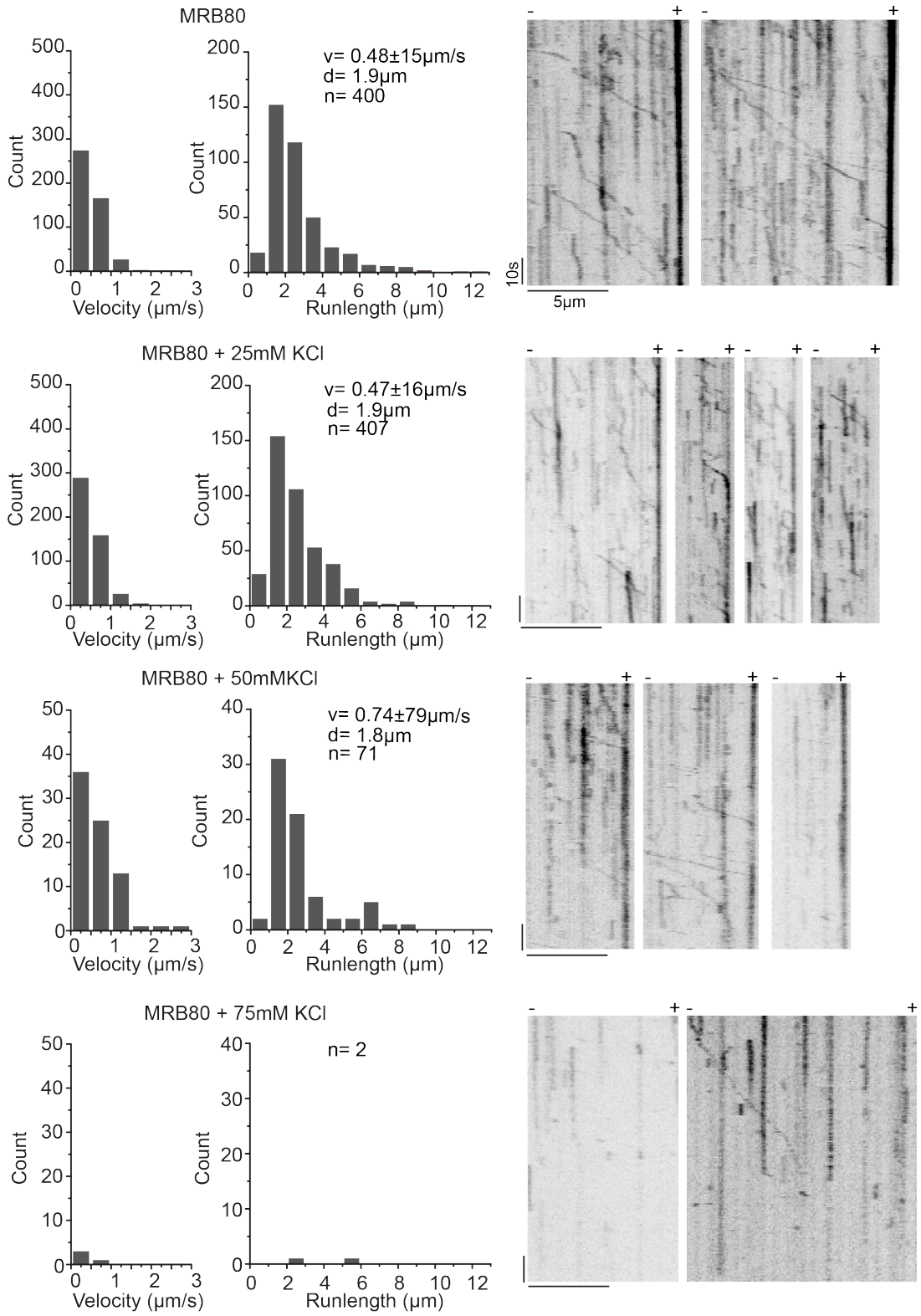

Figure 3.13: Buffer optimization for KIF1C

Kymographs and histogram of velocity and run length distributions depict effect of different salt concentration on the processivity and run length of KIF1CGFP. Image acquisition was at 2 fps.

3.5.2. Photobleaching of KIF1C

On the KIF1C-GFP kymographs, there were bright and dim runs observed. To address the heterogeneity in the assembly state of KIF1C, photo bleaching was carried out in the presence of AMP-PNP to lock the motors on the microtubules and to determine the oligomeric status of the pool of motors used in single molecule motility assay.

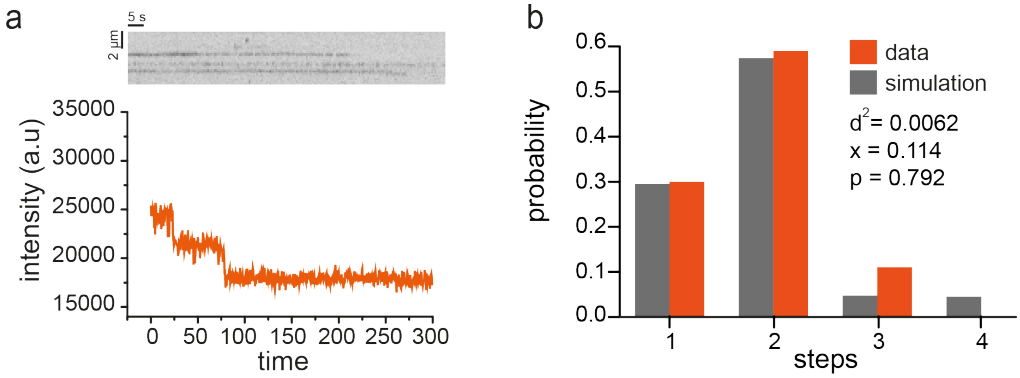

Figure 3.14: Photo Bleaching of KIF1C

Photo bleaching was carried out with KIF1C-GFP in a single molecule assay. (a) Representative kymograph and line plot showing the decrease in intensity over time. (b) Bar plot represents steps determined manually in orange and the best fit of a dimer/tetramer mixed binomial simulation in grey. d^2 is the sum of squared deviations, x is the fraction of tetramer and p is the fraction of fluorescently active GFP. Data represents three different movies analysed. n=108 motor traces. *The R code for mixed binomial model was written by Dr. Masanori Mishima.*

The intensity of KIF1C-GFP was measured over time then bleach steps were determined manually. A mixed binomial fit was performed on the bleach step distribution. The best fit is obtained if assuming a dimer to tetramer ratio of 7.8 and a fraction of inactive GFP fluorophores of 20.8%. That only 80% of GFP fluorophores are functional is in line with findings by others (Ulbrich and Isacoff, 2007). The data represented here indicate that the oligomeric state of KIF1C-GFP is not uniform, but the majority of motors in the preparation is dimeric with a small population of motors in a higher order assembly state.

3.6. Ezrin-FERM purification

In order to account for a control FERM domain in single molecule motility assays with KIF1C, the FERM domain of Ezrin was cloned and expressed in *E. coli* BL21 DE3 with an amino-terminal HA tag and a carboxy-terminal 6His tag. Purification was carried out in a two-step process with anion chromatography followed by affinity chromatography similar to $PTPN21_{1-381}$ purification. The protein was visualized on SDS-PAGE as a 41 kD protein (Fig 3.15).

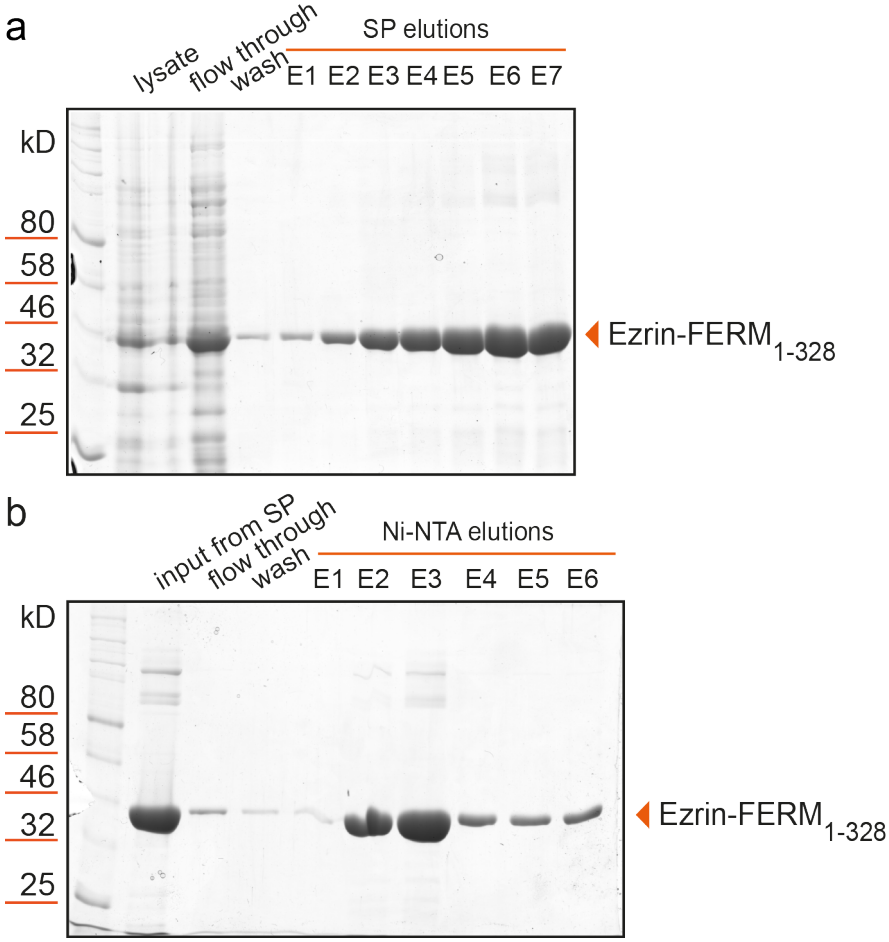

Figure 3.15: Purification of Ezrin-FERM domain

(a) Coomassie gel of HA-$Ezrin_{1-328}$-6His after anion exchange purification. The lysate was bound to SP-Sepharose beads and the column was washed with 50 mM NaCl and eluted with 200 mM NaCl. Elutions E1-E7 were pooled and bound to Ni-NTA beads for affinity chromatography. (b) Coomassie gel of HA-$Ezrin_{1-328}$-6His after affinity column purification. The input from SP-Sepharose was bound to Ni-NTA beads which was washed with 20 mM Imidazole Bacterial Ni-NTA Buffers and eluted with 150 mM Imidazole. Elutions E2-E6 were stored and used for subsequent experiments.

3.7. Single molecule assays with KIF1C-GFP, PTPN21-FERM and Ezrin-FERM

Single molecule motility assay was performed with KIF1C-GFP in the absence and presence of PTPN21-FERM and Ezrin-FERM. KIF1C-GFP was incubated with 125 nM of PTPN21-FERM or Ezrin-FERM for 15min before adding the rest of the motility mix (Table 17) and flowing into the chamber. In the control chamber with KIF1C-GFP alone, the elution buffer of PTPN21-FERM/Ezrin-FERM was added and incubated for 15min to correct for any buffer effects. Representative kymographs are shown below for KIF1C-GFP, KIF1C-GFP + PTPN21-FERM and KIF1C-GFP + Ezrin-FERM (Fig 3.16).

From the kymographs, the motors were scored as running if they moved with a velocity greater than 25 nm/s (green) or static - which did not move for the duration of the movie (grey). Runs with pause events or significant changes in speed were analysed as separate phases. Blind analysis was also carried out independently for an unbiased scoring of the data sets.

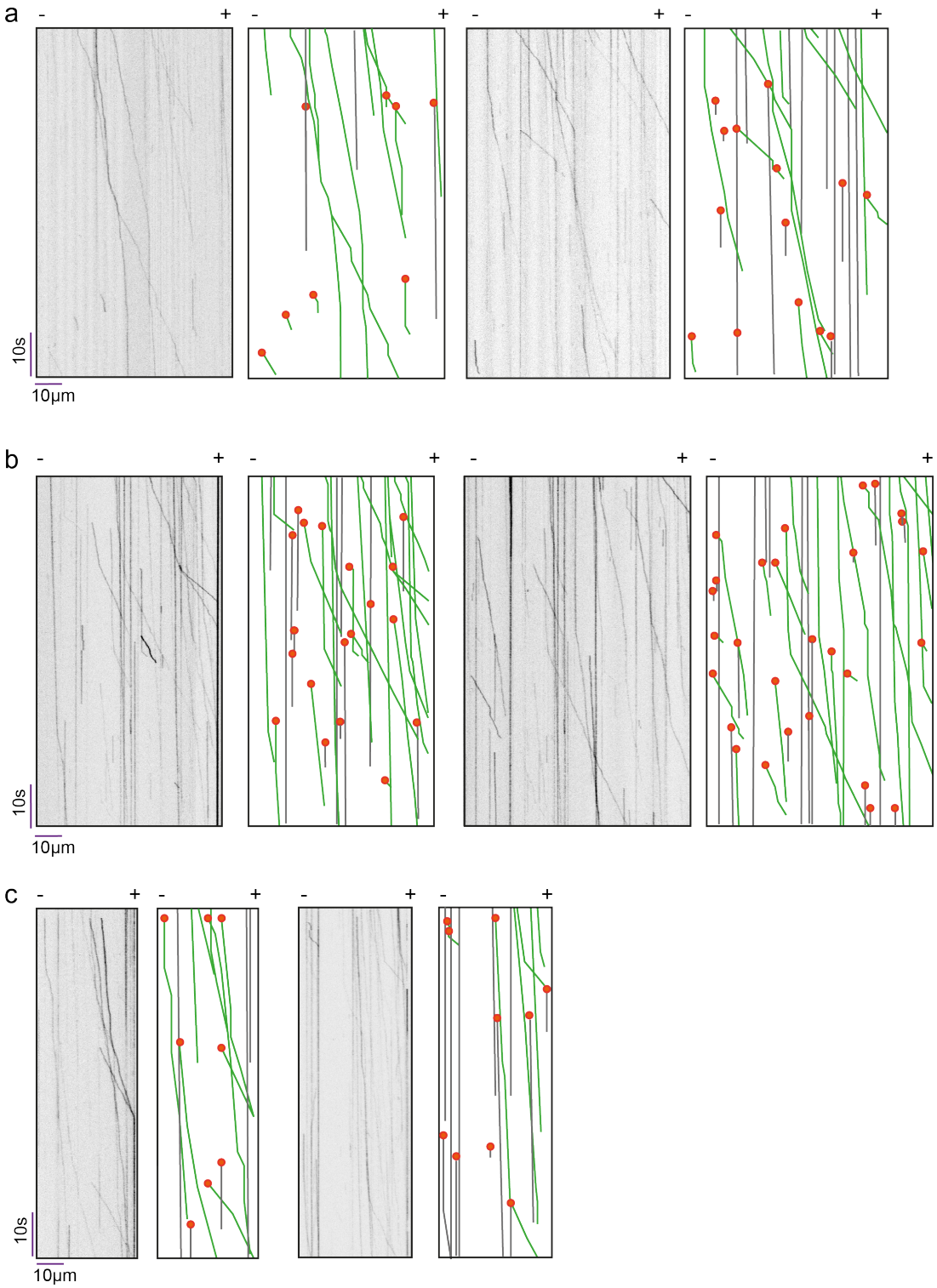

Figure 3.16: Single molecule motility assay with KIF1C-GFP, PTPN21-FERM and Ezrin-FERM

The movies were imaged at 10fps. Representative kymographs for (a) KIF1C-GFP alone, (b) with the addition PTPN21-FERM and (c) with Ezrin-FERM depict runs in green and static motors in grey and landing events in orange.

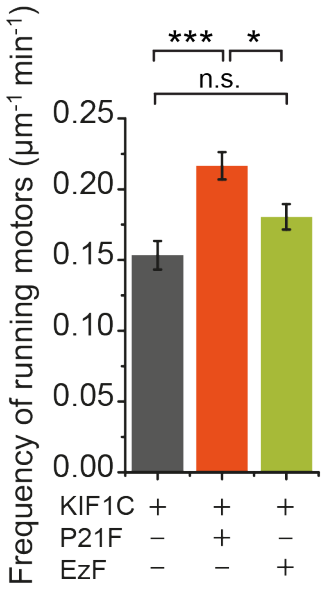

Figure 3.17: Frequency of running motors

The frequency of running motors is shown. Bar plots show mean±SEM from data pooled from three independent experiments. n=22-31 microtubules / 413-473 motors. Statistical significance (t-Test): *p<0.05. P21F: PTPN21-FERM, EzF: Ezrin-FERM.

It is evident that there is an increase in the number of motors landing with the addition of PTPN21-FERM domain. The quantification of the frequency of running motors per microtubule length per minute revealed that KIF1C alone has a frequency of 0.15±0.01 $\mu m^{-1}min^{-1}$ whereas the addition of PTPN21-FERM domain leads to a ~1.4fold increase (0.22±0.01 $\mu m^{-1}min^{-1}$) in the frequency of running motors observed. However, addition of Ezrin-FERM to KIF1C did not have a significant effect on the frequency of running motors (0.18±0.01 $\mu m^{-1}min^{-1}$). These data suggest that addition of PTPN21-FERM to KIF1C does indeed activate it thereby increasing the frequency of running motors. To probe deeper to determine if the addition of PTPN21-FERM domain increases the number motors landing or affects the interaction of KIF1C with microtubules, the landing rates and dwell times were calculated.

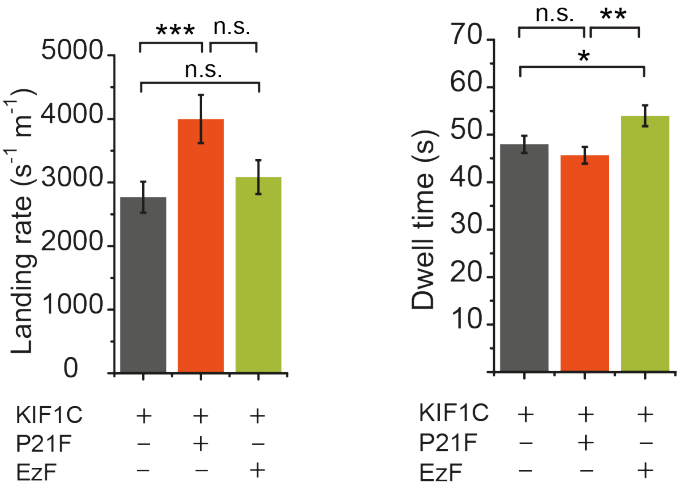

Figure 3.18: Landing rates and Dwell time.

The landing rates and dwell times are shown as bar plots with mean±SEM. Data pooled from 3 independent experiments. n=22-31 microtubules / 413-473 motors. Statistical significance (t-Test): * p<0.05, ** p<0.005, *** p<0.0005. P21F-PTPN21-FERM, EzF-EzrinFERM.

To quantify the landing rates, all the motors that landed depicted as orange dots in Fig 3.17 were counted and normalised to microtubule length and observation time. There was a significant increase of about ~1.4 fold in the landing rate of KIF1C motors to the microtubule when PTPN21-FERM domain was present (Fig 3.18). The landing rate of KIF1C alone was 2769±244 $s^{-1}m^{-1}$ which increased to 3998±379 $s^{-1}m^{-1}$ with PTPN21-FERM domain but not with Ezrin-FERM (3084±265 $s^{-1}m^{-1}$). The dwell times however did not show a significant difference between KIF1C (47.9±1.8 s) and PTPN21-FERM domain (45.6±1.7 s). The addition of Ezrin-FERM increased the dwell time significantly (53.9±2.1 s). These data suggest that PTPN21-FERM activates KIF1C and by virtue of this, there are more motors landing onto the microtubules. The data has been quantified by means of a blind analysis independently and has been repeated with different protein preparations and the results observed are consistent suggesting that indeed PTPN21-FERM domain activates KIF1C motors.

Next, to determine if PTPN21-FERM domain influenced the velocity or run length of KIF1C, the distributions for the same were plotted as shown in Fig 3.19. Addition of PTPN21-FERM or Ezrin-FERM did not have an effect on the

velocity but there was a reduction in the run length distributions of KIF1C. The run length decreased from 8.6±0.4 µm for KIF1C to 7.5±0.3 µm in the presence of PTPN21-FERM domain and to 7.8±0.3 µm with Ezrin-FERM.

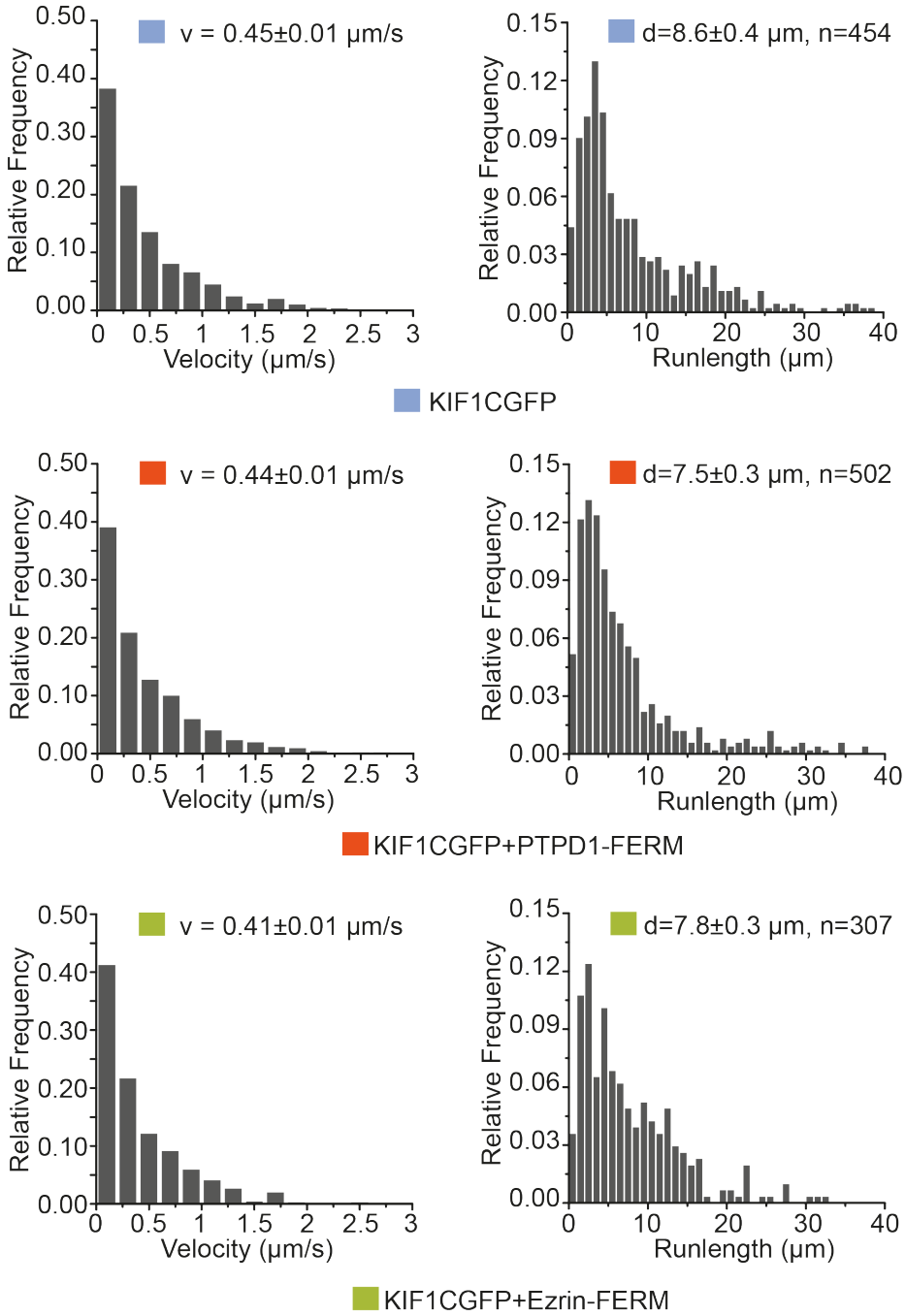

Figure 3.19: Velocity and Run length profile

Histograms depict velocity and run length for KIF1C in grey and KIF1C with PTPN21-FERM in orange and KIF1C plus Ezrin-FERM in green. The mean±SEM values are indicated for each condition.

Theoretically, the velocity profiles follow a Gaussian distribution and the run length follows an exponential decay (Vu et al., 2016). However, for superprocessive, truncated kinesin-3 motors normal distributions have been reported for both velocity and run lengths (Soppina et al., 2014). In our data, we frequently observe static and very slow motors. While static motors were excluded from the velocity analysis, the many slow motors result in an exponential distribution for the velocities. The prevalence of slow motors might be due to the presence of the tail that could interfere with motility. In gliding assays, a truncated version of KIF1C containing amino acids 1-679 showed fast motility of 2.0 ± 0.2 μm/s (Rogers et al, 2001). The distribution was normal similarly to other truncated kinesin-3 motors reported in the literature (Soppina and Verhey, 2014). The KIF1C run length could be exponential in nature if one considers that detecting very short runs (<500 nm) is difficult and thus likely to be underrepresented in the dataset. However, two limitations restrict the measured run length in these assays: the length of the microtubules (typically ~10-15 μm) restricts detection of long runs and many of the slow-moving motors were present for the entire duration of the 3 min movie, suggesting that also the timing might restrict run length. The data presented have not been corrected for these effects. Thus, further experiments with increased microtubule length (20-30 μm) are required to validate the data.

3.8. Conclusion

The data observed here reveal that KIF1C is a dimer in solution in a possibly compact state and elongates at high salt concentrations. This is similar to kinesin-1 conformation change in which the motor protein transitions from 9 S to 6 S as the ionic strength increases (Hackney et al., 1992). For kinesin-1, a small peptide region in the tail of kinesin-1 binds to the motor domain to inhibit it (Friedman and Vale, 1999, Stock et al., 1999, Coy et al., 1999). Crystal structure of kinesin-1 dimeric motor heads reveals a “double lockdown” mechanism where the movement of the motor heads is restricted due to the cross-linking at the coiled coil region and tail domains (Kaan et al., 2011). Similarly, for KIF1C, cross link mass spectrometry validated the

compact state by the cross links that were observed between the tail and motor domain. Addition of PTPN21-FERM domain relieves the autoinhibition and activates the pool of motors, similar to the activation of kinesin-1 by JIP-3 (Watt et al., 2015, Sun et al., 2011).

Taken together, these data suggest that KIF1C is a dimer in solution and the PTPN21-FERM domain does indeed activate KIF1C as shown by the frequency of running motors and the landing events. Binding of PTPN21-FERM domain relieves the tail-block autoinhibition of KIF1C and the motor can now step along microtubules and/or bind cargo and more active motors are observed moving on the microtubules.

Chapter 4 REGULATION OF KIF1C ACTIVITY IN CELLS

4.1. Disrupting the tail-motor interaction results in a hyper active KIF1C

In cells, motor activity is tightly regulated in the absence of cargo by keeping it in an autoinhibited state to avoid microtubule crowding and futile ATP consumption (Verhey et al., 1998). The results in Chapter 3 suggest that KIF1C exists in an autoinhibited tail-block state which is activated by the binding of the phosphatase PTPN21. To test if disrupting the tail-motor interaction sites relieves the autoinhibition and creates a dominant active KIF1C, the tail regions that made contacts with the motor domain based on cross-linked mass spectrometry data were mutated and/or deleted. The substitutions made were designed to hinder the interactions either by charge reversal mutations, substitution with alanine or deletion of domains (Fig 4.1). It is important to note that the amino acids selected for substitutions were based on the cross-link mass spectrometry data alone. It is possible that the actual interaction surface is quite far away in the primary sequence.

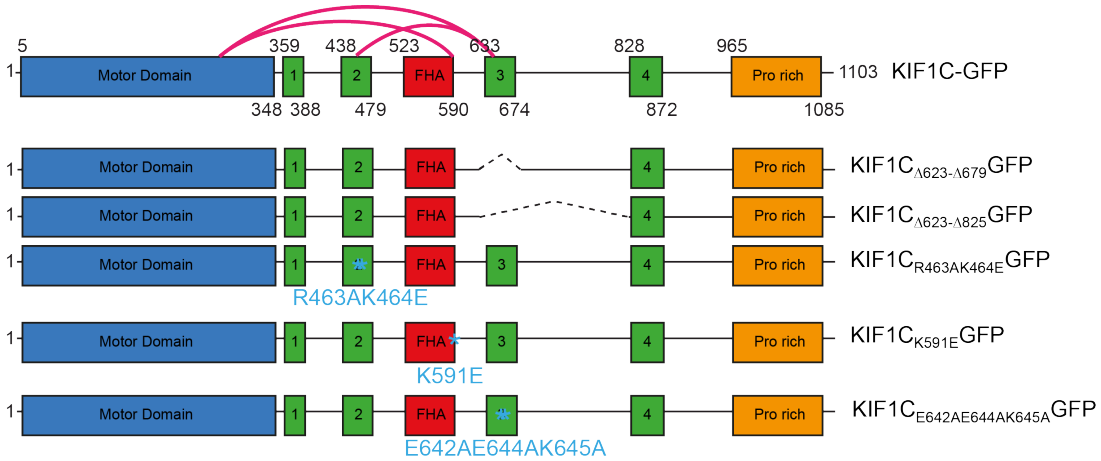

Figure 4.1: KIF1C deletion and mutation constructs

Primary structure of KIF1C depicting deletion (dotted line) and mutation (blue asterisk) constructs generated based on cross-link mass spectrometry links identified

in Chapter 3 (pink arches). Arg463 and Lys464 in the second coiled coil region were mutated to Ala and Glu respectively to generate KIF1C$_{R463AK464E}$GFP. Lys591 in the FHA domain was mutated to Glu to generate KIF1C$_{K591E}$GFP and Glu642, Glu644 and Lys645 in the third coiled coil region were mutated to Ala to generate KIF1C$_{E642AE644EK645A}$GFP. The third coiled coil deletion constructs KIF1C$_{\Delta623\text{-}\Delta679}$GFP and were KIF1C$_{\Delta623\text{-}\Delta825}$GFP were already available in lab.

In Retinal pigmented epithelial (RPE) cells, KIF1C accumulates dynamically at the tip of the tail and delivers the fibronectin receptor $\alpha5\beta1$-integrin into the cell tail which is required for the maturation of trailing adhesions and maintenance of cell tails (Theisen et al., 2012). We used the tail accumulation of KIF1C as a read out for motor activity. We co-expressed KIF1C-mCherry and KIF1C-GFP in RPE cells. The quantification of the mean enrichment of KIF1C at the tail and the front relative to cytoplasmic levels reveal that both mCherry and GFP tagged full-length KIF1C constructs accumulate to a similar extent but there is a higher level of accumulation observed at the tail than the front (Fig 4.2a). Hence, we used this assay to determine the activity of the mutants and deletions in comparison to full-length KIF1C-mCherry.

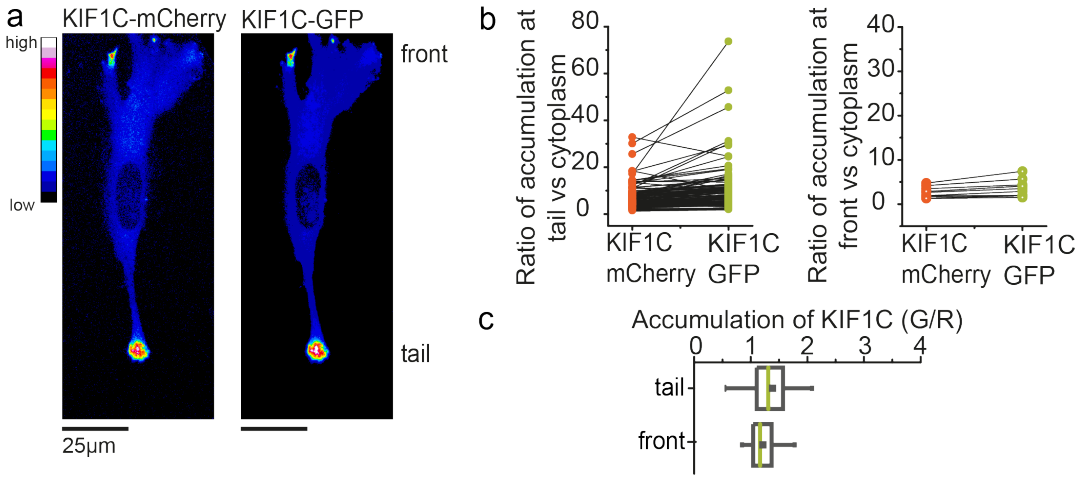

Figure 4.2: KIF1C localisation in RPE cells

(a) RPE cells were co-transfected with KIF1C-mCherry and KIF1C-GFP and imaged 24hr post transfection. KIF1C accumulates at the tip of the tails. Images were adjusted using ImageJ to similar cytoplasmic background. The calibration bar represents the intensity profile for the images. (b) Line series represents ratio of accumulation of KIF1C measured in the tail versus cytoplasm. (c) Box plot depicts ratio of KIF1C accumulation relative to cytoplasmic levels, measured in GFP versus mCherry channels at the tail and at the front. Green line represents the median. Data pooled from three independent experiments, n=26-98.

To assess accumulation of mutants, RPE cells were co-transfected with KIF1C-mCherry and the deletions or mutations with a GFP tag. Cells were imaged 24 hr post transfection. Image analysis revealed that most of the cells lacked tails in the deletion constructs and were round in shape (Fig 4.3 a). For comparison, similar shape cells were chosen for KIF1C-mCherry quantification. Both the deletions, KIF1C$_{\Delta 623\text{-}\Delta 679}$GFP and KIF1C$_{\Delta 623\text{-}\Delta 825}$GFP localized towards the periphery and the quantification of mean accumulation of the "accumulation peaks" revealed higher accumulation of the deletion constructs (3.6±0.58 and 3.9±0.65) than that observed for full length-KIF1C (1.3±0.04) albeit the full-length protein is delocalized (presumably by dimerization with the truncated constructs) and accumulates without a rear bias. This suggests a hyperactive phenotype for the deletion constructs. Subsequently, unpublished data from the Straube lab (Zwetsloot et al., *unpublished*) show that the cells transfected with deletion constructs make tails and the tail to cytoplasm ratio was found to be increased for the KIF1C deletion constructs in comparison to wildtype. This is consistent with the data observed here.

Next, RPE cells were co-transfected with KIF1C-mCherry and the mutations KIF1C$_{R463AK464E}$GFP, KIF1C$_{K591E}$GFP and KIF1C$_{E642AE644AK645A}$GFP. Image analysis and quantification of mean accumulation at the rear and the front revealed that the mutation R463A and K464E in the second coiled coil region resulted in dramatically increased accumulation in the tail (6.7±0.8) and the front of the cell (6.4±0.8). The FHA domain mutation K591E led to a slight increase in accumulation (2.2±0.1 at the tail and 1.6±0.1 at the front). The triple mutant in the third coiled coil domain did not show a significant difference in accumulation (1.4±0.1 and 1.3±0.04 at the rear and front) in comparison to wt KIF1C (1.3±0.04 and 1.2±0.04 at the rear and front) (Fig 4.4a).

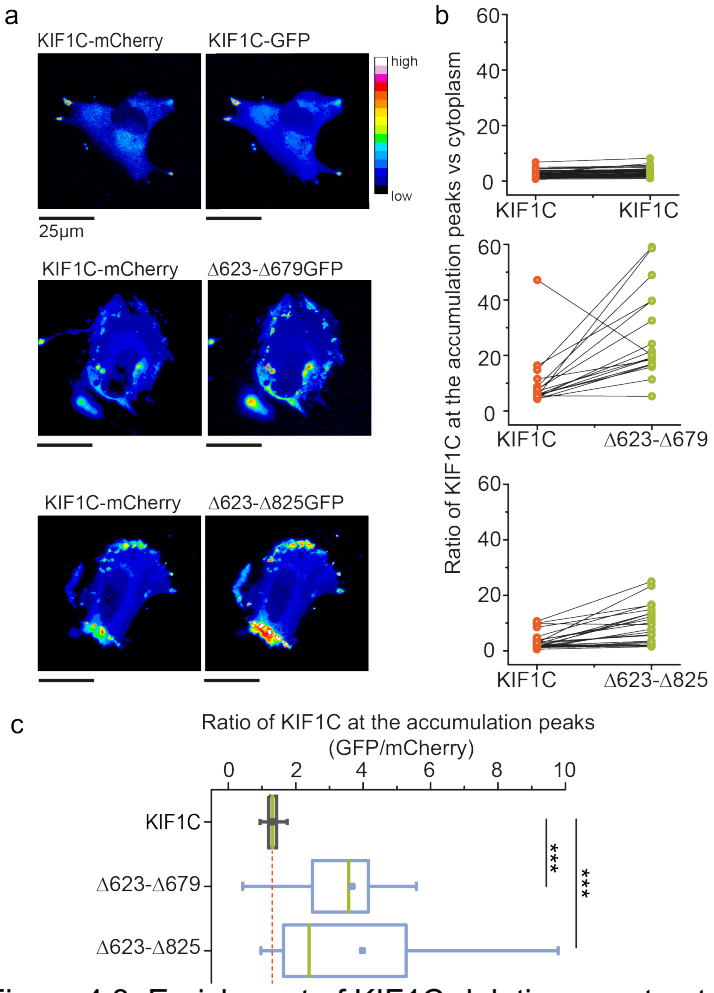

Figure 4.3: Enrichment of KIF1C-deletion constructs

(a) RPE cells were co-transfected with full-length KIF1C-mCherry and deletion constructs tagged with GFP and imaged 24hr post infection. Images were adjusted using ImageJ to similar cytoplasmic background. The calibration bar represents the intensity profile for the images. (b) Line series represents ratio of KIF1C measured in the accumulation peaks versus cytoplasm. (c) Box plot depicts ratio of KIF1C relative to cytoplasmic levels, measured in GFP versus mCherry channels at the accumulation peaks. Green line represents the median. Orange line represents the wt level for reference. Data pooled from three independent experiments, n=17-38. Statistical significance (t-Test): *** $p<0.0005$.

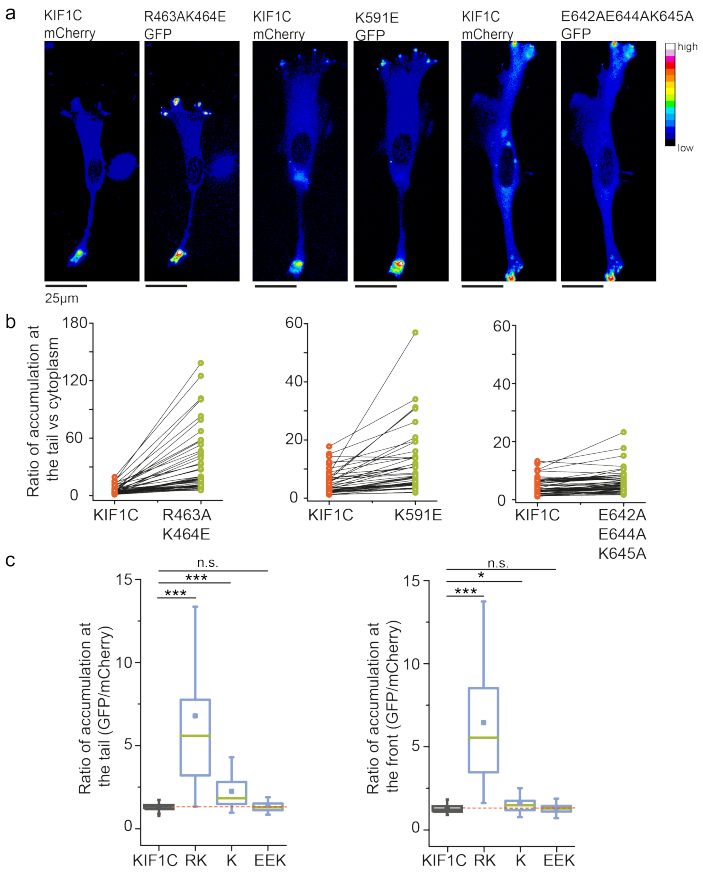

Figure 4.4: Enrichment of KIF1C mutation constructs

(a) RPE cells were co-transfected with KIF1C-mCherry and KIF1C-mutation constructs and imaged 24hr post transfection. Images were adjusted using ImageJ to similar cytoplasmic background. The calibration bar represents the intensity profile for the images. (b) Line series represents ratio of accumulation of KIF1C measured in the tail versus cytoplasm. (c) Box plot depicts ratio of accumulation relative to cytoplasmic levels, measured in GFP versus mCherry channels at the tail and front. Green line represents the median. Orange line represents the wt level for reference. Data pooled from three independent experiments, n=26-48. Statistical significance (t-Test): *p<0.05. RK- R463AK464E, K- K591E, EEK- E642AE644AK645A.

Deleting the entire third coiled coil region or the point mutations in the second coiled coil region of KIF1C both of which have been shown to interact via cross-link mass spectrometry, resulted in higher accumulation of the constructs at the tail and the front of the cell. This phenotype suggests hyperactivity of the motor protein and indicates that in the absence of the third coiled coil domain interacting with the motor domain and second coiled coil region, the motor domain is free to make contacts with the microtubule surface and is no longer held in an autoinhibited state. Alternative explanations to

hyperactivity would be that the observed increase in accumulation is due to a higher retention of the mutant constructs at microtubule plus-ends or a decrease in minus-end transport due to the inability to bind an adaptor protein. Either of those would also results in the motors accumulating to a greater extent than wildtype KIF1C at the edge of the cell without the requirement of the motors moving more or faster.

4.2. The Proline-rich region is required for KIF1C localisation in cells

For KIF1C to accumulate at the tip of the tail in migrating cells, but not everywhere at the periphery, it either needs to have a bias to the rear or be retained specifically at the tail tip. It could be possible that KIF1C is anchored at microtubule plus ends in the rear by interactions with other proteins exclusively present in the rear of the cell. Thus, KIF1C would walk to all microtubule ends but is specifically retained at the cell rear. To determine the structural domains of KIF1C contributing to the rear accumulation in cells, various truncations of KIF1C were tested for their ability to accumulate at the tip of the tails in RPE cells in comparison to full-length KIF1C.

The series of truncations that were available in lab were used for this purpose - KIF1C$_{1\text{-}490}$GFP which is a minimal construct with the motor domain and two coiled coils, KIF1C$_{1\text{-}610}$GFP which includes regions until the end of the FHA domain, KIF1C$_{1\text{-}822}$GFP further includes the third coiled coil and KIF1C$_{1\text{-}912}$GFP includes the fourth coiled coil domain. In addition to these constructs, KIF1C$_{1\text{-}950}$GFP which lacks the proline-rich region and KIF1C$_{1\text{-}1043}$GFP which lacks the binding regions of Rab6 and 14-3-3 proteins were generated. Truncation sites were chosen considering database predictions of coiled-coil, globular regions and unstructured regions – the latter were used for positioning truncations to minimise the probability of misfolding of the resulting protein (Fig 4.5).

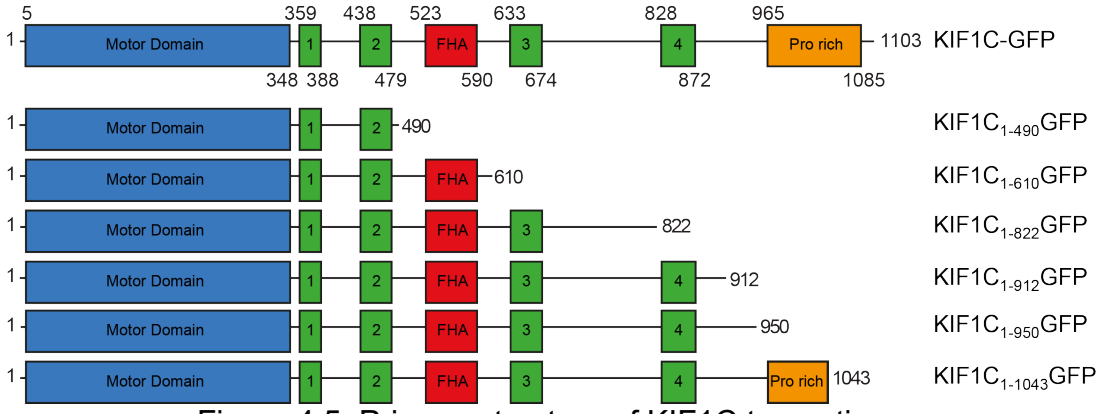

Figure 4.5: Primary structure of KIF1C truncations

KIF1C was truncated at various positions in unstructured regions in the C-terminal tail region to identify the structural domains contributing to the rear accumulation in cells.

RPE cells were co-transfected with full-length KIF1C-mCherry and truncated KIF1C-GFP constructs to determine the localisation phenotypes of the different truncations in comparison to full-length KIF1C. Previous reports from our lab have shown that KIF1C localises at the tip of the tail in migrating cells and is important for directional persistence in these cells (Theisen et al., 2012). The co-transfection of wildtype KIF1C is important since the status of the tail determines how much KIF1C accumulates - forming tails show increase in KIF1C accumulation and retracting tails show a rapid decrease in KIF1C accumulation (Theisen et al., 2012). Thus, KIF1C-mCherry serves as an internal control for the tail state. Image analysis and quantification of mean accumulation at the rear or front and in cytoplasm revealed differences in the localization pattern of the KIF1C truncations in comparison to full-length motor. For comparison, we also measured accumulation at the front of the cell.

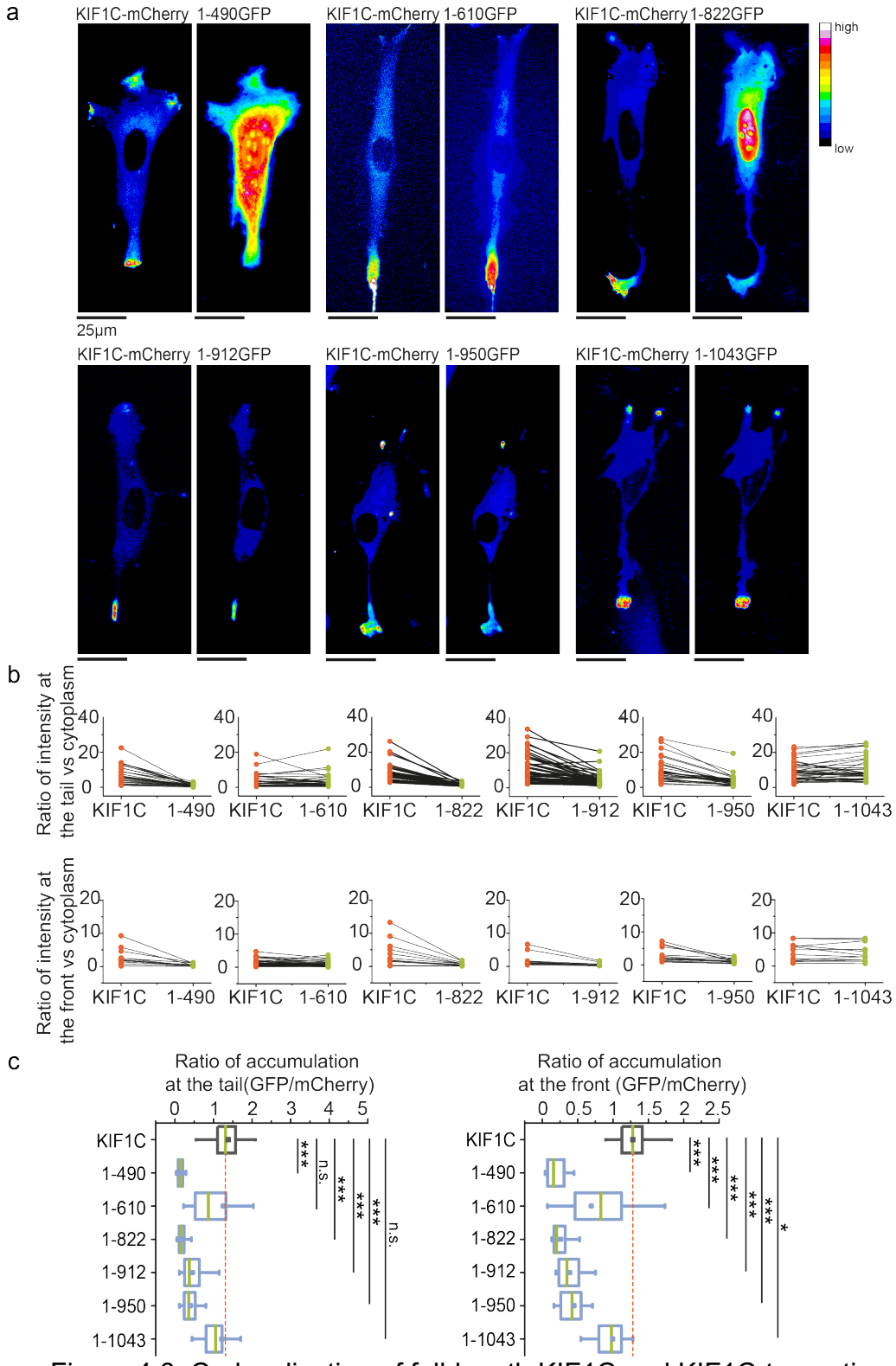

Figure 4.6: Co-localisation of full-length KIF1C and KIF1C-truncations

(a) RPE cells were co-transfected with full-length KIF1C-mCherry and KIF1C-truncation-GFP and imaged 24hr post transfection. Images were adjusted using ImageJ to similar cytoplasmic background. The calibration bar represents the intensity profile for the images. (b) Line series represents ratio of accumulation of

KIF1C measured in the tail versus cytoplasm and front versus cytoplasm. (c) Box plot depicts ratio of accumulation relative to cytoplasmic levels, measured in GFP versus mCherry channels at the tail and front. Green line represents the median. Orange line represents the wt level for reference. Data pooled from three independent experiments, n=10-98. Statistical significance (t-Test): *p<0.05.

The KIF1C$_{1\text{-}490}$GFP construct was found to be mainly in the cytoplasm (Fig 4.6a). The tail and front accumulation was significantly reduced to 10% of the full-length motor. This construct comprises of the motor domain along with the two coiled coils only. But, since we find this construct to be mainly cytosolic, it suggests that the domains in the tail are indeed required for proper localisation of KIF1C in the cell.

The KIF1C$_{1\text{-}610}$GFP construct which includes the tail until the FHA domain was seen decorating microtubules throughout the cell (Fig 4.7). But, it did not co-localize with full-length KIF1C very well and was excluded from regions where full-length KIF1C was present.

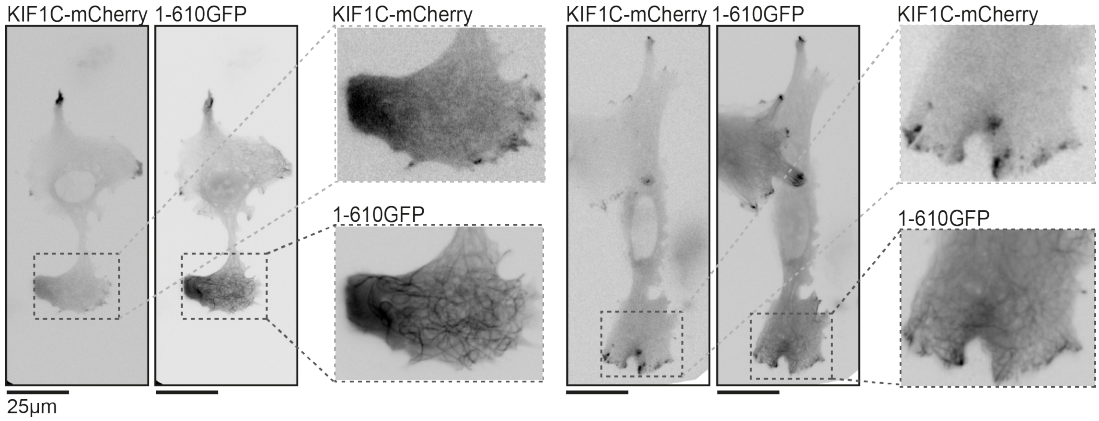

Figure 4.7: KIF1C$_{1\text{-}610}$GFP decorates microtubules

RPE cells co-transfected with KIF1C-mCherry and KIF1C$_{1\text{-}610}$GFP. Microtubule decoration was observed in KIF1C$_{1\text{-}610}$GFP (inset).

The KIF1C$_{1\text{-}822}$GFP construct localizes to the nucleus and does not accumulate in the tail (0.1±0.01) or front (0.1±0.01). This truncation possesses the FHA domain along with the PTPN21 and Myosin IIA binding site. Upon closer inspection, there is a predicted nuclear localisation signal identified near the truncation site which might become exposed in the truncation and explain the mislocalization.

The KIF1C$_{1-912}$GFP and KIF1C$_{1-950}$GFP constructs which exclude the proline-rich region as well as 14-3-3 and Rab6 binding regions localize to the rear and front to some extent, but not as strongly as the full-length. Finally, with the inclusion of the proline-rich region in the construct KIF1C$_{1-1043}$GFP there was complete co-localisation observed (1.2±0.1) between full-length KIF1C and the truncated construct at the tail and front with a higher accumulation at the tail. From literature it is known that the truncated motors are often dominant active since the tail is no longer present to interfere with the motor head to keep it in an autoinhibited state (Soppina et al., 2014, Hammond et al., 2009). But, the results observed here indicate that truncating the tail region of KIF1C results in a pool of motors that is mainly cytoplasmic. It remains to be seen in-vitro if the 1-490 construct behaves as a dominant active motor. Although we set out to determine the structural regions contributing to rear accumulation, we found that truncating the tail region of KIF1C not only affects the tail localisation but the front localisation as well, suggesting that the proline-rich region is important for the activity of the motor to walk to the cell periphery rather than any specific retention or bias towards the rear. Further experiments are required to decipher how exactly the proline-rich region mediates the efficient localisation of KIF1C in cells. One possibility is that the cargo adapters and Rabs that bind in this region are keeping the motor in an active conformation.

4.3. 14-3-3 proteins negatively regulate KIF1C activity

14-3-3 adapter proteins are known to regulate kinesin motor activity (Douglas et al., 2010, Yoshimura et al., 2010). These proteins recognize and bind to phosphoserine or phosphothreonine proteins, thereby regulating the kinesin motor activity (Fu et al., 2000, Tzivion and Avruch, 2002). For KIF13B, a kinesin-3 family member, it has been shown that the motor exists in an autoinhibited state (Yamada et al., 2007) and upon phosphorylation by Par1b/MARK2, which is a microtubule affinity regulating kinase, 14-3-3β binds and promotes the intramolecular interaction of KIF13B motor and tail domains. This in turn negatively regulates KIF13B microtubule binding, resulting in the

dispersal of the motor in the cytoplasm and a reduction in cell protrusion and axon formation (Yoshimura et al., 2010).

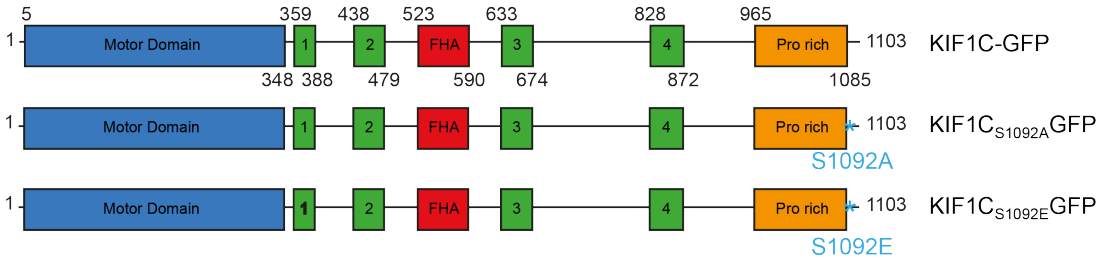

Figure 4.8: KIF1C deletion and mutation constructs

KIF1C was truncated at various positions in unstructured regions in the C-terminal tail region to identify the structural domain contributing to the rear accumulation in cells.

KIF1C has been shown to interact with 14-3-3 proteins in a yeast two-hybrid screen in a phosphorylation-dependent manner via the phosphorylation of Serine 1092 by an unknown kinase (Dorner et al., 1999) but the functional consequence of the binding of 14-3-3 proteins to KIF1C remains to be elucidated. To understand the physiological significance of the interaction between 14-3-3 proteins and KIF1C, Ser1092 was mutated to Alanine to disrupt the binding of 14-3-3 proteins and Ser1092 to Glutamate to generate a phosphomimetic mutant – although it is known that phosphomimetic mutations of 14-3-3 tend not to work and replicate the finding of nonphosphorylatable Alanine mutations (Johnson et al., 2010) (Figure 4.8).

RPE cells were co-transfected with KIF1C-mCherry and the mutations KIF1C$_{S1092A}$GFP and KIF1C$_{S1092E}$GFP. Image analysis and quantification of the mean intensities at the rear and the front revealed that both point mutants accumulate at the tail (2.0±0.1 and 2.0±0.09) and the front (1.9±0.2 and 1.5±0.09) of the cells to a greater extent than full-length KIF1C (Fig 4.9). This suggests that 14-3-3 binding is required to control the levels of KIF1C accumulation or motility in the cell via negative regulation. In the absence of this, there is higher accumulation observed. Thus 14-3-3 binding negatively regulates KIF1C accumulation or motility.

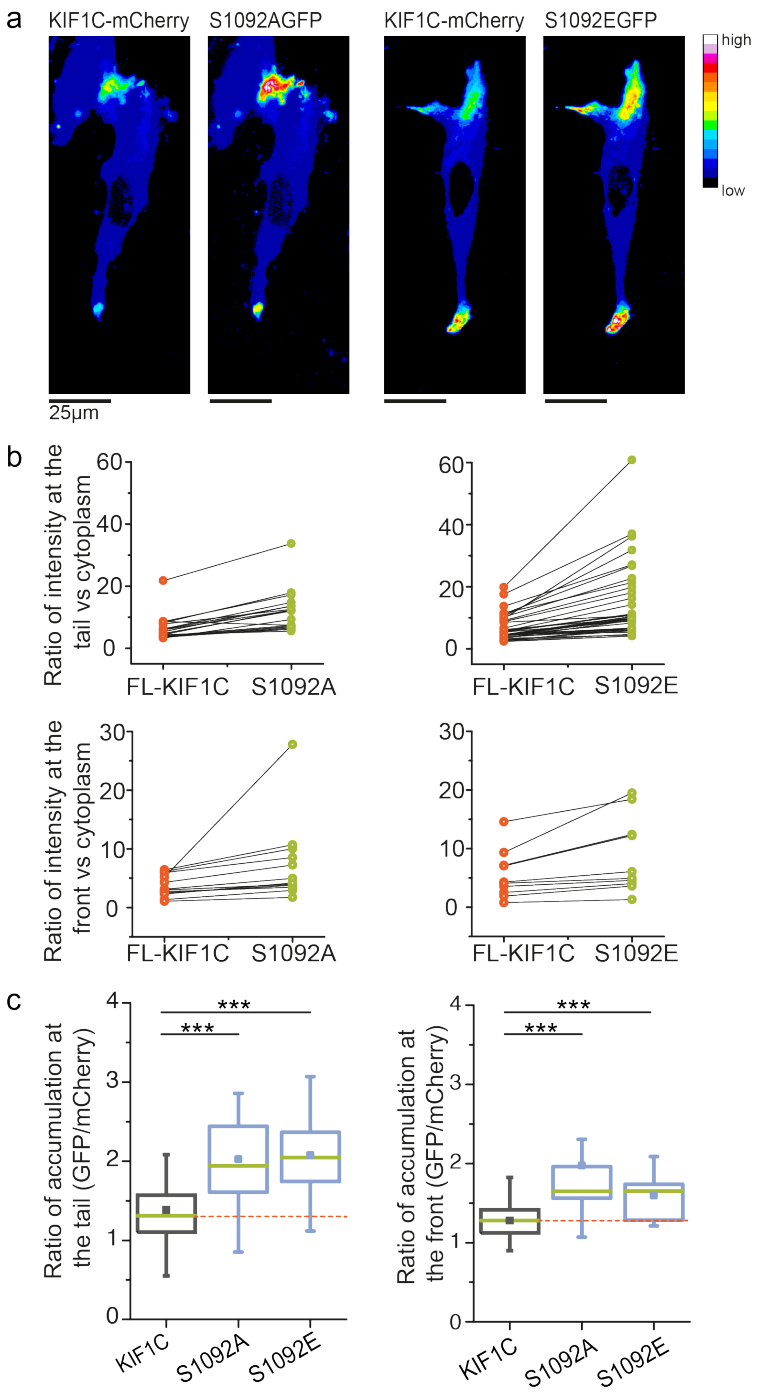

Figure 4.9: Enrichment of the 14-3-3 mutants at front and rear of the cell. (a) RPE cells were co-transfected with full-length KIF1C-mCherry and KIF1C-mutants-GFP and imaged 24hr post transfection. Images were adjusted using ImageJ to similar cytoplasmic background. The calibration bar represents the intensity profile for the images. (b) Line series represents ratio of accumulation of KIF1C measured in the tail versus cytoplasm and front versus cytoplasm. (c) Box plot depicts ratio of accumulation relative to cytoplasmic levels, measured in GFP versus mCherry channels at the tail and front. Green line represents the median. Orange line represents the wt levels. Data pooled from three independent experiments, n=10-98. Statistical significance (t-Test): *p<0.05.

4.4. Conclusion

The results discussed here suggest that the deletion of the third coiled coil domain results in a dominant active KIF1C which is consistent with the crosslink mass spectrometry data observed in Chapter 3 which show that the third coiled coil domain crosslinks with the second coiled coil and motor domain. In the absence of the coiled coil domains, the tail is no longer able to make contacts with the motor domain thereby making it dominant active. Using KIF1C truncations tagged with a GFP fluorophore it was found that the proline rich domain at the C-terminus of the motor protein is required for proper localization of KIF1C in cells. One of the limitations of this study is that the relative expression of mCherry-tagged wild-type and GFP-tagged mutants cannot easily be controlled for. However, based on Western blot analysis of our stable KIF1C-GFP cell line that expresses roughly comparable levels to endogenous protein (Theisen et al., 2012), we know how endogenous level localisation looks like and that expression above those levels results in aberrant, highly elongated cell shape and accumulation of KIF1C elsewhere in the cell. Thus, for data analysis, only low to medium expressing cells were selected and total cell levels were measured to control for relative expression levels (Table 20). The construct KIF1C$_{R463AK464E}$GFP that resulted in massive accumulation was actually expressed less than the other GFP constructs suggesting that the accumulation phenotype observed is not due to higher expression.

Total cell fluorescence, mean ± SD		
	KIF1C mCherry	GFP
KIF1C	9.3 ± 5.4	87.6 ± 45.6
KIF1C$_{R463AK464E}$GFP	11.5± 5.4	38.2 ± 19.7
KIF1C$_{K591E}$GFP	14.3 ± 10.0	51.6 ± 34.8
KIF1C$_{E642AE644AK645A}$GFP	15.4 ± 9.8	54.9 ± 36.0

Table 20: Total cell fluorescence

The total cell fluorescence levels were measured for different KIF1C constructs (n=11 to 28). The mean ± SD are reported above.

Taken together, these results are consistent with a model whereby binding of PTPN21 activates KIF1C (Chapter 3) and 14-3-3 protein binding negatively regulates KIF1C activity. None of the truncation experiments showed a specific loss of tail accumulation while retaining enrichment at the periphery, suggesting that defects observed are likely due to reduced motor activity rather than interaction with a potential tail-specific interaction partner that mediates retention. The absence of this might suggest that tail retention is due to limited retrograde transport opportunities in the tail rather than specific retention.

CHAPTER 5 FORCE GENERATION AND PATIENT MUTANTS

Kinesin-3 mediated long-distance cargo transport is essential for cellular maintenance and function (Kern et al., 2013) (Otsuka et al., 1991). The motors transport cargo by walking along microtubules, converting the chemical energy generated by ATP hydrolysis into mechanical work (Chang et al., 2013, Cross, 2016). It is evident from literature that the kinesin-3 motor proteins can walk substantial distances before falling off from the microtubule track making them highly processive and particularly suited for long-distance transport (Soppina et al., 2014). A characteristic feature of these motor proteins is the presence of a stretch of positively charged lysine residues designated as the K-loop in the motor domain which has been shown to enhance microtubule binding (Soppina and Verhey, 2014) (Rogers et al., 2001). Mutations identified in the motor domain of the KIF1 family members have been shown to cause neurological disorders, hereditary spastic paraplegia and cerebellar dysfunction in humans (Caballero Oteyza et al., 2014, Erlich et al., 2011) (Dor et al., 2014). However, little is known about the force generation for kinesin-3 members and how the motor proteins respond to load in a normal and diseased condition. For truncated monomeric KIF1A, it has been shown that the motor moves by a biased Brownian motion in 8 nm steps against a load of up to 0.15 pN (Okada et al., 2003). To elucidate the single molecule mechanics of KIF1C and to probe the effect of the mutations identified in patients, optical trapping and single molecule motility assays were employed.

5.1. Optical Trap

Optical trapping was carried out in collaboration with Dr. Algirdas Toleikis (AT), Cross Lab, CMCB, University of Warwick. Force generation experiments were performed together with AT and the analysis of the traces was done using code written by AT unless mentioned otherwise. The details of the optical trap used here were published previously by (Carter and Cross, 2005).

Optical traps use a highly-focussed laser beam to generate force in the order of piconewtons to be able to physically hold and move a dielectric particle - a polystyrene bead with a diameter of 560 nm in this case. The refraction of the infra-red laser by the polystyrene bead transfers momentum to the bead and tends to centre it in the beam, thereby creating a trapping potential. The same effect generates returning force whenever the bead is pulled off-centre by the attached motor protein. The further the motor walks away from the trap centre, the greater is the force experienced. The position of the bead is tracked and the motions of the motor under load inferred (Fig 5.1).

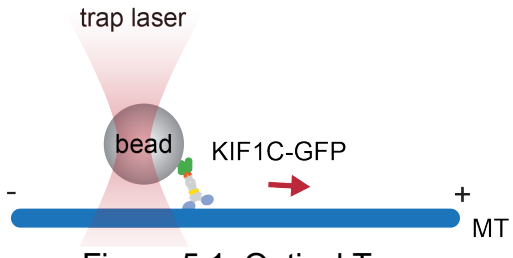

Figure 5.1: Optical Trap

Schematic of a single kinesin motor attached to the bead. The motor displaces the bead from the centre of the trap while walking along microtubules (MT) immobilised on a glass surface. The bead's position relative to the centre of the trap is recorded. Figure not to scale.

5.1.1. Stepping behaviour of wildtype-KIF1C

Human KIF1C-GFP wildtype purified from insect cells described in Chapter 3 was used at concentrations such that less than 20% of the beads moved along microtubules. The Poisson distribution determines the probability of a given number of events occurring in a fixed interval of space or time (Ahrens and Dieter, 1974). In our optical trapping experiments, we observed that 20% of beads moved along the microtubules. This means, P (0), which is the probability of beads that do not move is 0.8. From P (0), the average

number of kinesins bound per bead (x) was calculated to be 0.2231 (Fig. 5.2). Based on this, the probability of a single dimeric motor bound to a moving bead was found to be 89% and that for more than 2 motors bound was 11% (Fig. 5.2).

$$P(n) = \frac{e^{-x} \cdot x^{n}}{n!}$$

n= number of kinesins per bead
x= average number of kinesins bound per bead
e= Euler's number

For 20% beads moving,

$$P(0) = \frac{e^{-x} \cdot x^{0}}{0!} = 0.8, \therefore x = -\ln(0.8) = 0.2231$$

$$P(1) = 0.178$$

$$P(>1) = 0.022$$

Moving beads with 2 or more motors,

$$\frac{P(>1)}{P(1)+ P(>1)} = \frac{0.022}{0.178+ 0.022} = 11\%$$

Figure 5.2: Poisson distribution

Poisson distribution for the number of motors bound to the bead (k) is calculated for 20% beads moving. The probability of a bead moving with 2 or more motors was found to be 11%.

The trap was calibrated before the start of the experiment and from the traces generated, a step finding algorithm that uses a moving window t-test was used to detect steps (Fig 5.3 a) (Carter and Cross, 2005). From the traces collected, the step sizes for all detectable steps were plotted against force (Fig 5.3 b). Steps detection started at 1 pN force since the amplitude of any steps detected below this threshold would be close to that of system noise and therefore unreliable. At low force, the frequency of forward steps (blue) taken is higher and as the force (load) increases, it reduces. At 0 pN force, KIF1C-GFP was observed to walk processively with a velocity of ~550 nm/s along microtubules which is close to the single molecule results discussed in chapter 3. The mean step size for KIF1C-GFP from the forward step size distributions (Fig 5.4 a) was around 7.4 nm, which is close to the 8 nm spacing observed for squid kinesin head domain bound to the same microtubule protofilament (Song and Mandelkow, 1993) (Svoboda et al., 1993). However, the backward step size was distributed more broadly without any dominating step size (Fig 5.4 b).

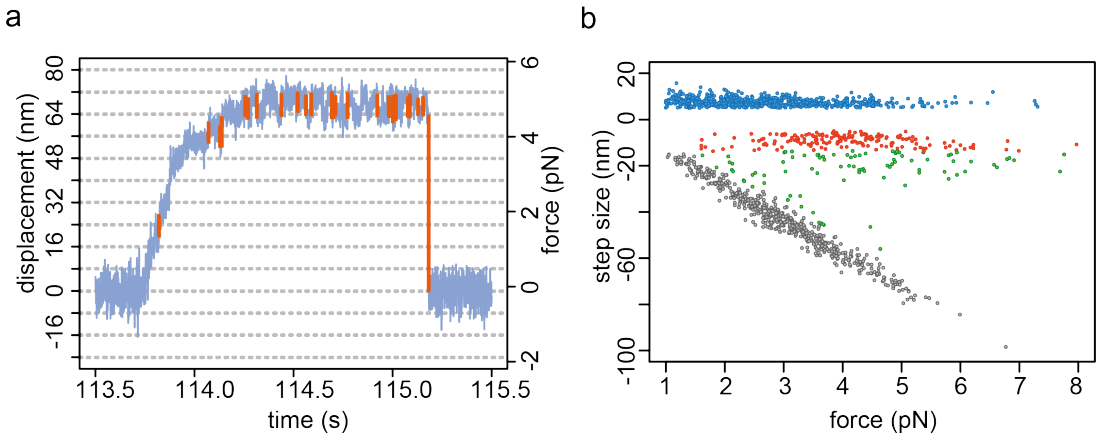

Figure 5.3: KIF1C-GFP motor trace under the trap and detected steps

(a) KIF1C-GFP wildtype was bound to 560 nm polystyrene beads and added to a flow cell with microtubules immobilised on the glass surface. Under the load of the trap, KIF1C-GFP walks along the microtubule and the trace recorded at 20 kHz and mean-filtered to 1 kHz (1 ms) is shown in blue. Y-axis on the left shows distance moved. Time is on the X-axis and force experienced by the motor on the Y-axis is on the right. Horizontal grid lines are drawn 8 nm apart, depicting the expected step size. The steps detected using the step-finder are highlighted in orange. Parameters used in step finder algorithm - t-test score threshold=30, minimum step size=5 nm, minimum force=1 pN, moving average, n=20 (1 ms). (b) The sizes of all detected steps (n=1279) are plotted on Y-axis with the corresponding force experienced in piconewtons on X-axis. Forward steps are represented in blue, backward steps in orange. At higher forces, the motor is unable to make any more forward steps and falls back to the centre of the trap. This is known as a drop-off and is depicted in grey. If the motor re-attaches following a drop-off, we called this a slip, shown in green.

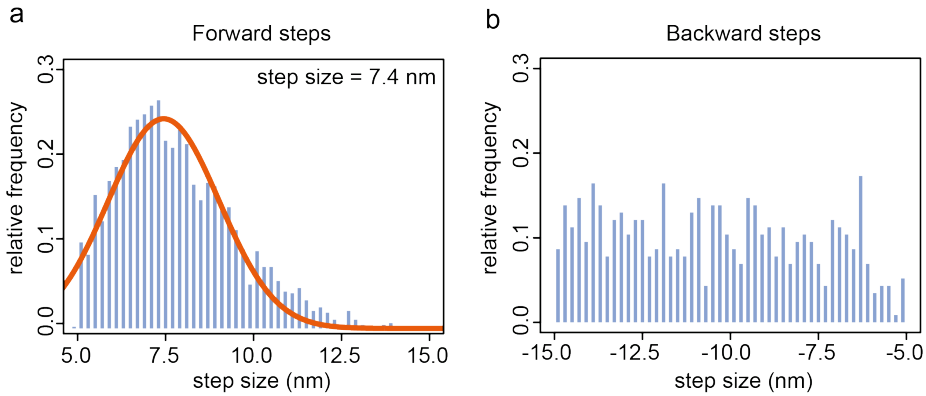

Figure 5.4: Step size distributions of Forward steps and Backward steps

From the steps detected, the relative frequency of forward steps (n=394). and backward steps (n=153) were plotted against step size (nm). The step size from the forward step distribution was found to be 7.4 nm for KIF1C-GFP. Data pooled from three independent experiments with two independent protein preparations.

5.1.2. Dwell times for wildtype-KIF1C

The dwell times represent the time between two consecutive steps taken by the motor - the time during which each motor domain remains bound to the microtubule between steps. Steps below 1 pN force were disregarded since the traces have high noise and steps cannot be assigned reliably. The dwell time for KIF1C-GFP at 2 pN was found to be 34 ms. As the load increases the dwell time was found to increase to 188 ms at 6 pN after which it plateaus. At 8 pN the dwell time dropped to 84 ms (Fig 5.5). This could be for at least two reasons. First, the number of data points at 8 pN is low and the error large. So, the reduction might not be significant and level out when more data are collected for example by moving the stage to push more motors into the high force regime. Secondly, only 2 out of the 37 traces contribute to the data points above 8 pN. It is possible that these two beads had two motors bound as from the Poisson distribution (Fig 5.2), the expected fraction of moving beads with two or more motors bound is 11%. It would be expected that for a pair of motors the dwell time would be shorter. To rule out this possibility, trapping assays need to be repeated with a lower rate of average kinesin per bead, i.e. a lower moving bead rate and high force data collected under conditions where high force is reached by moving the stage to above stall force levels.

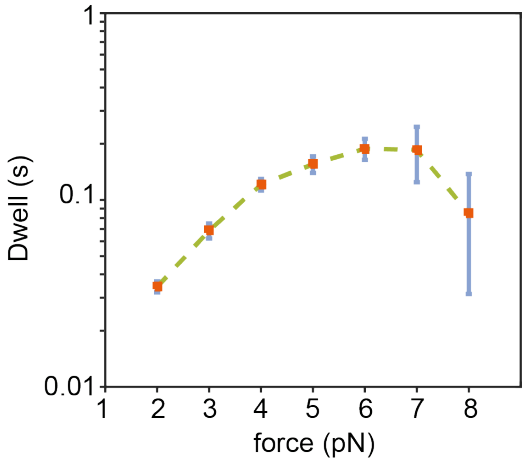

Figure 5.5: Dwell times for KIF1C-GFP

The dwell times were determined from the steps detected and were manually verified for an authentic dwell event. The dwell times were plotted on a Y-axis (log scale) against force in piconewtons. Data points were binned every 1 pN and the standard error is represented in blue error bars.

5.1.3. Stall force for wildtype-KIF1C

Stall force is the force experienced by the motor at which the probability of forward stepping is equal to that of backward stepping and there is no net forward movement observed. Stall force can be determined by plotting the ratios fore step : back step ratio versus load as shown in Fig 5.6. The stall force for KIF1C-GFP was found to be ~5.5 pN.

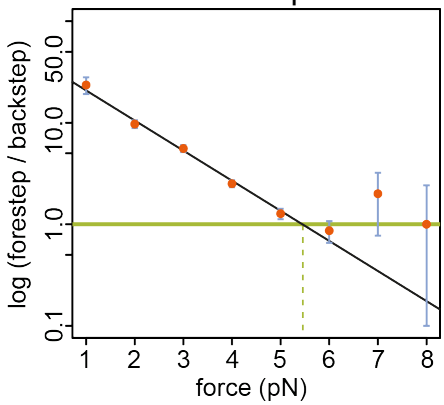

Figure 5.6: Stall force for KIF1C-GFP

Ratio of fore step and back step (log scale) on Y-axis is plotted against increasing force in piconewtons on X-axis. The error bars represent SE. The stall force is determined to be ~5.5 pN when the ratio of fore step to back step is 1, depicted by the intersection of the green and black line.

5.1.4. Force-velocity curve for wildtype-KIF1C

At lower force the motor experiences least load and the velocity is highest. As the load is progressively increased, the velocity progressively decreases until the motor ultimately stalls. At 0 pN, the velocity of KIF1C was found to be ~550 nm/s. As the force (load) increases, the velocity starts to decrease and diminishes around 5-6 pN which is the maximum force experienced by the motor (Fig 5.7).

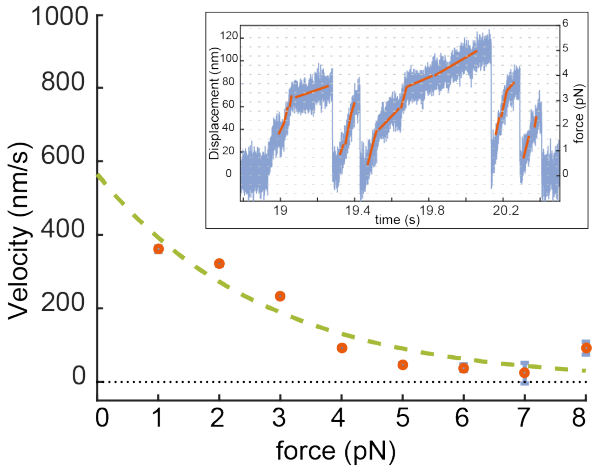

Figure 5.7: Force – velocity curve for KIF1C-GFP

The velocity calculated from the slope of the linear fits (orange lines) at 20 nm trace intervals (inset) was plotted against force in piconewtons to generate a force-velocity curve. *The MATLAB code to determine the velocity was written by Dr. Anup Das, School of Engineering, University of Warwick.*

5.2. HSP causing Patient Mutants identified in KIF1C

Hereditary spastic paraplegia (HSP) is a genetic disorder characterised by the spasticity of lower limbs. Since kinesin-3 motors are implicated in long-haul transport, this might explain why the lower limbs are preferentially affected in these patients. Mutations identified in two different families in KIF1C are present in the highly-conserved motor domain region (Fig 5.8). This could potentially affect the microtubule binding and ATP hydrolysis domains thereby hindering motor function.

Exome sequencing of a family diagnosed with HSP revealed that the parents were carriers of mutations KIF1CPro176Leu and KIF1CGly102Ala (Caballero Oteyza et al., 2014). KIF1CPro176Leu lies in the motor domain and close to the microtubule interaction region whereas KIF1CGly102Ala is present in the highly-conserved nucleotide binding p-loop. KIF1CGly102Ala mutation renders the motor inactive keeping it in a rigor state (Dorner et al., 1998). The parents had one copy of wildtype and one copy of the mutation, but the offspring had both mutant variants expressed together which developed into a diseased condition. Previously reported studies using localisation phenotypes in COS-7 African green monkey cell lines reveal that wildtype KIF1C was able to rescue the perinuclear mislocalization of the mutant

KIF1CGly102Ala, but the mutant KIF1CPro176Leu protein does not rescue this defect, suggesting that pathogenicity occurs when these variants are expressed together, as observed in the patients (Caballero Oteyza et al., 2014). Another mutation KIF1CArg169Trp that lies in the motor domain was identified by whole exome analysis in another family as a missense mutation (Dor et al., 2014) but functional studies are lacking. To gain a better understanding of these mutations and how they affect the motor's ability to carry out long-distance transport, the two mutants KIF1CPro176Leu and KIF1CArg169Trp were chosen (Fig 5.8) for subsequent experiments.

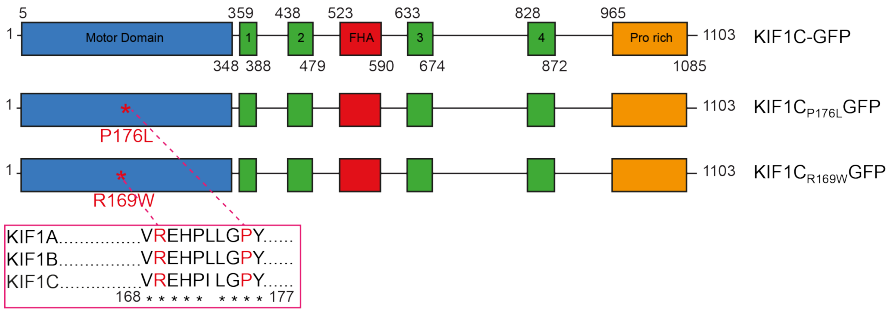

Figure 5.8: Structure of Kinesin-3 motor domain depicting HSP mutations
Primary structure of KIF1C depicting the mutations P176L and R169W in the motor domain identified in HSP patients with sequence conservation between KIF1 family members. The mutations are highlighted in red.

5.2.1. Purification of full-length KIF1C-GFP$_{P176L}$

KIF1C-GFP$_{P176L}$ was expressed in SF9 insect cells with an amino-terminal 6HIS tag and a carboxy-terminal GFP tag. Purification was carried out in a two-step process by anion exchange chromatography using SP-Sepharose beads and affinity chromatography using Ni-NTA beads similar to the wildtype KIF1C-GFP.

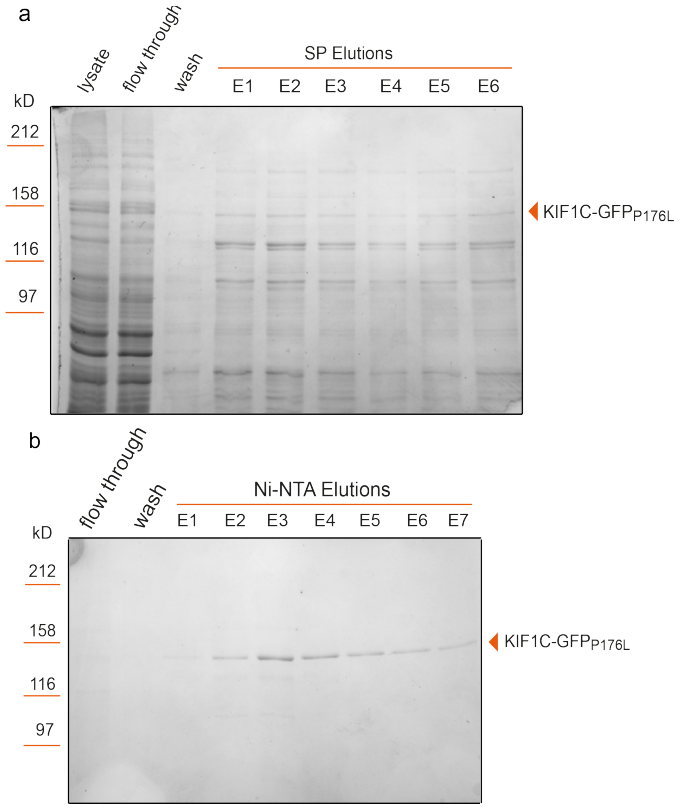

Figure 5.9: Purification of full-length KIF1C-GFP$_{P176L}$

(a) Coomassie gel of 6His-KIF1C-GFP$_{P176L}$ after anion exchange chromatography. The lysate was bound to SP-Sepharose beads and the column was washed with 150 mM NaCl and eluted with 300 mM NaCl. Elutions E1-E6 were pooled and bound to Ni-NTA beads for affinity chromatography. (b) Coomassie gel of 6His-KIF1C-GFP$_{P176L}$ after affinity chromatography. The elutions E1-E6 from SP were bound to Ni-NTA beads and washed with 50 mM Imidazole and eluted with 150 mM Imidazole. Elutions E2 – E7 were stored for subsequent experiments.

5.2.2. Purification of KIF1C-GFP$_{R169W}$

KIF1C-GFP$_{R169W}$ was expressed in SF9 insect cells with an amino-terminal 6HIS tag and a carboxy-terminal GFP tag. Purification was carried out in a two-step process by anion exchange chromatography using SP-Sepharose beads and affinity chromatography using Ni-NTA beads similar to the wildtype KIF1C-GFP protein.

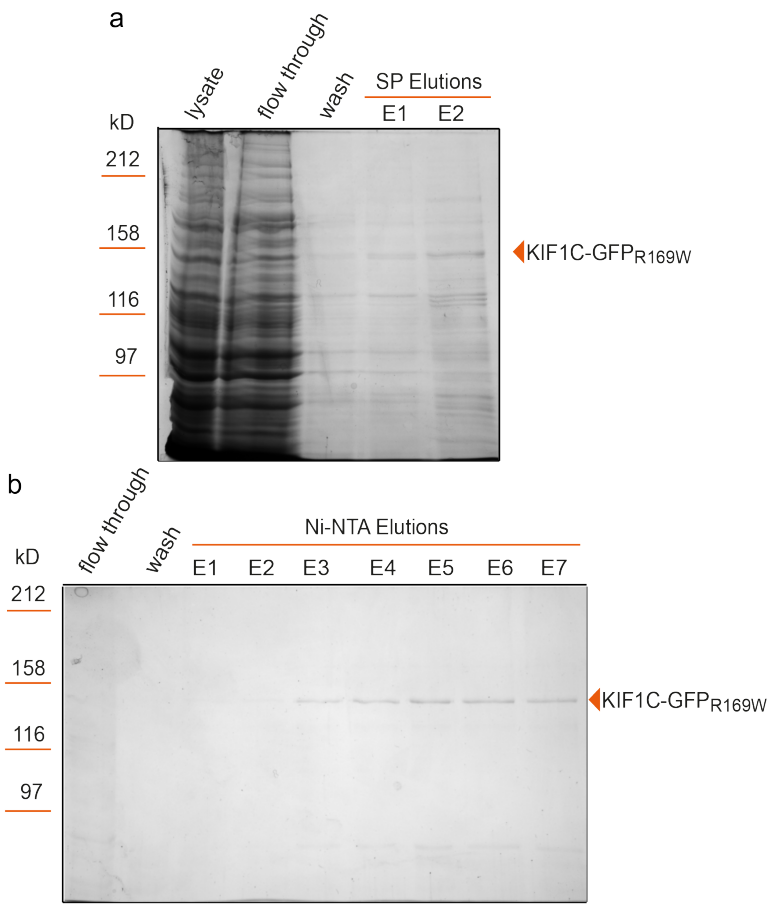

Figure 5.10: Purification of full-length KIF1C-GFP$_{R169W}$

(a) Coomassie gel of 6His-KIF1C- GFP$_{R169W}$ after anion exchange chromatography. The lysate was bound to SP-Sepharose beads and the column was washed with 150 mM NaCl and eluted with 300 mM NaCl. Elutions E1-E4 (E3-E4 not on gel) were pooled and bound to Ni-NTA beads for affinity chromatography. (b) Coomassie gel of 6His-KIF1C- GFP$_{R169W}$ after affinity chromatography. The elutions E1-E4 from SP were bound to Ni-NTA beads and washed with 50 mM Imidazole and eluted with 150 mM Imidazole. Elutions E3 – E7 were pooled and stored for subsequent experiments.

5.2.3. Single molecule behaviour

To establish the effect of the mutations on the motor protein and to determine if the mutations interfere with the ability of the motor protein to walk single molecule motility assays were performed with labelled microtubules

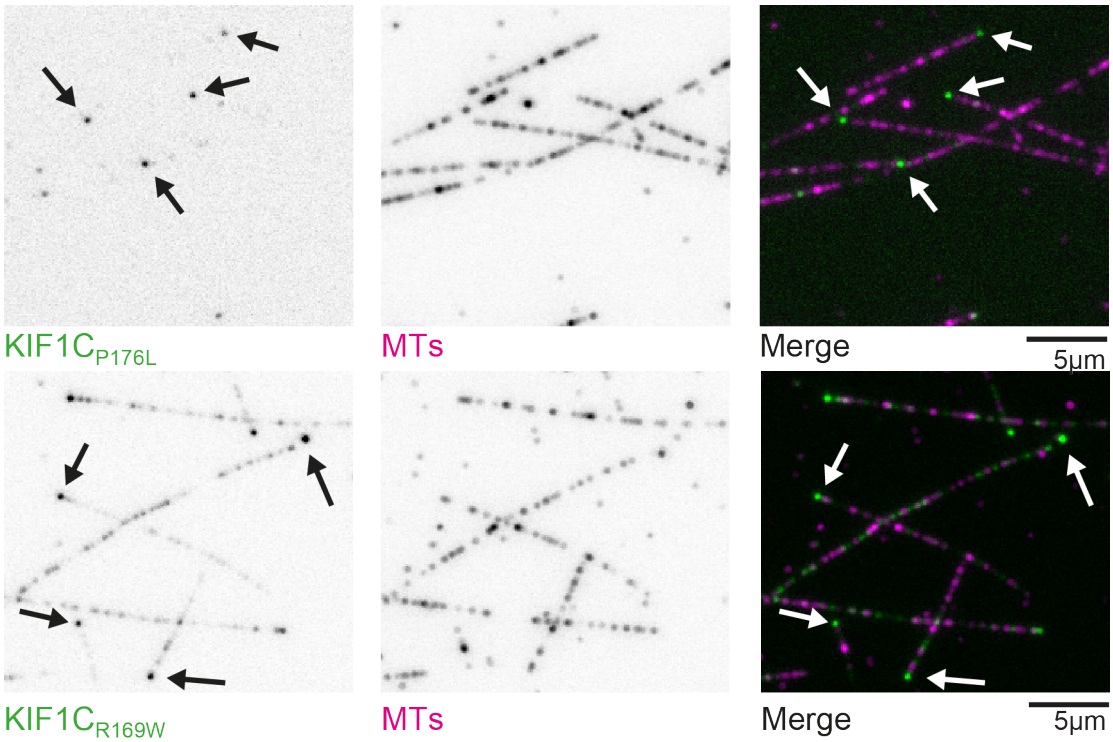

Figure 5.11: KIF1C patient mutants accumulate at plus-ends of MTs

(a) KIF1C$_{P176L}$ (b) KIF1C$_{R169W}$ was added to a chamber with microtubules (MT) immobilised on a glass surface. Both KIF1C patient mutants were observed moving to the plus-ends of the microtubules. Arrow heads indicate KIF1C$_{mut}$ accumulation at microtubule plus-ends. KIF1C$_{mut}$ in green and microtubules are in magenta. KIF1C$_{mut}$ – KIF1C mutant

Both KIF1C patient mutant proteins, KIF1C-GFP$_{P176L}$ and KIF1C-GFP$_{R169W}$ showed plus-end accumulation along microtubules in the single molecule motility assays. The mutants are able to move processively but there are also diffusion events observed on the kymographs (Fig 5.11). KIF1C-GFP$_{P176L}$ behaved more like KIF1C wt but had a reduced velocity, whereas KIF1C-GFP$_{R169W}$ showed a marked reduction in velocity and run length.

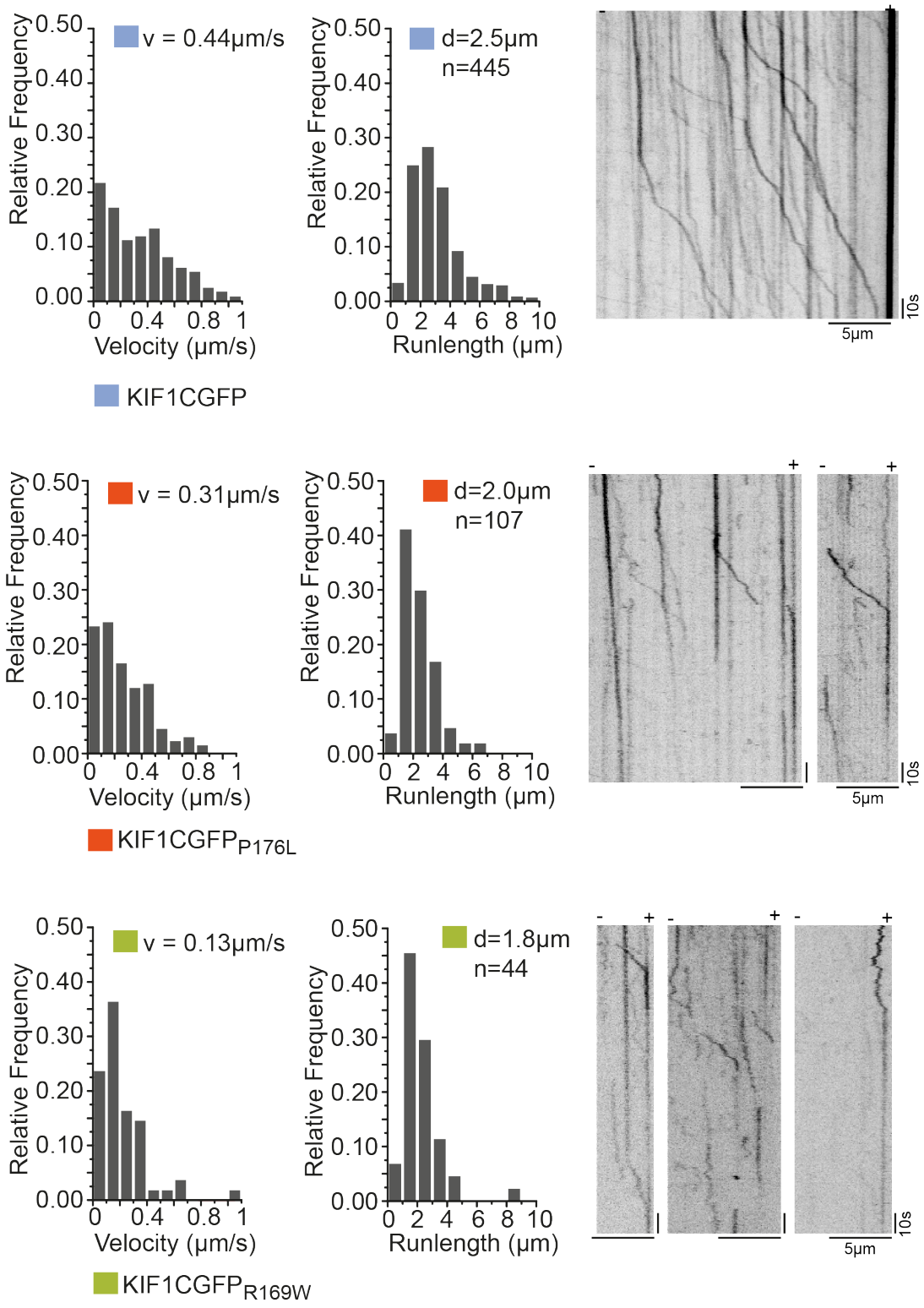

Figure 5.12: Velocity and Run distributions

Histograms depict velocity and run length for KIF1C-GFP (blue), KIF1C-GFP$_{P176L}$ (orange) and KIF1C-GFP$_{R169W}$ (green). The mean values are indicated for each condition. V=velocity, d=run length. Representative kymographs show motility pattern.

5.2.4. Stepping behaviour of mutants

From the single molecule motility assays, it was clear that the mutants are active and can reach microtubule plus ends with a reduction in velocity and run length compared to KIF1C. Next, to probe how these mutants behaved under the load of the trap, optical trapping was carried out.

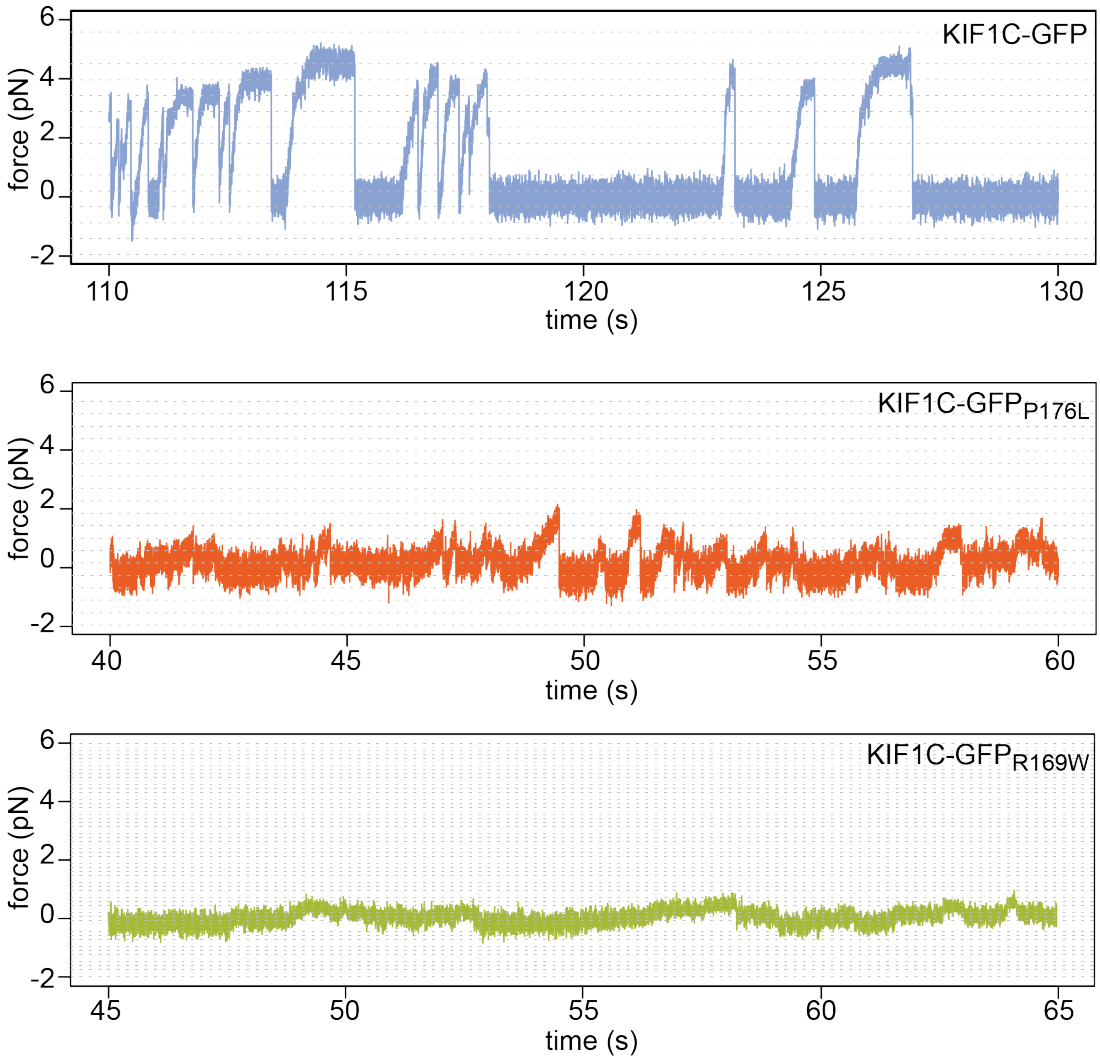

Figure 5.13: Stepping traces of KIF1C wt and patient mutants

Representative traces for KIF1C-GFP (blue), KIF1C-GFP$_{P176L}$ (orange) and KIF1C-GFP$_{R169W}$ (green) under the load of the trap, plotted with force in piconewtons on Y-axis and time in X-axis. The trap laser power for wt KIF1C was 400 mW and that for the mutants was 100 mW.

The experiment was first performed at 400 mW laser power and KIF1C wt walked along microtubules but the patient mutants struggled to step along microtubules. Most of the beads were checked for the presence of a motor by letting it run with the trap off (zero load). This showed that the motor is indeed

bound to the bead but struggles to walk when the trap is switched on. Next, the laser was reduced to 100 mW and runs were observed for KIF1C-GFP$_{P176L}$ but it could only generate / step against forces up to 2 pN. KIF1C-GFP$_{R169W}$ was found to be bound to beads, when the trap was turned off the bead would move small distances but even with 100 mW laser power, this mutant was unable to walk along microtubules.

5.3. Conclusion

From these data, it was observed that the patient mutants are able to step along microtubules without any load but under load the mutant motor proteins struggle to take forward steps. Both pathogenic point mutations tested lie in the motor domain close to the microtubule interaction region and nucleotide hydrolysis site. Further experiments (ATPase and microtubule binding assays) are required to determine which aspect of function is defective and thereby understand how these single point mutations affect the motor proteins cargo transporting capacity under load.

CHAPTER 6 DISCUSSION

6.1. Overview

KIF1C is a kinesin-3 family motor protein that is involved in the transport of dense core vesicles in neurons (Lipka et al., 2016), α5β1 integrin transport to the cell protrusions and maintenance of cell tails in migrating cells (Theisen et al., 2012). In accordance with its function in long distance transport, mutations in KIF1C cause hereditary spastic paraplegia in humans (Dor et al., 2014) (Caballero Oteyza et al., 2014). In this study, the various aspects of KIF1C regulation along with biochemical and mechanical properties of KIF1C and that of the patient mutants were addressed.

6.2. KIF1C is an autoinhibited dimer

In order to transport cargo efficiently across long distances, kinesin motors need to step processively along microtubules. This is achieved by either functioning as dimers (Atherton et al., 2014) or in teams of multiple monomeric units (Oriola and Casademunt, 2013, Soppina and Verhey, 2014, Rogers et al., 2001). For kinesin-3 motor proteins, there are reports suggesting that both these modes are employed. Kinesin-3 family members such as KIF1A and KIF13A exist as monomers and are activated via dimerization (Soppina et al., 2014, Okada and Hirokawa, 1999, Tomishige et al., 2002). Whereas KIF13B and KIF16B are dimers with a tail block which is relieved upon cargo and/or adapter binding (Farkhondeh et al., 2015, Yamada et al., 2007, Yoshimura et al., 2010, Hammond et al., 2009). We show here that KIF1C is a dimer in solution which has a slight shift in migration with the increase ionic strength suggesting that the motor might be in an equilibrium between extended and compact states. At physiological salt concentrations,

KIF1C adopts a compact conformation and transitions to an elongated state at higher ionic strength. This is similar to data reported for kinesin-1, which also undergoes a conformation change from a compact state in low ionic strength to an extended one in high ionic strength (Hackney et al., 1992). Using rotary shadow electron microscopy, the closed, folded state has been visualised for kinesin-1, while KIF1A appeared to be circular and compact with the tail close to the motor domain (Hirokawa, 1998, Hackney et al., 1992).

From the hydrodynamic analysis, the calculated mass of KIF1C was 239 kD which is close to the predicted mass of a KIF1C for a dimeric motor (308 kD). This is consistent with earlier findings that in intact cells under transient overexpression, the motor protein dimerizes (Dorner et al., 1999).

We employed cross-link mass spectrometry to validate the conformation state of KIF1C and found that the tail domain of KIF1C, specifically the third coiled coil (CC3) and FHA region made contacts with the second coiled coil (CC2) and the motor domain. This could mean that the tail region engages the motor heads and making them unavailable to bind microtubules. From kinesin-1 data it is known that the tail domain binds to the motor domain via the neck coiled coil region to keep it in a closed auto inhibitory state (Friedman and Vale, 1999, Stock et al., 1999, Coy et al., 1999). Similarly, reports for KIF16B also suggest that the second and third coiled coil make contacts with the motor domain to keep it in an autoinhibited state (Farkhondeh et al., 2015). We used deletion constructs of KIF1C lacking the third coiled coil region to determine if they are hyperactive. If the third coiled coil domain makes contacts with the motor domain then in the absence of this region, the motor should be hyperactive. The third coiled coil deletion construct was seen accumulating at all plus-ends without a rear bias and the cells observed lacked tails and were circular in shape, displaying a hyperactive phenotype and consistent with the cross-links identified by mass spectrometry.

Taken together, the hydrodynamic analysis and cross-link mass spectrometry data suggest that KIF1C is in a compact conformation with the tail making contacts with the motor domain to keep it in a “closed” tail block state. However, the cross-link mass spectrometry experiments were performed only

once. Further experiments including repetitions of the cross-linking mass spectrometry and negative stain electron microscopy would help validate the results observed. The mutations generated were based solely on cross-link data. The exact interaction surfaces could be elsewhere. Co-crystallization studies with KIF1C motor domain and tail peptides would also help give insight into the interaction sites. FRAP (fluorescence recovery after photo bleaching) experiments in cells could help understand what happens when the hyperactive motor reaches the plus-end, it would be interesting to know if there is a bi-directional movement occurring or if the motors are stuck at the periphery since negative regulation via autoinhibition is not possible. However, it is known in KIF1C depleted cells the tail lifespan is reduced and there is loss of directional persistence (Theisen et al., 2012). In addition to this, in-vitro experiments such as purifying the deletion constructs and the coiled coil two mutant proteins and testing for their activity in a single molecule assay would also give insight into the activity of these constructs.

6.3. PTPN21 FERM domain is an activator of KIF1C

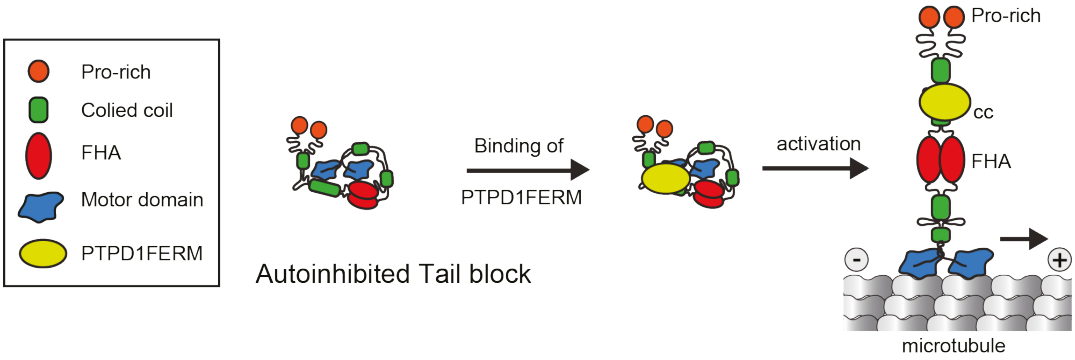

Figure 6.1: Mechanism of KIF1C activation
KIF1C is in a autoinhibited tail-block state which gets activated upon binding to PTPN21 FERM domain and lands on microtubules.

Activation of an autoinhibited motor by cargo interaction has been observed for many kinesins where the motor is activated either by binding to its cargo directly (Yamada et al., 2007) or by cargo adapter proteins that mediate motor activation and cargo loading (Wagner et al., 2009, Hsu et al., 2011, Wu et al., 2016). PTPN21 FERM domain was identified to interact with KIF1C in a yeast two-hybrid screen (Dorner et al., 1998). Previous reports

generated in the lab (Bachmann et al, unpublished) indicated that PTPN21, a scaffolding phosphatase restores KIF1C mediated α5-integrin transport when overexpressed in KIF1C-depleted cells. This led to a hypothesis in which KIF1C is in a closed autoinhibited state, and the binding of PTPN21 relieves autoinhibition. However, there is also the possibility that PTPN21 FERM domain activates another kinesin motor in cells, such as KIF16B which is also known to interact with PTPN21 (Carlucci et al., 2010).

Cross-linking mass spectrometry experiments with PTPN21 FERM domain and KIF1C revealed a lack of crosslinks between KIF1C coiled coil region and motor domain. Instead, there were new crosslinks identified between KIF1C and PTPN21 FERM domain. The absence of the crosslinks between the coiled coil regions and the motor domain supports the idea that maybe the binding of PTPN21 FERM domain has relieved KIF1C autoinhibition. Furthermore, single molecule motility assays with KIF1C and PTPN21 FERM domain showed a significant increase in the landing events and frequency of running motors observed. In addition, there was no difference in the frequency of running motors or landing rates between KIF1C and the FERM domain of Ezrin, suggesting that the effect is specific to the FERM domain of PTPN21 and KIF1C.

Thus, these data confirm that indeed PTPN21 FERM domain binds to KIF1C and relieves the inhibition of the tail region, thereby activating the motor. Further experiments are required to dissect the binding kinetics of KIF1C and PTPN21. It would be interesting to find out how many molecules of PTPN21 are bound to KIF1C. It would also be insightful to determine if PTPN21 remains bound to KIF1C after activation and waits until cargo binds to dissociate since premature dissociation might promote autoinhibition. It is known that adapter proteins recruit motors to the cargo and steer them (Wagner et al., 2009, Hsu et al., 2011). It is not clear whether PTPN21 is a cargo adapter protein and how its phosphatase activity is regulated. Additionally, experiments such as single molecule motility assays with KIF16B and PTPN21 FERM domain would determine if the activation via PTPN21 FERM domain is specific to KIF1C or redundant across kinesin-3 family members.

KIF1C has also been implicated in bi-directional transport in which there can either be a tug of war where the motors of opposite polarity pull against each other and the strongest team wins (Amrute-Nayak and Bullock, 2012, Derr et al., 2012) or by a steric inhibition mechanism where one of the motor is active while the other is in a weakly bound state contributing to the processivity of the entire complex (Hancock, 2014). However, KIF1C depletion studies have shown that there is loss of movement in both directions (Schlager et al., 2010, Theisen et al., 2012). KIF1C and dynein both bind to adapter proteins such as BICDR-1 and HOOK3 (Schlager et al., 2010, Redwine et al., 2017, Schlager et al., 2014) which are proposed to facilitate cooperation between the two motors. KIF1C and BICDR-1 also bind Rab6A (Schlager et al., 2010, Lee et al., 2015) linking both dynein and KIF1C to cargo. Rab6A binds KIF1C at the tail region and at the motor domain. The binding of Rab6A to the motor domain disrupts the motor's ability to walk along microtubules (Lee et al., 2015) while the consequence of the tail binding could promote cargo loading and activation. Rab6A could thereby act as a possible switch in bi-directional transport due to its ability to inhibit KIF1C. Other kinesin members such as KIF1A/UNC104 have also been reported to be involved in bi-directional transport (Tien et al., 2011). It has been hypothesized that the kinesin-3 motors cooperate with dynein to regulate bi-directional transport of cargo (Bielska et al., 2014), however the mechanism of this has been poorly understood. Recent cryo electron microscopy reports suggest that in the presence of BICDR-1, one dynactin unit acts as a scaffold and recruits four dynein heavy chains which results in an increase in both speed and force exerted by the dynein complex compared with a single, dimeric dynein-dynactin-BICD2 complex (Grotjahn et al., 2017, Urnavicius et al., 2017). However, it remains to be seen if PTPN21 binding results in an increase in KIF1C force generation and regulates switching of bidirectional transport complexes.

6.4. The Proline-rich region is required for KIF1C localisation in cells

In RPE cells, KIF1C accumulates at the tip of the tail and delivers α5β1 integrin receptors that are required for the maturation of trailing adhesion and maintenance of cell tails (Theisen et al., 2012). To address how KIF1C is retained at the tip of the tail, KIF1C truncation constructs were used in co-localization studies with full-length KIF1C which revealed that the proline-rich region in the C-terminus was necessary for efficient localisation of KIF1C at the front as well as rear, although it accumulates to a greater extent at the rear of the cell. Proline-rich regions are known to mediate protein-protein interactions (Williamson, 1994) and from the co-localization studies it is evident that the this region contributes to localization of KIF1C. The different proteins known to bind KIF1C via the proline-rich region are BICDR-1, 14-3-3 and Rab6 proteins. However, the construct $KIF1C_{1\text{-}1043}$GFP lacks the 14-3-3, Rab6 binding sites and part of BICDR-1 binding site (811-1090 amino acids). But the region that was found to be required for KIF1C localization was between 950-1043 amino acids, which suggests that this region possibly interacts with yet another unknown protein or it could be possible that any of the above-mentioned tail interacting proteins are involved in this interaction since the mapping sites are in close proximity. In future, experiments can be carried out using chimeric kinesin construct with the kinesin-1 head and KIF1C tail and vice versa. Kinesin-1 does not normally localize to the tail, if the chimeric kinesin-1 head - KIF1C tail construct now localizes to the tail and the vice versa if the KIF1C head - kinesin-1tail does not localize to the tail anymore it would validate that indeed it's the proline-rich region that mediates tail localization. Further to this, pull-down experiments in cell extracts with the proline-rich region could identify potential interactors that bind to this region and possibly anchor the motor protein at the tail and probe the mechanism by which the proline-rich region mediates KIF1C tail localization.

From the co-localization studies using KIF1C constructs it also became clear that the fourth coiled coil region (CC4) was important for dimerization of KIF1C. Previously it has been shown using yeast two-hybrid assay that the CC4 is sufficient to drive dimerization (Dorner et al., 1999). Here, it was

observed that the constructs lacking CC4 domain did not show any co-localization with FL-KIF1C, but the other constructs which included the CC4 domains showed co-localization with FL-KIF1C to varying extents suggesting that CC4 is important for dimerization.

6.5. 14-3-3 proteins negatively regulate KIF1C activity

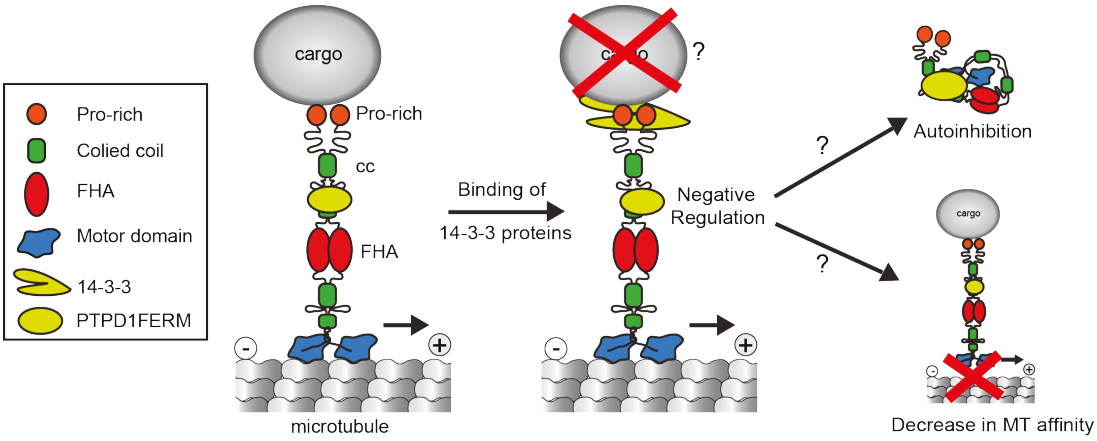

Figure 6.2: Negative regulation by 14-3-3 proteins

In cells, binding of 14-3-3 proteins negatively regulate KIF1C activity. This could be either by stabilizing the autoinhibition state or by reducing the microtubule affinity of the motor resulting in unbinding from the MT.

14-3-3 proteins are known to bind phosphoserine and/or phosphothreonine proteins and regulate their activity (Tzivion et al., 2001). There are seven mammalian isoforms and they exist as dimers (Fu et al., 2000). It is known that the phosphorylation of Ser1092 in KIF1C is required for 14-3-3 binding and mutating the Ser1092 to Ala results in disruption of 14-3-3 binding to KIF1C (Dorner et al., 1999). Here, the functional consequence of 14-3-3 binding was addressed by disrupting the interaction site using mutagenesis.

In cells, it was observed that the S1092A mutant accumulated at a higher level at the tail and front in comparison to wt KIF1C. This means that in the absence of 14-3-3 protein binding, there is higher accumulation observed in cells. These results suggest that 14-3-3 proteins negatively regulate KIF1C. It is known for KIF13B, a kinesin-3 family member that 14-3-3β binding promotes the autoinhibited state (Yoshimura et al., 2010). Similar reports for kinesin-1 and kinesin-6 also suggest the same (Ichimura et al., 2002, Geiger et al., 2014,

Douglas et al., 2010, Joseph et al., 2012) proposing that negative regulation by 14-3-3 proteins is a common mode to “turn off” the motor and it could potentially act as a switch and/or signal for other adapter proteins and/or cargo to bind and drive transport. The S1092E mutant also accumulated to the same extent as that of S1092A mutant. Literature suggests that the amino acid residues glutamate and aspartate do not serve as good phosphomimetic residues with respect to 14-3-3 binding to target proteins (Johnson et al., 2010), which explains why non-phosphorylatable and phosphomimicking mutations result in a similar phenotype. Further experiments in vitro such as microtubule binding assays and single molecule motility assays with purified 14-3-3 proteins and KIF1C would shed light on the mechanism of 14-3-3 regulation. It would be of interest to determine if the binding of 14-3-3 proteins to KIF1C reduces the affinity of the motor to the microtubules or it would promote the interaction between tail and the motor domain to keep the protein in an autoinhibited state as in case of KIF13B. It would also be interesting to identify the kinase that phosphorylates KIF1C at Ser1092 and other potential sites and to determine when and where KIF1C is phosphorylated. Is the kinase present in the vicinity of KIF1C? If so, what is the upstream signalling pathway that determines the phosphorylation status of KIF1C remains to be addressed.

6.6. Force generation of KIF1C and HSP causing patient mutants

The single molecule mechanics of KIF1C gave insight into the mechanical properties of the motor protein. The K-loop is a feature that is specific to kinesin-3 members. Previously it has been shown that this stretch of positively charged lysine residues enhances microtubule binding (Rogers et al., 2001). Since KIF1C is implicated in long distance cargo transport in neurons (Lipka et al., 2016) and disease causing mutations (Caballero Oteyza et al., 2014), it was essential to elucidate these properties. KIF1C was found to walk processively along microtubules under the load of the trap. The step-size of KIF1C was found to be 7.4 nm which is similar to the step-size of kinesin-1 motor protein (8 nm), which corresponds to the distance between microtubule heterodimeric subunits (Svoboda et al., 1993). The stall force for

KIF1C was found to be ~5.5 pN at which the net forward and backward movement is equal. From literature, it is known that dynein has a stall force of around 0.5-1.5 pN (Torisawa et al., 2014, Rai et al., 2013) and kinesin-1 can stall to about 6 pN (Visscher et al., 1999) which is similar to the stall force of KIF1C measured here, suggesting that KIF1C can also generate opposing forces required in bi-directional transport. More recently it has been shown that the DDR complex (dynein, dynactin, BICDR-1) can generate large resistive forces of upto 6.5 pN and can now compete with kinesin motors in a tug-of-war scenario (Urnavicius et al., 2017).

Hereditary spastic paraplegia (HSP) presents with stiffness of the lower limbs and axon degeneration due to defects in various cellular processes one being cargo transport (Blackstone, 2012). It is thought that the efficiency of the motor transport is affected since the mutated motor is either slower or has reduced microtubule affinity (Ebbing et al., 2008). The HSP causing patient mutants in KIF1C that were tested here were able to reach the plus-ends of microtubules with no cargo or load attached. However, they struggled to walk along microtubules under the load of the trap even at low laser power (100mW). This may be due the mutations being present in the well conserved microtubule binding and ATP hydrolysis regions. This in turn might lead to the inability of the motor to generate forces and take forward steps in the presence of the load/cargo attached to the tail. Reports for kinesin-1 and KIF1A suggest that mutation in the motor domain result in lack of stimulation of the motor ATPase and reduced microtubule affinity (Reid et al., 2002, Erlich et al., 2011, Crimella et al., 2012, Dion et al., 2009). However, the mechanism of these HSP causing mutations remains unclear.

6.7. Conclusion

Kinesin-3 family of motor proteins are important neuronal long distance cargo transporters. They are particularly suited for long haul transport since they are highly processive. Hence, it is essential to understand the mode of regulation as well as their mechanism of motor activation since mutations in these motor proteins cause neurological disorders and motor impairments in

humans. However, it has been unclear as to what the mode of activation for this family of motors is (Siddiqui and Straube, 2017).

In this study, we determine the mechanism of activation and elucidate the oligomeric status of KIF1C. The study presented here is consistent with a model in which KIF1C is a dimer which is autoinhibited by its tail region. The PTPN21-FERM domain activates KIF1C. While in cells, the proline-rich region is necessary for proper localisation and the binding of 14-3-3 proteins negatively regulates KIF1C activity. Further to this, the HSP causing disease mutations that were tested, walked along microtubules and reached plus-ends in the absence of a cargo but failed to do the same under load of the trap.

The study presented here has shed light on the mechanism of regulation of KIF1C. However, further experiments are required to better understand if the FERM domain of PTPN21 stabilises the open conformation and since the FERM domain also interacts with KIF16B which is another kinesin-3, Could this be a general mode of activation for kinesin-3 family remains to be seen.

CHAPTER 7 BIBLIOGRAPHY

A, C. U., E, W., B, K., C, J. & A, P. S. 2014. Treatment of trochanteric fractures with the gamma3 nail - methodology and early results of a prospective consecutive monitored clinical case series. *Open Orthop J,* 8**,** 466-73.

AHMED, S. M., THERIAULT, B. L., UPPALAPATI, M., CHIU, C. W., GALLIE, B. L., SIDHU, S. S. & ANGERS, S. 2012. KIF14 negatively regulates Rap1a-Radil signaling during breast cancer progression. *J Cell Biol,* 199**,** 951-67.

AHRENS, J. H. & DIETER, U. 1974. Computer methods for sampling from gamma, beta, poisson and bionomial distributions. *Computing,* 12**,** 223-246.

AL-BASSAM, J., CUI, Y., KLOPFENSTEIN, D., CARRAGHER, B. O., VALE, R. D. & MILLIGAN, R. A. 2003. Distinct conformations of the kinesin Unc104 neck regulate a monomer to dimer motor transition. *J Cell Biol,* 163**,** 743-53.

ALLY, S., LARSON, A. G., BARLAN, K., RICE, S. E. & GELFAND, V. I. 2009. Opposite-polarity motors activate one another to trigger cargo transport in live cells. *J Cell Biol,* 187**,** 1071-82.

AMRUTE-NAYAK, M. & BULLOCK, S. L. 2012. Single-molecule assays reveal that RNA localization signals regulate dynein-dynactin copy number on individual transcript cargoes. *Nat Cell Biol,* 14**,** 416-23.

ATHERTON, J., FARABELLA, I., YU, I. M., ROSENFELD, S. S., HOUDUSSE, A., TOPF, M. & MOORES, C. A. 2014. Conserved mechanisms of microtubule-stimulated ADP release, ATP binding, and force generation in transport kinesins. *Elife,* 3**,** e03680.

ATHERTON, J., HOUDUSSE, A. & MOORES, C. 2013. MAPping out distribution routes for kinesin couriers. *Biol Cell,* 105**,** 465-87.

AULCHENKO, Y. S., HOPPENBROUWERS, I. A., RAMAGOPALAN, S. V., BROER, L., JAFARI, N., HILLERT, J., LINK, J., LUNDSTROM, W., GREINER, E., DESSA SADOVNICK, A., GOOSSENS, D., VAN BROECKHOVEN, C., DEL-FAVERO, J., EBERS, G. C., OOSTRA, B. A., VAN DUIJN, C. M. & HINTZEN, R. Q. 2008. Genetic variation in the

KIF1B locus influences susceptibility to multiple sclerosis. *Nat Genet,* 40**,** 1402-3.

BACHMANN, A. & STRAUBE, A. 2015. Kinesins in cell migration. *Biochem Soc Trans,* 43**,** 79-83.

BELYY, V., SCHLAGER, M. A., FOSTER, H., REIMER, A. E., CARTER, A. P. & YILDIZ, A. 2016. The mammalian dynein-dynactin complex is a strong opponent to kinesin in a tug-of-war competition. *Nat Cell Biol,* 18**,** 1018-24.

BHUWANIA, R., CASTRO-CASTRO, A. & LINDER, S. 2014. Microtubule acetylation regulates dynamics of KIF1C-powered vesicles and contact of microtubule plus ends with podosomes. *Eur J Cell Biol,* 93**,** 424-37.

BIELSKA, E., SCHUSTER, M., ROGER, Y., BEREPIKI, A., SOANES, D. M., TALBOT, N. J. & STEINBERG, G. 2014. Hook is an adapter that coordinates kinesin-3 and dynein cargo attachment on early endosomes. *J Cell Biol,* 204**,** 989-1007.

BLACKSTONE, C. 2012. Cellular pathways of hereditary spastic paraplegia. *Annu Rev Neurosci,* 35**,** 25-47.

BLATNER, N. R., WILSON, M. I., LEI, C., HONG, W., MURRAY, D., WILLIAMS, R. L. & CHO, W. 2007. The structural basis of novel endosome anchoring activity of KIF16B kinesin. *EMBO J,* 26**,** 3709-19.

BRINGMANN, H., SKINIOTIS, G., SPILKER, A., KANDELS-LEWIS, S., VERNOS, I. & SURREY, T. 2004. A kinesin-like motor inhibits microtubule dynamic instability. *Science,* 303**,** 1519-22.

BRITTO, M., GOULET, A., RIZVI, S., VON LOEFFELHOLZ, O., MOORES, C. A. & CROSS, R. A. 2016. Schizosaccharomyces pombe kinesin-5 switches direction using a steric blocking mechanism. *Proc Natl Acad Sci U S A,* 113**,** E7483-E7489.

CABALLERO OTEYZA, A., BATTALOGLU, E., OCEK, L., LINDIG, T., REICHBAUER, J., REBELO, A. P., GONZALEZ, M. A., ZORLU, Y., OZES, B., TIMMANN, D., BENDER, B., WOEHLKE, G., ZUCHNER, S., SCHOLS, L. & SCHULE, R. 2014. Motor protein mutations cause a new form of hereditary spastic paraplegia. *Neurology,* 82**,** 2007-16.

CAI, D., MCEWEN, D. P., MARTENS, J. R., MEYHOFER, E. & VERHEY, K. J. 2009. Single molecule imaging reveals differences in microtubule track selection between Kinesin motors. *PLoS Biol,* 7**,** e1000216.

CARLIER, M. F. & PANTALONI, D. 2007. Control of actin assembly dynamics in cell motility. *J Biol Chem,* 282**,** 23005-9.

CARLUCCI, A., PORPORA, M., GARBI, C., GALGANI, M., SANTORIELLO, M., MASCOLO, M., DI LORENZO, D., ALTIERI, V., QUARTO, M., TERRACCIANO, L., GOTTESMAN, M. E., INSABATO, L. & FELICIELLO, A. 2010. PTPD1 supports receptor stability and mitogenic signaling in bladder cancer cells. *J Biol Chem,* 285**,** 39260-70.

CARTER, N. J. & CROSS, R. A. 2005. Mechanics of the kinesin step. *Nature,* 435**,** 308-12.

CHANG, Q., NITTA, R., INOUE, S. & HIROKAWA, N. 2013. Structural basis for the ATP-induced isomerization of kinesin. *J Mol Biol,* 425**,** 1869-80.

COY, D. L., HANCOCK, W. O., WAGENBACH, M. & HOWARD, J. 1999. Kinesin's tail domain is an inhibitory regulator of the motor domain. *Nat Cell Biol,* 1**,** 288-92.

CRIMELLA, C., BASCHIROTTO, C., ARNOLDI, A., TONELLI, A., TENDERINI, E., AIROLDI, G., MARTINUZZI, A., TRABACCA, A., LOSITO, L., SCARLATO, M., BENEDETTI, S., SCARPINI, E., SPINICCI, G., BRESOLIN, N. & BASSI, M. T. 2012. Mutations in the motor and stalk domains of KIF5A in spastic paraplegia type 10 and in axonal Charcot-Marie-Tooth type 2. *Clin Genet,* 82**,** 157-64.

CROSS, R. A. 2016. Review: Mechanochemistry of the kinesin-1 ATPase. *Biopolymers,* 105**,** 476-82.

DELEVOYE, C., MISEREY-LENKEI, S., MONTAGNAC, G., GILLES-MARSENS, F., PAUL-GILLOTEAUX, P., GIORDANO, F., WAHARTE, F., MARKS, M. S., GOUD, B. & RAPOSO, G. 2014. Recycling endosome tubule morphogenesis from sorting endosomes requires the kinesin motor KIF13A. *Cell Rep,* 6**,** 445-54.

DERR, N. D., GOODMAN, B. S., JUNGMANN, R., LESCHZINER, A. E., SHIH, W. M. & RECK-PETERSON, S. L. 2012. Tug-of-war in motor protein ensembles revealed with a programmable DNA origami scaffold. *Science,* 338**,** 662-5.

DION, P. A., DAOUD, H. & ROULEAU, G. A. 2009. Genetics of motor neuron disorders: new insights into pathogenic mechanisms. *Nat Rev Genet,* 10**,** 769-82.

DIXIT, R., ROSS, J. L., GOLDMAN, Y. E. & HOLZBAUR, E. L. 2008. Differential regulation of dynein and kinesin motor proteins by tau. *Science,* 319**,** 1086-9.

DOR, T., CINNAMON, Y., RAYMOND, L., SHAAG, A., BOUSLAM, N., BOUHOUCHE, A., GAUSSEN, M., MEYER, V., DURR, A., BRICE, A., BENOMAR, A., STEVANIN, G., SCHUELKE, M. & EDVARDSON, S.

2014. KIF1C mutations in two families with hereditary spastic paraparesis and cerebellar dysfunction. *J Med Genet,* 51**,** 137-42.

DORNER, C., CIOSSEK, T., MULLER, S., MOLLER, P. H., ULLRICH, A. & LAMMERS, R. 1998. Characterization of KIF1C, a new kinesin-like protein involved in vesicle transport from the Golgi apparatus to the endoplasmic reticulum. *J Biol Chem,* 273**,** 20267-75.

DORNER, C., ULLRICH, A., HARING, H. U. & LAMMERS, R. 1999. The kinesin-like motor protein KIF1C occurs in intact cells as a dimer and associates with proteins of the 14-3-3 family. *J Biol Chem,* 274**,** 33654-60.

DOUGLAS, M. E., DAVIES, T., JOSEPH, N. & MISHIMA, M. 2010. Aurora B and 14-3-3 coordinately regulate clustering of centralspindlin during cytokinesis. *Curr Biol,* 20**,** 927-33.

DRERUP, C. M., LUSK, S. & NECHIPORUK, A. 2016. Kif1B Interacts with KBP to Promote Axon Elongation by Localizing a Microtubule Regulator to Growth Cones. *J Neurosci,* 36**,** 7014-26.

DUROCHER, D. & JACKSON, S. P. 2002. The FHA domain. *FEBS Letters,* 513**,** 58-66.

EBBING, B., MANN, K., STAROSTA, A., JAUD, J., SCHOLS, L., SCHULE, R. & WOEHLKE, G. 2008. Effect of spastic paraplegia mutations in KIF5A kinesin on transport activity. *Hum Mol Genet,* 17**,** 1245-52.

EDDE, B., ROSSIER, J., LE CAER, J. P., DESBRUYERES, E., GROS, F. & DENOULET, P. 1990. Posttranslational glutamylation of alpha-tubulin. *Science,* 247**,** 83-5.

EFIMOVA, N., GRIMALDI, A., BACHMANN, A., FRYE, K., ZHU, X., FEOKTISTOV, A., STRAUBE, A. & KAVERINA, I. 2014. Podosome-regulating kinesin KIF1C translocates to the cell periphery in a CLASP-dependent manner. *J Cell Sci,* 127**,** 5179-88.

ELLURU, R. G., BLOOM, G. S. & BRADY, S. T. 1995. Fast axonal transport of kinesin in the rat visual system: functionality of kinesin heavy chain isoforms. *Mol Biol Cell,* 6**,** 21-40.

ENDOW, S. A. 1999. Determinants of molecular motor directionality. *Nat Cell Biol,* 1**,** E163-7.

ERICKSON, H. P. 2009. Size and shape of protein molecules at the nanometer level determined by sedimentation, gel filtration, and electron microscopy. *Biol Proced Online,* 11**,** 32-51.

ERLICH, Y., EDVARDSON, S., HODGES, E., ZENVIRT, S., THEKKAT, P., SHAAG, A., DOR, T., HANNON, G. J. & ELPELEG, O. 2011. Exome

sequencing and disease-network analysis of a single family implicate a mutation in KIF1A in hereditary spastic paraparesis. *Genome Res,* 21**,** 658-64.

ETIENNE-MANNEVILLE, S. 2010. From signaling pathways to microtubule dynamics: the key players. *Curr Opin Cell Biol,* 22**,** 104-11.

FARKHONDEH, A., NIWA, S., TAKEI, Y. & HIROKAWA, N. 2015. Characterizing KIF16B in neurons reveals a novel intramolecular "stalk inhibition" mechanism that regulates its capacity to potentiate the selective somatodendritic localization of early endosomes. *J Neurosci,* 35**,** 5067-86.

FEHLING, S. K., NODA, T., MAISNER, A., LAMP, B., CONZELMANN, K. K., KAWAOKA, Y., KLENK, H. D., GARTEN, W. & STRECKER, T. 2013. The microtubule motor protein KIF13A is involved in intracellular trafficking of the Lassa virus matrix protein Z. *Cell Microbiol,* 15**,** 315-34.

FISCHER VON MOLLARD, G., SUDHOF, T. C. & JAHN, R. 1991. A small GTP-binding protein dissociates from synaptic vesicles during exocytosis. *Nature,* 349**,** 79-81.

FRIEDMAN, D. S. & VALE, R. D. 1999. Single-molecule analysis of kinesin motility reveals regulation by the cargo-binding tail domain. *Nat Cell Biol,* 1**,** 293-7.

FU, H., SUBRAMANIAN, R. R. & MASTERS, S. C. 2000. 14-3-3 proteins: structure, function, and regulation. *Annu Rev Pharmacol Toxicol,* 40**,** 617-47.

FU, M. M. & HOLZBAUR, E. L. 2014. Integrated regulation of motor-driven organelle transport by scaffolding proteins. *Trends Cell Biol,* 24**,** 564-74.

FUCHS, F. 2004. Role of Unc104/KIF1-related Motor Proteins in Mitochondrial Transport in Neurospora crassa. *Molecular Biology of the Cell,* 16**,** 153-161.

GEIGER, J. C., LIPKA, J., SEGURA, I., HOYER, S., SCHLAGER, M. A., WULF, P. S., WEINGES, S., DEMMERS, J., HOOGENRAAD, C. C. & ACKER-PALMER, A. 2014. The GRIP1/14-3-3 pathway coordinates cargo trafficking and dendrite development. *Dev Cell,* 28**,** 381-93.

GELL, C., FRIEL, C. T., BORGONOVO, B., DRECHSEL, D. N., HYMAN, A. A. & HOWARD, J. 2011. Purification of tubulin from porcine brain. *Methods Mol Biol,* 777**,** 15-28.

GERSON-GURWITZ, A., THIEDE, C., MOVSHOVICH, N., FRIDMAN, V., PODOLSKAYA, M., DANIELI, T., LAKAMPER, S., KLOPFENSTEIN, D.

R., SCHMIDT, C. F. & GHEBER, L. 2011. Directionality of individual kinesin-5 Cin8 motors is modulated by loop 8, ionic strength and microtubule geometry. *EMBO J,* 30**,** 4942-54.

GILBERT, S. P., WEBB, M. R., BRUNE, M. & JOHNSON, K. A. 1995. Pathway of processive ATP hydrolysis by kinesin. *Nature,* 373**,** 671-6.

GOTZE, M., PETTELKAU, J., FRITZSCHE, R., IHLING, C. H., SCHAFER, M. & SINZ, A. 2015. Automated assignment of MS/MS cleavable cross-links in protein 3D-structure analysis. *J Am Soc Mass Spectrom,* 26**,** 83-97.

GROTJAHN, D. A., CHOWDHURY, S., XU, Y., MCKENNEY, R. J., SCHROER, T. & LANDER, G. 2017. Cryo-electron tomography reveals that dynactin recruits a team of dyneins for processive motility. *bioRxiv*.

GRUNEBERG, U., NEEF, R., LI, X., CHAN, E. H., CHALAMALASETTY, R. B., NIGG, E. A. & BARR, F. A. 2006. KIF14 and citron kinase act together to promote efficient cytokinesis. *J Cell Biol,* 172**,** 363-72.

GUARDIA, C. M., FARIAS, G. G., JIA, R., PU, J. & BONIFACINO, J. S. 2016. BORC Functions Upstream of Kinesins 1 and 3 to Coordinate Regional Movement of Lysosomes along Different Microtubule Tracks. *Cell Rep,* 17**,** 1950-1961.

HACKNEY, D. D., LEVITT, J. D. & SUHAN, J. 1992. Kinesin undergoes a 9 S to 6 S conformational transition. *J Biol Chem,* 267**,** 8696-701.

HALL, D. H. & HEDGECOCK, E. M. 1991. Kinesin-related gene unc-104 is required for axonal transport of synaptic vesicles in C. elegans. *Cell,* 65**,** 837-47.

HALLAK, M. E., RODRIGUEZ, J. A., BARRA, H. S. & CAPUTTO, R. 1977. Release of tyrosine from tyrosinated tubulin. Some common factors that affect this process and the assembly of tubulin. *FEBS Lett,* 73**,** 147-50.

HAMMET, A., PIKE, B. L., MCNEES, C. J., CONLAN, L. A., TENIS, N. & HEIERHORST, J. 2003. FHA domains as phospho-threonine binding modules in cell signaling. *IUBMB Life,* 55**,** 23-7.

HAMMOND, J. W., CAI, D., BLASIUS, T. L., LI, Z., JIANG, Y., JIH, G. T., MEYHOFER, E. & VERHEY, K. J. 2009. Mammalian Kinesin-3 motors are dimeric in vivo and move by processive motility upon release of autoinhibition. *PLoS Biol,* 7**,** e72.

HANCOCK, W. O. 2014. Bidirectional cargo transport: moving beyond tug of war. *Nat Rev Mol Cell Biol,* 15**,** 615-28.

HERRMANN, H., BAR, H., KREPLAK, L., STRELKOV, S. V. & AEBI, U. 2007. Intermediate filaments: from cell architecture to nanomechanics. *Nat Rev Mol Cell Biol,* 8**,** 562-73.

HIROKAWA, N. 1998. Kinesin and dynein superfamily proteins and the mechanism of organelle transport. *Science,* 279**,** 519-26.

HIROKAWA, N. & NODA, Y. 2008. Intracellular transport and kinesin superfamily proteins, KIFs: structure, function, and dynamics. *Physiol Rev,* 88**,** 1089-118.

HIROKAWA, N., NODA, Y., TANAKA, Y. & NIWA, S. 2009. Kinesin superfamily motor proteins and intracellular transport. *Nat Rev Mol Cell Biol,* 10**,** 682-96.

HIROKAWA, N., PFISTER, K. K., YORIFUJI, H., WAGNER, M. C., BRADY, S. T. & BLOOM, G. S. 1989. Submolecular domains of bovine brain kinesin identified by electron microscopy and monoclonal antibody decoration. *Cell,* 56**,** 867-78.

HOEPFNER, S., SEVERIN, F., CABEZAS, A., HABERMANN, B., RUNGE, A., GILLOOLY, D., STENMARK, H. & ZERIAL, M. 2005. Modulation of receptor recycling and degradation by the endosomal kinesin KIF16B. *Cell,* 121**,** 437-50.

HORIGUCHI, K., HANADA, T., FUKUI, Y. & CHISHTI, A. H. 2006. Transport of PIP3 by GAKIN, a kinesin-3 family protein, regulates neuronal cell polarity. *J Cell Biol,* 174**,** 425-36.

HSU, C. C., MONCALEANO, J. D. & WAGNER, O. I. 2011. Sub-cellular distribution of UNC-104(KIF1A) upon binding to adaptors as UNC-16(JIP3), DNC-1(DCTN1/Glued) and SYD-2(Liprin-alpha) in C. elegans neurons. *Neuroscience,* 176**,** 39-52.

HUNG, C. O. & COLEMAN, M. P. 2016. KIF1A mediates axonal transport of BACE1 and identification of independently moving cargoes in living SCG neurons. *Traffic,* 17**,** 1155-1167.

HUO, L., YUE, Y., REN, J., YU, J., LIU, J., YU, Y., YE, F., XU, T., ZHANG, M. & FENG, W. 2012. The CC1-FHA tandem as a central hub for controlling the dimerization and activation of kinesin-3 KIF1A. *Structure,* 20**,** 1550-61.

HUTAGALUNG, A. H. & NOVICK, P. J. 2011. Role of Rab GTPases in membrane traffic and cell physiology. *Physiol Rev,* 91**,** 119-49.

ICHIMURA, T., WAKAMIYA-TSURUTA, A., ITAGAKI, C., TAOKA, M., HAYANO, T., NATSUME, T. & ISOBE, T. 2002. Phosphorylation-dependent interaction of kinesin light chain 2 and the 14-3-3 protein. *Biochemistry,* 41**,** 5566-72.

IKEGAMI, K., HEIER, R. L., TARUISHI, M., TAKAGI, H., MUKAI, M., SHIMMA, S., TAIRA, S., HATANAKA, K., MORONE, N., YAO, I., CAMPBELL, P. K., YUASA, S., JANKE, C., MACGREGOR, G. R. & SETOU, M. 2007. Loss of alpha-tubulin polyglutamylation in ROSA22 mice is associated with abnormal targeting of KIF1A and modulated synaptic function. *Proc Natl Acad Sci U S A,* 104**,** 3213-8.

INSALL, R. & MACHESKY, L. 2001. Cytoskeleton. *eLS.* John Wiley & Sons, Ltd.

JANKE, C. 2014. The tubulin code: molecular components, readout mechanisms, and functions. *J Cell Biol,* 206**,** 461-72.

JOHNSON, C., CROWTHER, S., STAFFORD, M. J., CAMPBELL, D. G., TOTH, R. & MACKINTOSH, C. 2010. Bioinformatic and experimental survey of 14-3-3-binding sites. *Biochem J,* 427**,** 69-78.

JOSEPH, N., HUTTERER, A., POSER, I. & MISHIMA, M. 2012. ARF6 GTPase protects the post-mitotic midbody from 14-3-3-mediated disintegration. *EMBO J,* 31**,** 2604-14.

KAAN, H. Y., HACKNEY, D. D. & KOZIELSKI, F. 2011. The structure of the kinesin-1 motor-tail complex reveals the mechanism of autoinhibition. *Science,* 333**,** 883-5.

KERN, J. V., ZHANG, Y. V., KRAMER, S., BRENMAN, J. E. & RASSE, T. M. 2013. The Kinesin-3, Unc-104 Regulates Dendrite Morphogenesis and Synaptic Development in Drosophila. *Genetics,* 195**,** 59-72.

KEVENAAR, J. T., BIANCHI, S., VAN SPRONSEN, M., OLIERIC, N., LIPKA, J., FRIAS, C. P., MIKHAYLOVA, M., HARTERINK, M., KEIJZER, N., WULF, P. S., HILBERT, M., KAPITEIN, L. C., DE GRAAFF, E., AHKMANOVA, A., STEINMETZ, M. O. & HOOGENRAAD, C. C. 2016. Kinesin-Binding Protein Controls Microtubule Dynamics and Cargo Trafficking by Regulating Kinesin Motor Activity. *Curr Biol,* 26**,** 849-61.

KLOPFENSTEIN, D. R., TOMISHIGE, M., STUURMAN, N. & VALE, R. D. 2002. Role of phosphatidylinositol(4,5)bisphosphate organization in membrane transport by the Unc104 kinesin motor. *Cell,* 109**,** 347-58.

KOPP, P., LAMMERS, R., AEPFELBACHER, M., WOEHLKE, G., RUDEL, T., MACHUY, N., STEFFEN, W. & LINDER, S. 2006. The kinesin KIF1C and microtubule plus ends regulate podosome dynamics in macrophages. *Mol Biol Cell,* 17**,** 2811-23.

KRATCHMAROV, R., KRAMER, T., GRECO, T. M., TAYLOR, M. P., CH'NG, T. H., CRISTEA, I. M. & ENQUIST, L. W. 2013. Glycoproteins gE and gI are required for efficient KIF1A-dependent anterograde axonal transport of alphaherpesvirus particles in neurons. *J Virol,* 87**,** 9431-40.

L'HERNAULT, S. W. & ROSENBAUM, J. L. 1985. Chlamydomonas alpha-tubulin is posttranslationally modified by acetylation on the epsilon-amino group of a lysine. *Biochemistry,* 24**,** 473-8.

LAWRENCE, C. J., DAWE, R. K., CHRISTIE, K. R., CLEVELAND, D. W., DAWSON, S. C., ENDOW, S. A., GOLDSTEIN, L. S., GOODSON, H. V., HIROKAWA, N., HOWARD, J., MALMBERG, R. L., MCINTOSH, J. R., MIKI, H., MITCHISON, T. J., OKADA, Y., REDDY, A. S., SAXTON, W. M., SCHLIWA, M., SCHOLEY, J. M., VALE, R. D., WALCZAK, C. E. & WORDEMAN, L. 2004. A standardized kinesin nomenclature. *J Cell Biol,* 167**,** 19-22.

LEE, P. L., OHLSON, M. B. & PFEFFER, S. R. 2015. Rab6 regulation of the kinesin family KIF1C motor domain contributes to Golgi tethering. *Elife,* 4.

LI, J., LEE, G. I., VAN DOREN, S. R. & WALKER, J. C. 2000. The FHA domain mediates phosphoprotein interactions. *J Cell Sci,* 113 Pt 23**,** 4143-9.

LIPKA, J., KAPITEIN, L. C., JAWORSKI, J. & HOOGENRAAD, C. C. 2016. Microtubule-binding protein doublecortin-like kinase 1 (DCLK1) guides kinesin-3-mediated cargo transport to dendrites. *EMBO J,* 35**,** 302-18.

LO, K. Y., KUZMIN, A., UNGER, S. M., PETERSEN, J. D. & SILVERMAN, M. A. 2011. KIF1A is the primary anterograde motor protein required for the axonal transport of dense-core vesicles in cultured hippocampal neurons. *Neurosci Lett,* 491**,** 168-73.

LUDUENA, R. F. & WOODWARD, D. O. 1975. Alpha- and beta-tubulin: separation and partial sequence analysis. *Ann N Y Acad Sci,* 253**,** 272-83.

MA, Y. Z. & TAYLOR, E. W. 1995. Mechanism of microtubule kinesin ATPase. *Biochemistry,* 34**,** 13242-51.

MATSUSHITA, M., TANAKA, S., NAKAMURA, N., INOUE, H. & KANAZAWA, H. 2004. A novel kinesin-like protein, KIF1Bbeta3 is involved in the movement of lysosomes to the cell periphery in non-neuronal cells. *Traffic,* 5**,** 140-51.

MATSUSHITA, M., YAMAMOTO, R., MITSUI, K. & KANAZAWA, H. 2009. Altered motor activity of alternative splice variants of the mammalian kinesin-3 protein KIF1B. *Traffic,* 10**,** 1647-54.

MIKI, H., OKADA, Y. & HIROKAWA, N. 2005. Analysis of the kinesin superfamily: insights into structure and function. *Trends Cell Biol,* 15**,** 467-76.

NAKAGAWA, T., SETOU, M., SEOG, D., OGASAWARA, K., DOHMAE, N., TAKIO, K. & HIROKAWA, N. 2000. A novel motor, KIF13A, transports

mannose-6-phosphate receptor to plasma membrane through direct interaction with AP-1 complex. *Cell,* 103**,** 569-81.

NAKAJIMA, K., TAKEI, Y., TANAKA, Y., NAKAGAWA, T., NAKATA, T., NODA, Y., SETOU, M. & HIROKAWA, N. 2002. Molecular Motor KIF1C Is Not Essential for Mouse Survival and Motor-Dependent Retrograde Golgi Apparatus-to-Endoplasmic Reticulum Transport. *Molecular and Cellular Biology,* 22**,** 866-873.

NAKAJIMA, K. & TANAKA, Y. 2010. Exclusion of Kif1c as a candidate gene for anthrax toxin susceptibility. *Microb Pathog,* 48**,** 188-90.

NANGAKU, M., SATO-YOSHITAKE, R., OKADA, Y., NODA, Y., TAKEMURA, R., YAMAZAKI, H. & HIROKAWA, N. 1994. KIF1B, a novel microtubule plus end-directed monomeric motor protein for transport of mitochondria. *Cell,* 79**,** 1209-20.

NIWA, S., TANAKA, Y. & HIROKAWA, N. 2008. KIF1Bbeta- and KIF1A-mediated axonal transport of presynaptic regulator Rab3 occurs in a GTP-dependent manner through DENN/MADD. *Nat Cell Biol,* 10**,** 1269-79.

NOVICK, P. & ZERIAL, M. 1997. The diversity of Rab proteins in vesicle transport. *Curr Opin Cell Biol,* 9**,** 496-504.

OKADA, Y., HIGUCHI, H. & HIROKAWA, N. 2003. Processivity of the single-headed kinesin KIF1A through biased binding to tubulin. *Nature,* 424**,** 574-7.

OKADA, Y. & HIROKAWA, N. 1999. A processive single-headed motor: kinesin superfamily protein KIF1A. *Science,* 283**,** 1152-7.

OKADA, Y. & HIROKAWA, N. 2000. Mechanism of the single-headed processivity: diffusional anchoring between the K-loop of kinesin and the C terminus of tubulin. *Proc Natl Acad Sci U S A,* 97**,** 640-5.

OKADA, Y., YAMAZAKI, H., SEKINE-AIZAWA, Y. & HIROKAWA, N. 1995. The neuron-specific kinesin superfamily protein KIF1A is a unique monomeric motor for anterograde axonal transport of synaptic vesicle precursors. *Cell,* 81**,** 769-80.

ORIOLA, D. & CASADEMUNT, J. 2013. Cooperative force generation of KIF1A Brownian motors. *Phys Rev Lett,* 111**,** 048103.

OTSUKA, A. J., JEYAPRAKASH, A., GARCIA-ANOVEROS, J., TANG, L. Z., FISK, G., HARTSHORNE, T., FRANCO, R. & BORN, T. 1991. The C. elegans unc-104 gene encodes a putative kinesin heavy chain-like protein. *Neuron,* 6**,** 113-22.

PECKHAM, M. 2011. Coiled coils and SAH domains in cytoskeletal molecular motors. *Biochem Soc Trans,* 39**,** 1142-8.

POLLOCK, N., DE HOSTOS, E. L., TURCK, C. W. & VALE, R. D. 1999. Reconstitution of membrane transport powered by a novel dimeric kinesin motor of the Unc104/KIF1A family purified from Dictyostelium. *J Cell Biol,* 147**,** 493-506.

POPCHOCK, A. R., TSENG, K. F., WANG, P., KARPLUS, P. A., XIANG, X. & QIU, W. 2017. The mitotic kinesin-14 KlpA contains a context-dependent directionality switch. *Nat Commun,* 8**,** 13999.

RAI, A. K., RAI, A., RAMAIYA, A. J., JHA, R. & MALLIK, R. 2013. Molecular adaptations allow dynein to generate large collective forces inside cells. *Cell,* 152**,** 172-82.

RAPPSILBER, J. 2011. The beginning of a beautiful friendship: cross-linking/mass spectrometry and modelling of proteins and multi-protein complexes. *J Struct Biol,* 173**,** 530-40.

RAPPSILBER, J., MANN, M. & ISHIHAMA, Y. 2007. Protocol for micro-purification, enrichment, pre-fractionation and storage of peptides for proteomics using StageTips. *Nat Protoc,* 2**,** 1896-906.

RASHID, D. J., BONONI, J., TRIPET, B. P., HODGES, R. S. & PIERCE, D. W. 2005. Monomeric and dimeric states exhibited by the kinesin-related motor protein KIF1A. *J Pept Res,* 65**,** 538-49.

REDEKER, V., LEVILLIERS, N., SCHMITTER, J. M., LE CAER, J. P., ROSSIER, J., ADOUTTE, A. & BRE, M. H. 1994. Polyglycylation of tubulin: a posttranslational modification in axonemal microtubules. *Science,* 266**,** 1688-91.

REDWINE, W. B., DESANTIS, M. E., HOLLYER, I., HTET, Z. M., TRAN, P. T., SWANSON, S. K., FLORENS, L., WASHBURN, M. P. & RECK-PETERSON, S. L. 2017. The human cytoplasmic dynein interactome reveals novel activators of motility. *Elife,* 6.

REID, E., KLOOS, M., ASHLEY-KOCH, A., HUGHES, L., BEVAN, S., SVENSON, I. K., GRAHAM, F. L., GASKELL, P. C., DEARLOVE, A., PERICAK-VANCE, M. A., RUBINSZTEIN, D. C. & MARCHUK, D. A. 2002. A kinesin heavy chain (KIF5A) mutation in hereditary spastic paraplegia (SPG10). *Am J Hum Genet,* 71**,** 1189-94.

REN, J., HUO, L., WANG, W., ZHANG, Y., LI, W., LOU, J., XU, T. & FENG, W. 2016. Structural Correlation of the Neck Coil with the Coiled-coil (CC1)-Forkhead-associated (FHA) Tandem for Active Kinesin-3 KIF13A. *J Biol Chem,* 291**,** 3581-94.

ROGERS, K. R., WEISS, S., CREVEL, I., BROPHY, P. J., GEEVES, M. & CROSS, R. 2001. KIF1D is a fast non-processive kinesin that demonstrates novel K-loop-dependent mechanochemistry. *EMBO J,* 20**,** 5101-13.

ROOSTALU, J., HENTRICH, C., BIELING, P., TELLEY, I. A., SCHIEBEL, E. & SURREY, T. 2011. Directional switching of the kinesin Cin8 through motor coupling. *Science,* 332**,** 94-9.

SAGONA, A. P., NEZIS, I. P., PEDERSEN, N. M., LIESTOL, K., POULTON, J., RUSTEN, T. E., SKOTHEIM, R. I., RAIBORG, C. & STENMARK, H. 2010. PtdIns(3)P controls cytokinesis through KIF13A-mediated recruitment of FYVE-CENT to the midbody. *Nat Cell Biol,* 12**,** 362-71.

SCARABELLI, G., SOPPINA, V., YAO, X. Q., ATHERTON, J., MOORES, C. A., VERHEY, K. J. & GRANT, B. J. 2015. Mapping the Processivity Determinants of the Kinesin-3 Motor Domain. *Biophys J,* 109**,** 1537-40.

SCHLAGER, M. A., KAPITEIN, L. C., GRIGORIEV, I., BURZYNSKI, G. M., WULF, P. S., KEIJZER, N., DE GRAAFF, E., FUKUDA, M., SHEPHERD, I. T., AKHMANOVA, A. & HOOGENRAAD, C. C. 2010. Pericentrosomal targeting of Rab6 secretory vesicles by Bicaudal-D-related protein 1 (BICDR-1) regulates neuritogenesis. *EMBO J,* 29**,** 1637-51.

SCHLAGER, M. A., SERRA-MARQUES, A., GRIGORIEV, I., GUMY, L. F., ESTEVES DA SILVA, M., WULF, P. S., AKHMANOVA, A. & HOOGENRAAD, C. C. 2014. Bicaudal d family adaptor proteins control the velocity of Dynein-based movements. *Cell Rep,* 8**,** 1248-56.

SCHLUTER, O. M., SCHMITZ, F., JAHN, R., ROSENMUND, C. & SUDHOF, T. C. 2004. A complete genetic analysis of neuronal Rab3 function. *J Neurosci,* 24**,** 6629-37.

SCHNEIDER, R., KORTEN, T., WALTER, WILHELM J. & DIEZ, S. 2015. Kinesin-1 Motors Can Circumvent Permanent Roadblocks by Side-Shifting to Neighboring Protofilaments. *Biophysical Journal,* 108**,** 2249-2257.

SCHOLEY, J. M. 2013. Kinesin-2: a family of heterotrimeric and homodimeric motors with diverse intracellular transport functions. *Annu Rev Cell Dev Biol,* 29**,** 443-69.

SEITZ, A., KOJIMA, H., OIWA, K., MANDELKOW, E. M., SONG, Y. H. & MANDELKOW, E. 2002. Single-molecule investigation of the interference between kinesin, tau and MAP2c. *EMBO J,* 21**,** 4896-905.

SEITZ, A. & SURREY, T. 2006. Processive movement of single kinesins on crowded microtubules visualized using quantum dots. *EMBO J,* 25**,** 267-77.

SHIN, H., WYSZYNSKI, M., HUH, K. H., VALTSCHANOFF, J. G., LEE, J. R., KO, J., STREULI, M., WEINBERG, R. J., SHENG, M. & KIM, E. 2003. Association of the kinesin motor KIF1A with the multimodular protein liprin-alpha. *J Biol Chem,* 278**,** 11393-401.

SIDDIQUI, N. & STRAUBE, A. 2017. Intracellular Cargo Transport by Kinesin-3 Motors. *Biochemistry (Mosc),* 82**,** 803-815.

SONG, Y. H. & MANDELKOW, E. 1993. Recombinant kinesin motor domain binds to beta-tubulin and decorates microtubules with a B surface lattice. *Proc Natl Acad Sci U S A,* 90**,** 1671-5.

SOPPINA, V., NORRIS, S. R., DIZAJI, A. S., KORTUS, M., VEATCH, S., PECKHAM, M. & VERHEY, K. J. 2014. Dimerization of mammalian kinesin-3 motors results in superprocessive motion. *Proc Natl Acad Sci U S A,* 111**,** 5562-7.

SOPPINA, V. & VERHEY, K. J. 2014. The family-specific K-loop influences the microtubule on-rate but not the superprocessivity of kinesin-3 motors. *Mol Biol Cell,* 25**,** 2161-70.

SPLINTER, D., TANENBAUM, M. E., LINDQVIST, A., JAARSMA, D., FLOTHO, A., YU, K. L., GRIGORIEV, I., ENGELSMA, D., HAASDIJK, E. D., KEIJZER, N., DEMMERS, J., FORNEROD, M., MELCHIOR, F., HOOGENRAAD, C. C., MEDEMA, R. H. & AKHMANOVA, A. 2010. Bicaudal D2, dynein, and kinesin-1 associate with nuclear pore complexes and regulate centrosome and nuclear positioning during mitotic entry. *PLoS Biol,* 8**,** e1000350.

STEINMETZ, M. O. & AKHMANOVA, A. 2008. Capturing protein tails by CAP-Gly domains. *Trends Biochem Sci,* 33**,** 535-45.

STETTLER, O., MOYA, K. L., ZAHRAOUI, A. & TAVITIAN, B. 1994. Developmental changes in the localization of the synaptic vesicle protein rab3A in rat brain. *Neuroscience,* 62**,** 587-600.

STOCK, M. F., GUERRERO, J., COBB, B., EGGERS, C. T., HUANG, T. G., LI, X. & HACKNEY, D. D. 1999. Formation of the compact confomer of kinesin requires a COOH-terminal heavy chain domain and inhibits microtubule-stimulated ATPase activity. *J Biol Chem,* 274**,** 14617-23.

SUN, F., ZHU, C., DIXIT, R. & CAVALLI, V. 2011. Sunday Driver/JIP3 binds kinesin heavy chain directly and enhances its motility. *EMBO J,* 30**,** 3416-29.

SVOBODA, K., SCHMIDT, C. F., SCHNAPP, B. J. & BLOCK, S. M. 1993. Direct observation of kinesin stepping by optical trapping interferometry. *Nature,* 365**,** 721-7.

TANAKA, Y., NIWA, S., DONG, M., FARKHONDEH, A., WANG, L., ZHOU, R. & HIROKAWA, N. 2016. The Molecular Motor KIF1A Transports the TrkA Neurotrophin Receptor and Is Essential for Sensory Neuron Survival and Function. *Neuron,* 90**,** 1215-29.

THEISEN, U., STRAUBE, E. & STRAUBE, A. 2012. Directional persistence of migrating cells requires Kif1C-mediated stabilization of trailing adhesions. *Dev Cell,* 23**,** 1153-66.

TIEN, N. W., WU, G. H., HSU, C. C., CHANG, C. Y. & WAGNER, O. I. 2011. Tau/PTL-1 associates with kinesin-3 KIF1A/UNC-104 and affects the motor's motility characteristics in C. elegans neurons. *Neurobiol Dis,* 43**,** 495-506.

TOMISHIGE, M., KLOPFENSTEIN, D. R. & VALE, R. D. 2002. Conversion of Unc104/KIF1A kinesin into a processive motor after dimerization. *Science,* 297**,** 2263-7.

TONG, Y., TEMPEL, W., WANG, H., YAMADA, K., SHEN, L., SENISTERRA, G. A., MACKENZIE, F., CHISHTI, A. H. & PARK, H. W. 2010. Phosphorylation-independent dual-site binding of the FHA domain of KIF13 mediates phosphoinositide transport via centaurin alpha1. *Proc Natl Acad Sci U S A,* 107**,** 20346-51.

TORISAWA, T., ICHIKAWA, M., FURUTA, A., SAITO, K., OIWA, K., KOJIMA, H., TOYOSHIMA, Y. Y. & FURUTA, K. 2014. Autoinhibition and cooperative activation mechanisms of cytoplasmic dynein. *Nat Cell Biol,* 16**,** 1118-24.

TORRES, J. Z., SUMMERS, M. K., PETERSON, D., BRAUER, M. J., LEE, J., SENESE, S., GHOLKAR, A. A., LO, Y. C., LEI, X., JUNG, K., ANDERSON, D. C., DAVIS, D. P., BELMONT, L. & JACKSON, P. K. 2011. The STARD9/Kif16a kinesin associates with mitotic microtubules and regulates spindle pole assembly. *Cell,* 147**,** 1309-23.

TSUNETOSHI, T., OTSUKA, A., MIKAMI, H., KATAHIRA, K., MORIGUCHI, A. & OGIHARA, T. 1991. Effect of cromakalim (BRL 34915) on hemodynamic and electrocardiographic changes induced by endothelin in dogs. *Basic Res Cardiol,* 86**,** 49-55.

TZIVION, G. & AVRUCH, J. 2002. 14-3-3 proteins: active cofactors in cellular regulation by serine/threonine phosphorylation. *J Biol Chem,* 277**,** 3061-4.

TZIVION, G., SHEN, Y. H. & ZHU, J. 2001. 14-3-3 proteins; bringing new definitions to scaffolding. *Oncogene,* 20**,** 6331-8.

UENO, H., HUANG, X., TANAKA, Y. & HIROKAWA, N. 2011. KIF16B/Rab14 molecular motor complex is critical for early embryonic development by transporting FGF receptor. *Dev Cell,* 20**,** 60-71.

ULBRICH, M. H. & ISACOFF, E. Y. 2007. Subunit counting in membrane-bound proteins. *Nat Methods,* 4**,** 319-21.

URNAVICIUS, L., LAU, C. K., ELSHENAWY, M. M., MORALES-RIOS, E., MOTZ, C., YILDIZ, A. & CARTER, A. P. 2017. Cryo-EM shows how dynactin recruits two dyneins for faster movement. *bioRxiv*.

VALE, R. D. 1996. Switches, latches, and amplifiers: common themes of G proteins and molecular motors. *J Cell Biol,* 135**,** 291-302.

VALE, R. D., CASE, R., SABLIN, E., HART, C. & FLETTERICK, R. 2000. Searching for kinesin's mechanical amplifier. *Philos Trans R Soc Lond B Biol Sci,* 355**,** 449-57.

VAN DER VAART, B., AKHMANOVA, A. & STRAUBE, A. 2009. Regulation of microtubule dynamic instability. *Biochem Soc Trans,* 37**,** 1007-13.

VERHEY, K. J., LIZOTTE, D. L., ABRAMSON, T., BARENBOIM, L., SCHNAPP, B. J. & RAPOPORT, T. A. 1998. Light chain-dependent regulation of Kinesin's interaction with microtubules. *J Cell Biol,* 143**,** 1053-66.

VICENTE-MANZANARES, M., WEBB, D. J. & HORWITZ, A. R. 2005. Cell migration at a glance. *J Cell Sci,* 118**,** 4917-9.

VISSCHER, K., SCHNITZER, M. J. & BLOCK, S. M. 1999. Single kinesin molecules studied with a molecular force clamp. *Nature,* 400**,** 184-9.

VU, H. T., CHAKRABARTI, S., HINCZEWSKI, M. & THIRUMALAI, D. 2016. Discrete Step Sizes of Molecular Motors Lead to Bimodal Non-Gaussian Velocity Distributions under Force. *Phys Rev Lett,* 117**,** 078101.

WAGNER, O. I., ESPOSITO, A., KOHLER, B., CHEN, C. W., SHEN, C. P., WU, G. H., BUTKEVICH, E., MANDALAPU, S., WENZEL, D., WOUTERS, F. S. & KLOPFENSTEIN, D. R. 2009. Synaptic scaffolding protein SYD-2 clusters and activates kinesin-3 UNC-104 in C. elegans. *Proc Natl Acad Sci U S A,* 106**,** 19605-10.

WASILKO, D. J., LEE, S. E., STUTZMAN-ENGWALL, K. J., REITZ, B. A., EMMONS, T. L., MATHIS, K. J., BIENKOWSKI, M. J., TOMASSELLI, A. G. & FISCHER, H. D. 2009. The titerless infected-cells preservation and scale-up (TIPS) method for large-scale production of NO-sensitive

human soluble guanylate cyclase (sGC) from insect cells infected with recombinant baculovirus. *Protein Expr Purif,* 65**,** 122-32.

WATT, D., DIXIT, R. & CAVALLI, V. 2015. JIP3 Activates Kinesin-1 Motility to Promote Axon Elongation. *J Biol Chem,* 290**,** 15512-25.

WATTERS, J. W., DEWAR, K., LEHOCZKY, J., BOYARTCHUK, V. & DIETRICH, W. F. 2001. Kif1C, a kinesin-like motor protein, mediates mouse macrophage resistance to anthrax lethal factor. *Curr Biol,* 11**,** 1503-11.

WEDLICH-SOLDNER, R. 2002. A balance of KIF1A-like kinesin and dynein organizes early endosomes in the fungus Ustilago maydis. *The EMBO Journal,* 21**,** 2946-2957.

WESTERHOLM-PARVINEN, A., VERNOS, I. & SERRANO, L. 2000. Kinesin subfamily UNC104 contains a FHA domain: boundaries and physicochemical characterization. *FEBS Lett,* 486**,** 285-90.

WICKSTEAD, B., GULL, K. & RICHARDS, T. A. 2010. Patterns of kinesin evolution reveal a complex ancestral eukaryote with a multifunctional cytoskeleton. *BMC Evol Biol,* 10**,** 110.

WILLIAMSON, M. P. 1994. The structure and function of proline-rich regions in proteins. *Biochem J,* 297 (Pt 2)**,** 249-60.

WU, G. H., MUTHAIYAN SHANMUGAM, M., BHAN, P., HUANG, Y. H. & WAGNER, O. I. 2016. Identification and Characterization of LIN-2(CASK) as a Regulator of Kinesin-3 UNC-104(KIF1A) Motility and Clustering in Neurons. *Traffic,* 17**,** 891-907.

XING, B. M., YANG, Y. R., DU, J. X., CHEN, H. J., QI, C., HUANG, Z. H., ZHANG, Y. & WANG, Y. 2012. Cyclin-dependent kinase 5 controls TRPV1 membrane trafficking and the heat sensitivity of nociceptors through KIF13B. *J Neurosci,* 32**,** 14709-21.

XU, H., CHOE, C., SHIN, S. H., PARK, S. W., KIM, H. S., JUNG, S. H., YIM, S. H., KIM, T. M. & CHUNG, Y. J. 2014. Silencing of KIF14 interferes with cell cycle progression and cytokinesis by blocking the p27(Kip1) ubiquitination pathway in hepatocellular carcinoma. *Exp Mol Med,* 46**,** e97.

XUE, X., JAULIN, F., ESPENEL, C. & KREITZER, G. 2010. PH-domain-dependent selective transport of p75 by kinesin-3 family motors in non-polarized MDCK cells. *Journal of Cell Science,* 123**,** 1732-1741.

YAMADA, K. H., HANADA, T. & CHISHTI, A. H. 2007. The Effector Domain of Human Dlg Tumor Suppressor Acts as a Switch That Relieves Autoinhibition of Kinesin-3 Motor GAKIN/KIF13B. *Biochemistry,* 46**,** 10039-10045.

YAMADA, K. H., NAKAJIMA, Y., GEYER, M., WARY, K. K., USHIO-FUKAI, M., KOMAROVA, Y. & MALIK, A. B. 2014. KIF13B regulates angiogenesis through Golgi to plasma membrane trafficking of VEGFR2. *J Cell Sci,* 127**,** 4518-30.

YONEKAWA, Y., HARADA, A., OKADA, Y., FUNAKOSHI, T., KANAI, Y., TAKEI, Y., TERADA, S., NODA, T. & HIROKAWA, N. 1998. Defect in synaptic vesicle precursor transport and neuronal cell death in KIF1A motor protein-deficient mice. *J Cell Biol,* 141**,** 431-41.

YOSHIMURA, Y., TERABAYASHI, T. & MIKI, H. 2010. Par1b/MARK2 phosphorylates kinesin-like motor protein GAKIN/KIF13B to regulate axon formation. *Mol Cell Biol,* 30**,** 2206-19.

YUE, Y., SHENG, Y., ZHANG, H. N., YU, Y., HUO, L., FENG, W. & XU, T. 2013. The CC1-FHA dimer is essential for KIF1A-mediated axonal transport of synaptic vesicles in C. elegans. *Biochem Biophys Res Commun,* 435**,** 441-6.

ZERIAL, M. & MCBRIDE, H. 2001. Rab proteins as membrane organizers. *Nat Rev Mol Cell Biol,* 2**,** 107-17.

ZHOU, R., NIWA, S., GUILLAUD, L., TONG, Y. & HIROKAWA, N. 2013. A molecular motor, KIF13A, controls anxiety by transporting the serotonin type 1A receptor. *Cell Rep,* 3**,** 509-19.